INFILTRATION CONTROLS IN A TALLGRASS PRAIRIE AT A HILLSLOPE SCALE

by

SARAH D. AUVENSHINE

B.S., University of Illinois at Urbana-Champaign, 2003

A THESIS

submitted in partial fulfillment of the requirements for the degree

MASTER OF SCIENCE

Department of Civil Engineering
College of Engineering

KANSAS STATE UNIVERSITY
Manhattan, Kansas

2011

Approved by:

Major Professor
David G. Chandler

Copyright

Abstract

Infiltration capacity influences the ability of a soil to absorb and transmit water through macropores and micropores of the soil structure. Infiltration is primarily influenced by the soil type, which is dependent on a number of factors including parent material, climate, biological activity, and topography. Spatial controls of land use, land cover, soil texture, slope position, slope gradient and slope aspect are a few of the variables influencing infiltration capacity within a uniform soil type.

The goals of the thesis are to (1) quantify the spatial distribution of soil hydraulic properties at the surface of a hillslope using one measurement method - the automated mini-disk tension infiltrometer - and several analysis methods, (2) determine the dependence of depth on soil hydraulic properties using two measurement methods, and (3) compare the results of the investigation with information from the soil survey and soil investigations.

First, automated mini-disk infiltrometers were used to determine soil hydraulic properties at ten sites along a hillslope in Konza Prairie Natural Research Area. Several analysis methods were used to extract hydraulic conductivity and sorptivity values from the infiltration data. Next, large intact soil cores were extracted from three selected sites at the same hillslope and analyzed at six depths using a large disk infiltrometer. Finally, the six segments of the large soil cores were analyzed using the same methods as the field measurements with the mini-disk infiltrometers.

The results of the field investigation at the ten sites show a variability of soil hydraulic properties over an assumed homogeneous landscape. The values of hydraulic conductivity and sorptivity are dependent on the method of analysis. An empirically based approach produced more realistic values than a physically based approach.

The results of the laboratory investigation of the three extracted soil cores also show a dependence of method of analysis and measurement. In addition, the results show a complex relationship among landscape position, depth, and soil structure.

Finally, while soil surveys and soil descriptions can provide detailed information on soil properties, an infiltration investigation at a detailed spatial scale provides quantitative values for soil hydraulic properties.

Table of Contents

List of Figures

List of Tables

Acknowledgements

I would like to acknowledge the many people who helped me in my graduate studies and in the creation of my thesis. I would like to acknowledge the late Dan Riener for his testing and field measurements of the mini-disk infiltrometers, Dr. DeAnn Presley for her soil descriptions of the sites, the Civil Engineering Shop for ordering and fabricating the materials needed to conduct the experiments, my committee members, Dr. Dave Steward and Dr. Melinda Daniels, for their support and guidance.

A special acknowledgement goes to my advisor, Dr. David Chandler, for all of his time and patience in guiding me through my graduate studies.

Finally, I would like to thank my husband, Jess, who has been mostly loving and supportive of my educational pursuits.

CHAPTER 1 - Introduction

Objective

A primary resource for any hydrologic investigation is the soil survey. Three databases representing different soil geographic scales have been established by the Natural Resources Conservation Service (NRCS) of the U.S. Department of Agriculture (USDA). The three databases are, in increasing scale, (1) the National Soil Geographic Data Base (NATSGO), (2) State Soil Geographic Data Base (STATSGO), and (3) the Soil Survey Geographic Data Base (SSURGO). The SSURGO with the largest scale, between 1:12,000 and 1:31,680, provides the most detail. Tabular data of the soil properties are linked to maps providing a spatial reference. Soil survey information from SSURGO is adequate for most applications in agronomy or engineering, but additional information is needed to understand land use impact or the natural variation of the soil at a finer spatial scale.

Infiltration capacity influences the ability of a soil to absorb and transmit water through macropores and micropores of the soil structure. Infiltration is primarily influenced by the soil type, which is dependent on a number of factors including parent material, climate, biological activity, and topography. Spatial controls of land use, land cover, soil texture, slope position, slope gradient and slope aspect are a few of the variables influencing infiltration capacity within a uniform soil type.

The hydrologic response to the infiltration-runoff properties of the land cover are seen in the hydrograph. For a downstream response to a precipitation event in an impermeable watershed, all precipitation becomes runoff. The hydrograph is a sheep peak with a high discharge followed by a steep recession. For a completely permeable watershed, where the infiltration capacity of the soil exceeds the precipitation rate, all precipitation infiltrates into the soil. Assuming subsurface return flow, the corresponding hydrograph is longer with a shallower slope and small peak discharge. In reality, most hydrologic responses lie between these two extremes. With less infiltration capacity, the greater the runoff and the greater the peak discharge downstream.

Part of the job of the civil engineer is to manage the runoff response by offsetting development which typically decreases infiltration capacity, with best management practices that reduce or maintain the peak discharge. For land management applications, the higher runoff that

produces higher peak discharge result in greater erosion potential of both the soil on the land and the stream and river channels downstream.

The goals of the thesis are to (1) quantify the spatial distribution of soil hydraulic properties at the surface of a hillslope using one measurement method - the automated mini-disk tension infiltrometer - and several analysis methods, (2) determine the dependence of depth on soil hydraulic properties using two measurement methods, and (3) compare the results of the investigation with information from the soil survey and soil investigations.

First, automated mini-disk infiltrometers were used to determine soil hydraulic properties at ten sites along a hillslope in Konza Prairie Natural Research Area (KPRNA), a tallgrass prairie and a long-term ecological research station near Manhattan, KS. Several analysis methods were used to extract hydraulic conductivity and sorptivity values from the infiltration data. Next, large intact soil cores were extracted from three selected sites at the same hillslope and analyzed at six depths using a large disk infiltrometer. Finally, the six segments of the large soil cores were analyzed using the same methods as the field measurements with the mini-disk infiltrometers.

The results of the field investigation at the ten sites show a variability of soil hydraulic properties over an assumed homogeneous landscape. The values of hydraulic conductivity and sorptivity are dependent on the method of analysis. An empirically based approach produced more realistic values than a physically based approach.

The results of the laboratory investigation of the three extracted soil cores also show a dependence on the method of analysis and measurement. In addition, the results show a complex relationship among landscape position, depth, and soil structure.

Finally, while soil surveys and soil descriptions can provide detailed information on soil properties, an infiltration investigation at a detailed spatial resolution provides quantitative values for soil hydraulic properties.

Hydraulic conductivity varies over an assumed homogeneous landscape, in this case a tallgrass prairie in Konza Prairie Research Natural Area. By using automated mini-disk tension infiltrometers, several measurements of the unsaturated hydraulic conductivity at the surface can be collected quickly and easily at various landscape positions within a watershed. Unsaturated hydraulic conductivity is a function of soil moisture or tension, $K(\theta)$ or $K(h)$. From the data set, a statistical analysis produces a mean, standard deviation, and groupings of the data. In addition

to characterizing the spatial distribution of the surface hydraulic conductivity, a comparison of analysis methods can be made from the infiltration data.

Unsaturated hydraulic conductivity varies over a range of applied tensions or water pressure heads. By measuring infiltration over a range of tensions and at a several depths, information on the soil texture and soil structure can be inferred. That information can be used to create unsaturated flow models to characterize the flux of water through the soil, and the change in soil moisture and pressure head.

Organization of the Thesis

The thesis is broken into three independent experiments. The first is the field measurements at all ten sites using the mini-disk infiltrometers. The next two sections are laboratory measurements using both the mini-disk infiltrometers and large disk infiltrometers on large extracted soil cores from three selected sites.

Background and Previous Studies

Definition of Hydraulic Conductivity

Hydraulic conductivity, *K*, is defined by Darcy's law and is commonly written as

$$q = -K\frac{h}{l} \qquad \textbf{[1-1]}$$

where *q* is the specific discharge, or flux, of water through the soil, *h* is the head loss, and *l* is the length of the soil sample in the direction of specific discharge. The hydraulic gradient, *i*, can be substituted for the head loss per unit length, *h/l*. For saturated condition, hydraulic conductivity is a constant factor that is equal to the specific discharge per unit hydraulic gradient. Other terms for hydraulic conductivity are permeability or the Darcy coefficient of permeability. Intrinsic permeability, κ, which has also been called permeability, is a soil property, while hydraulic conductivity is dependent on both the fluid and the porous medium. Hydraulic conductivity and intrinsic permeability are related by

$$K = \frac{\kappa g \rho}{\mu} \qquad \textbf{[1-2]}$$

where *g* is the acceleration of gravity, ρ is the density of the fluid, and μ is the dynamic viscosity of the fluid. For this study, water is the fluid of interest. Due to temperature fluctuations between the field measurements and the laboratory measurements, adjustments of the hydraulic conductivity for temperature are required to have comparable results. The temperature effects are corrected with the following equation:

$$K_2 = K_1\frac{\mu_1}{\mu_2} \qquad \textbf{[1-3]}$$

where K_1 and K_2 are the hydraulic conductivities at temperatures T_1 and T_2, and μ_1 and μ_2 are the dynamic viscosities of the fluid at T_1 and T_2. The density of the water also changes with temperature but is considered insignificant compared to the change in dynamic viscosity and is not included in equation [1-3].

Applications for Hydraulic Conductivity

Hydraulic conductivity is used in applications of water flow through a porous medium. For an engineer or hydrologist, hydraulic conductivity is used in the creation of detailed

hydrologic models where surface water, typically originating from precipitation, is divided into runoff and infiltration. Runoff is a surface water component of the hydrologic cycle. Runoff from hillslopes flows towards lower elevations and collects in rivers, lakes or other surface water bodies; it can evaporate back into the atmosphere or infiltrate into the ground. Infiltration is water that percolates into the ground. Infiltration can be stored in the root zone and used by vegetation or it can percolate deeper to become groundwater. The division of precipitation into runoff and infiltration has applications in hydrological, environmental, and geotechnical investigations (Bronstert 1999). In the vadose zone, or the unsaturated zone between the ground surface and the water table, the prediction of solute transport, design of agricultural systems for water application or drainage, and environmental risk assessment requires knowledge of unsaturated soil hydraulic properties (Gribb et al 2004). For a soil scientist, a spatial characterization of soil hydraulic properties is used for land management and understanding erosion-deposition processes. A previous study of infiltration at KPRNA examined the effects of burning of a prairie on hillslope hydrology. Infiltration decreased, and runoff and sediment loss increased after burning, but the effects were temporary and disappeared after a few months (Duell, 1990).

Spatial Variability of Hydraulic Conductivity

The hydraulic properties of soil vary spatially as seen in the soil surveys where the soils are classified into soil unit. Each soil unit has estimated values for hydraulic conductivity at the surface and at depths corresponding to soil horizons. Hydraulic conductivity varies at the laterally at the surface and with depth. The hydraulic properties at the surface depend on ground cover, the slope and aspect (Casanova et al 2000), the position along the hillslope (Holden 2009), and can be affected by land use and land management practices (Kechavarzi et al 2009). Hydraulic properties like hydraulic conductivity have been expressed as an exponential function of depth (Beven 1997).

Lateral variability of hydraulic conductivity

The hydraulic conductivity of a soil varies laterally at the surface. In crop land, the type of tillage practice can impact the infiltration capacity of the soil. Minimum tillage and no tillage preserve the macropores of the soil structure and therefore have higher K(h) at near saturation (Kechavarzi et al 2009). Within plots, crop rows were shown to have greater infiltration than

trafficked interrows since the pore structure was destroyed in trafficked rows due to compaction (Mohanty et al 1994, Kechavarzi et al 2009) and the enhancement of infiltration capacity by vegetation (Thompson et al 2010). Spatial influence of the agricultural practices was not as great as the temporal or season variation in crop lands, and could be due to variation in the soil or hydric conditions (Heddadj and Gascuel-Odoux 1999).

Natural processes driven by topography are shown to affect hydraulic conductivity. Topography controls the processes for water distribution in a watershed, and therefore is linked to some soil attributes. Although a direct link between terrain and soil hydraulic properties are mixed (Elsenbeer et al 1992, Sobieraj et al 2002, Mohanty and Mousli 2000).

The aspect of the slope has been shown to be a factor in hydraulic conductivity and soil water retention. North facing slopes had lower K than the adjacent south facing slope, and K(h) tended to increase as the slope increased (Casanova et al 2000). Water retention is as much as 25% more on north facing slopes than on south facing slopes (Geroy et al 2011-IN PRESS).

The slope position can affect macropore flow by the sediment runoff response. Typically steeper slopes produce more runoff, and runoff and sediment transport are directly related. As runoff and sediment are transported down slope, macropores could potentially be filled with sediment further increasing runoff thereby creating feedback loops (Holden 2009).

Variability in the depth of hydraulic conductivity:

The depth dependence of hydraulic conductivity has been described as being an exponential relationship in the context of transmissivity (Beven 1997).

Reason for the change in hydraulic conductivity with respect to depth could be due directly to the soil horizons. As depth increases, the soil transitions from one layer or horizon to another in either a continuous or discontinuous transition. In the case of independent soil horizons, a function to describe the hydraulic conductivity versus depth is not possible with one continuous function. A step function with discontinuities between layers may be appropriate to model the hydraulic conductivity versus depth function. The soil texture and the soil properties change as depth increases, and typically the soil has less structure or a heavier texture either of which relates to lower hydraulic conductivity.

A physical reason for the decreased hydraulic conductivity with depth is due to the overburden of the soil (Rose et al 1965). As the depth increases, the soil has more mass above it, compressing it. The overburden compresses the soil pores decreasing the porosity. The pores

are the areas that would fill and transmit water, and therefore as the quantity and size of pores decrease, the ability of the soil to store and transmit water also decreases.

Length Scale

The length scale or the representative element area or representative element volume is dependent on the variability of soil hydraulic properties. The concept of the length scale is important for the development of measuring or sampling strategies and for modeling the hydrologic processes. Processes that effect hydraulic conductivity may occur at several scales (Zeleke and Si 2005). Biological activity may occur at a scale near the size of a shrub (1 m), while topography or soil texture may be orders of magnitude greater (100 m to 1000 m).

The length scale for a particular watershed may vary considerably depending on the type of model, the hydrologic processes involved in the model, and the variability of the parameters. A single deterministic length scale for a watershed independent of these considerations is not possible (Seyfried and Wilcox 1995).

Methods for Measuring Hydraulic Conductivity

Various methods are available to measure hydraulic conductivity but all come with tradeoffs between ease of application, ease of analysis, cost, time constraints, and the type of results obtained (Gribb et al 2004). The method to determine hydraulic conductivity can be broken into two parts – measurement and analysis. The measurement can either be conducted in the field or in the laboratory. The measurement tools utilized in either field or laboratory measurements have the basic goal of determining the relationship of the amount of water entering or passing through the medium with respect to time. Analytical procedures use the measurement output of flux per time and translate it into hydraulic conductivity and other soil hydraulic properties.

Laboratory Methods

The laboratory methods are direct applications of Darcy's law. In the laboratory the saturated hydraulic conductivity is commonly measured one of two ways: (1) constant-head method and (2) the falling-head method. The constant-head method applies a constant hydraulic head, h, to a volume of soil of length, l, and cross sectional area, A. The total discharge, Q, is measured over time, t, and the saturated hydraulic conductivity, K_{sat}, is calculate with

$$K_{sat} = \frac{Ql}{hAt} \quad \textbf{[1-4]}$$

The falling-head method measures the flow entering the soil sample from a standpipe with the hydraulic head, *h*, decreasing over time. The saturated hydraulic conductivity is calculated with

$$K_{sat} = \frac{aL}{A(t_2 - t_1)} \ln\left(\frac{h_1}{h_2}\right) \quad \textbf{[1-5]}$$

where a is the area of the standpipe, *A* and *l* are the cross sectional area and length of the soil, and h_1 and h_2 are the measured heights of water in the standpipe at t_1 and t_2.

The benefit of these laboratory measurements is their direct application of Darcy's law and, they are the standard methods to determine hydraulic conductivity. Although the analysis of the data is simple and straightforward, the drawback is the amount of time and effort required to perform the experiment. The soil is extracted from the site, stored and transported to the laboratory, and placed in into a device for measurement. Both methods require soil to be extracted and the soil samples to be fully saturated. The length of the experiment depends on the soil texture with less permeable materials taking longer to analyze than more permeable. The falling head method is typically used for less permeable soils like clay.

Another laboratory method is the multi-step outflow method used for determining unsaturated hydraulic conductivity. Using a negative pressure head, the flow rate of water through the soil sample is measured. A relationship between unsaturated hydraulic conductivity, pressure head, and soil moisture is determined for the soil. The multi-step outflow method allows a direct characterization of unsaturated flow and an understanding of the non-linear relationship between hydraulic conductivity, soil moisture, and pressure head.

In laboratory testing, hydraulic conductivity is often performed on disturbed or repacked columns with additional disturbances resulting in the transporting and storing of the samples. Strategies to minimize the disturbance include extracting large samples, encasing to protect during storage and transport, and controlling temperature and humidity.

Field Methods

Although field methods for measuring hydraulic conductivity can produce less accurate values due to poorly defined boundary conditions or assumptions of unsaturated flow, trade-offs in cost efficiency, time, and disturbance are advantages.

Field measurements of water infiltration allow for multiple measurements with relative ease for rapid characterization of the spatial variability of soil hydraulic properties. Field methods typically measure infiltration from a disk, pond, trench, or bore hole. An analysis specific for the measurement method would be used to translate infiltration into hydraulic conductivity. Approximate and semi-empirical analysis methods are used to characterize the spatial variability of field soils (Ahuja et al 1984). Sprinklers, single- or double-ring infiltrometer, borehole permeameter, and tension infiltrometer are a few methods or devices used in determining infiltration in the field. A brief descriptions of selected devices are shown in Table 1.1.

Measurement Device	Description	Measurement
Borehole permeameter	Cylindrical borehole capable of measuring field-saturated hydraulic conductivity at various depths	Infiltration rate into the cylindrical borehole
Single-ring Infiltrometer	Large ring is partially inserted into the ground and water is ponded inside the ring.	Infiltration rate from a ponded cylindrical source
Double-ring Infiltrometer	Similar to single-ring but with two concentric rings where constant head is supplied by the outer ring.	Infiltration rate from a ponded cylindrical source that is bounded by an outer ring, forcing one-dimensional downward flow
Tension infiltrometer	A disk applies a negative pressure head to the soil surface	Infiltration rate from a disk
Sprinkler	Simulates rainfall on a defined plot	Sediment and runoff exiting the plot

Table 1.1. Summary of selected devices used to measure hydraulic conductivity in the unsaturated zone

The sprinkler method simulates rainfall over a plot. With a known application rate verified by rain gauges, the infiltration of water into the soil can be determined by equating the simulated rainfall into infiltration and runoff. The runoff would be collected with a trough at the lower end of the plot and measured with a flume, weir, or other device capable of measuring volume over time. The difference in the simulated rainfall and the runoff would be the infiltration. A benefit to the sprinkler method is the capability to measure sediment loss. A benefit or drawback to the sprinkler method is that the results are averaged over the test plot. Variations within the plot cannot be determined. For finer spatial resolution, point measurements would be taken with another method like the tension infiltrometer.

A tension infiltrometer is a tool that measures unsaturated infiltration rates under a negative pressure head. Being able to apply a negative pressure head, or tension, is important for characterizing hydraulic properties of the vadose zone because it replicates the unsaturated flow conditions that occur above the water table. Hydraulic properties of the soils, sorptivity (S) and hydraulic conductivity (K) can be determined from the infiltration rates (Reynolds and Elrick 1991, Vandervaere et al 2000, Zhang 1997).

Several tension infiltrometer designs have been proposed and produced, but generally consist of three components – (1) a porous disk for the soil-water interface, (2) a water reservoir for storing the water and measuring the flux of water, and (3) a head control for managing the supply pressures (Perroux and White 1988). Using a Marriott tube in a bubble tower for the head control allows for measurements at various pressure heads. An alternative to the bubble tower is a capillary tube near the porous disk. Although a capillary tube does have advantages over the bubble tower (Madsen and Chandler 2007), it is limited in the range of applied pressures. Typical designs have one capillary tube capable of supplying a single negative pressure head. Measurement at one pressure head requires assumptions of soil texture and the soil moisture characteristic curve in order to determine soil hydraulic properties.

Automated mini-disk infiltrometers (Madsen and Chandler 2007) (Figure 1.1) allow for multiple measurements in the field with relative ease in order to understand both the statistical and spatial variability of soil hydraulic properties. The sampling strategy will determine the statistical or spatial inference of the soil hydraulic properties. Tension infiltrometers have been used to determine the soil hydraulic properties under different field conditions for agricultural management (Mohanty et al 1994) and rangeland management (Madsen et al 2008).

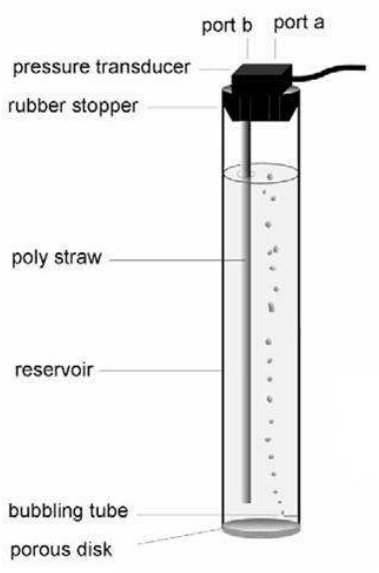

Figure 1.1. Diagram of the automated mini-disk infiltrometer (AMDI) (from Madsen and Chandler 2007)

Unsaturated flow Theory

Darcy's law as shown in equation [1-1] is specifically for saturated conditions when the pores in the soil are completely filled with water and no air remains. For unsaturated conditions, Richards equation is used.

$$\frac{\partial \theta}{\partial t} = \frac{\partial}{\partial z}\left(K(h)\frac{\partial h}{\partial z} \right) + \frac{\partial K(h)}{\partial z} \qquad \textbf{[1-6]}$$

The unsaturated hydraulic conductivity is a function of soil moisture or tension, K(θ) or K(h), with saturated hydraulic conductivity being a constant, K_{sat}. Soil moisture and tension are related through a non-linear soil-water retention function.

Unsaturated flow through the soil is controlled by the relationship between tension, water content, and the unsaturated hydraulic conductivity function K(h) or K(θ). The water content, or soil moisture, θ, is either the mass of water per unit mass of soil, or the volume of water per unit volume of soil. Tension, h, is also called matric suction head, pressure head, or soil water pressure head and has units of length. For example in this study, tension is expressed in unit of cm, and for unsaturated flow, h is negative.

Unsaturated flow is subject to hysteresis. The relationship between soil moisture and tension is path dependent. The wetting curve on the soil-water retention function will have a

lower tension than the draining curve for a given soil moisture content. Hysteresis does not affect hydraulic conductivity with respect to soil moisture. Measurements of infiltration examine only the wetting curve of the soil moisture retention function, and therefore hysteresis effects are not applicable to the study of infiltration.

Several relationships have been developed for the unsaturated hydraulic conductivity functions. A common function is the exponential relationship between pressure head and unsaturated hydraulic conductivity given by Gardner (1958)

$$K(h) = K_{sat} e^{\alpha h} \qquad \textbf{[1-7]}$$

where K_{sat} is the saturated hydraulic conductivity, α is a fitting parameter related to soil structure, and the tension, *h*, is negative. The fitting parameter, α, has also been called the sorptive number. Other empirical expressions relating tension to hydraulic conductivity have been developed and used (Mualem 1986), but the Gardner expression is commonly used because of its simplicity.

The relationship between tension and soil moisture is expressed through a soil-water characteristic curve. Several models have been proposed (Russo 1988). A commonly used model is described by van Genuchten (1980) as

$$\Theta = \left[\frac{1}{1 + (\alpha h)^n} \right]^m \qquad \textbf{[1-8]}$$

where α, *n* and *m* are fitting parameters that are soil dependent, *m* is given by $m = 1 - 1/n$, and Θ is the effective degree of saturation at soil moisture θ given by

$$\Theta = \frac{\theta - \theta_r}{\theta_s - \theta_r} \qquad \textbf{[1-9]}$$

where θ_r is the residual soil moisture, θ_s is the soil moisture at saturation.

For the van Genuchten (1980) soil-water characteristic curve, values for α and *n* can be directly determined using a hanging column or pressure plate measurements or assumed based on soil texture. Typical values for the van Genuchten parameters (α and *n*) for various soil textures have been published in Carsel and Parish (1988) and Schaap and Leij (1998).

Unsaturated hydraulic conductivity, K(h) or K(θ) for h less than zero and θ less than saturation, is a non-linear function dependent on moisture content and tension. The van Genuchten (1980) model provides K(Θ) in the following form:

$$\frac{K(\Theta)}{K_s} = \Theta^{1/2}\left[1-\left(1-\Theta^{1/m}\right)^m\right]^2 \qquad \textbf{[1-10]}$$

Infiltration Analysis Methods

First, the models used in the analysis of infiltration assume a homogeneous, isotropic soil. Tension is controlled, and cumulative infiltration is measured. The foundation of current the studies for tension disk infiltrometers (Bodner et al 2008, Dohnal et al 2010, Reynolds and Elrick 1991, Thompson et al 2010, Vandervaere et al 2000) is the Wooding (1968) solution to three-dimensional steady infiltration from a shallow pond which has been given as the following:

$$Q_S = \left(\frac{r}{G_d} + \pi r^2 \alpha\right)\phi \qquad \textbf{[1-11]}$$

where ϕ is the Kirchhoff transformation, α is the soil structure parameter used in the Gardner equation, G_d is a fitting parameter, and r is the radius of the pond, disk, or water source. The Kirchhoff transform can be approximated by

$$\phi_0 = \frac{K(h)}{\alpha} \qquad \textbf{[1-12]}$$

With the Kirchhoff transform, the Wooding solution can be expressed as

$$Q_S = \left(\frac{r}{G_d \alpha} + \pi r^2\right)K(h) \qquad \textbf{[1-13]}$$

and combining with the Gardner equation yields

$$Q_S = \left(\frac{r}{G_d \alpha} + \pi r^2\right)K_{sat} e^{\alpha h} \qquad \textbf{[1-14]}$$

With two measurements at differing tensions or radii, K_{sat} and α can be determined (Reynolds and Elrick1991). The Wooding-Gardner equation, [1-14], does not require measurements of soil moisture.

From an infiltration measurement, the typical output is cumulative infiltration, *I*, with respect to time. Cumulative infiltration is the volume of that has infiltrated the soil divided by the area of the disk or contact area and is measured in units of length. The simplest form of the infiltration equation is

$$I = C_1 t \qquad \textbf{[1-15]}$$

where C_1 is the infiltration rate, i, and is related to the hydraulic conductivity. Infiltration in the form of equation [1-15] shall be referred to as "simple infiltration" or "simple linear infiltration". The simple infiltration equation neglects any influence of early time sorptivity where infiltration is higher due to the change in soil moisture as the soil is imbibed. Another expression which does factor in sorptivity is the two-term expression for cumulative infiltration (Haverkamp et al 1994, Zhang 1997) given by

$$I = C_1\sqrt{t} + C_2 t \qquad \textbf{[1-16]}$$

where C_1 and C_2 are coefficients relating to sorptivity and hydraulic conductivity. Infiltration in the form of equation [1-16] shall be referred to as "cumulative infiltration". Haverkamp et al (1994) proposed the following physically based expressions valid for transient infiltration:

$$C_1 = S \qquad \textbf{[1-17]}$$

$$C_2 = K_n + \left[\left(\frac{2-b}{3}\right)\left(K - K_n\right) + \left[\frac{\gamma}{r\left(\theta - \theta_n\right)}\right]\right]S^2 \qquad \textbf{[1-18]}$$

Zhang (1997) gives empirical values for the relationship between C_1 and C_2 and sorptivity and hydraulic conductivity dependent on soil hydraulic function, soil type, and infiltrometer parameters.

An alternate approach (Vandervaere et al 2000) is a differentiated form of [1-16] with respect to the square root of time and is given as

$$\frac{dI}{d\sqrt{t}} = C_1 + 2C_2\sqrt{t} \qquad \textbf{[1-19]}$$

Vandervaere et al (2000) uses the same expressions for C_1 and C_2 as Haverkamp et al (1994). Infiltration in the form of equation [1-19**]** shall be referred to as "differential linearization".

The physically based approach from the Vandervaere and Haverkamp methods assumes flow is dominated by gravitational forces rather than lateral capillarity forces. With a small disk radius, the lateral capillary forces are more likely to dominate, and therefore the results of their methods become unreliable (Dohnal et al (2010).

CHAPTER 2 - Study Area

Konza Prairie Research Natural Area (KPRNA), a 3,487-ha long-term ecological research station, is located approximately 5 miles south of Manhattan, Kansas in Riley County. The mean annual temperature is 13°C with average annual precipitation of 844 mm based on the Konza weather station measurements between 1983 and 2009. The area is divided into numerous watersheds; the watersheds are subjected to various burning treatment frequencies or animal grazing. The watershed for this study is watershed 1D, a 40-ha watershed in the southeast quarter of KPRNA as shown in Figure 2.1. Watershed 1D is burned annually and is not subjected to grazing. Watershed 1D is a subbasin of Swede Creek while most of KPRNA is within the Kings Creek watershed.

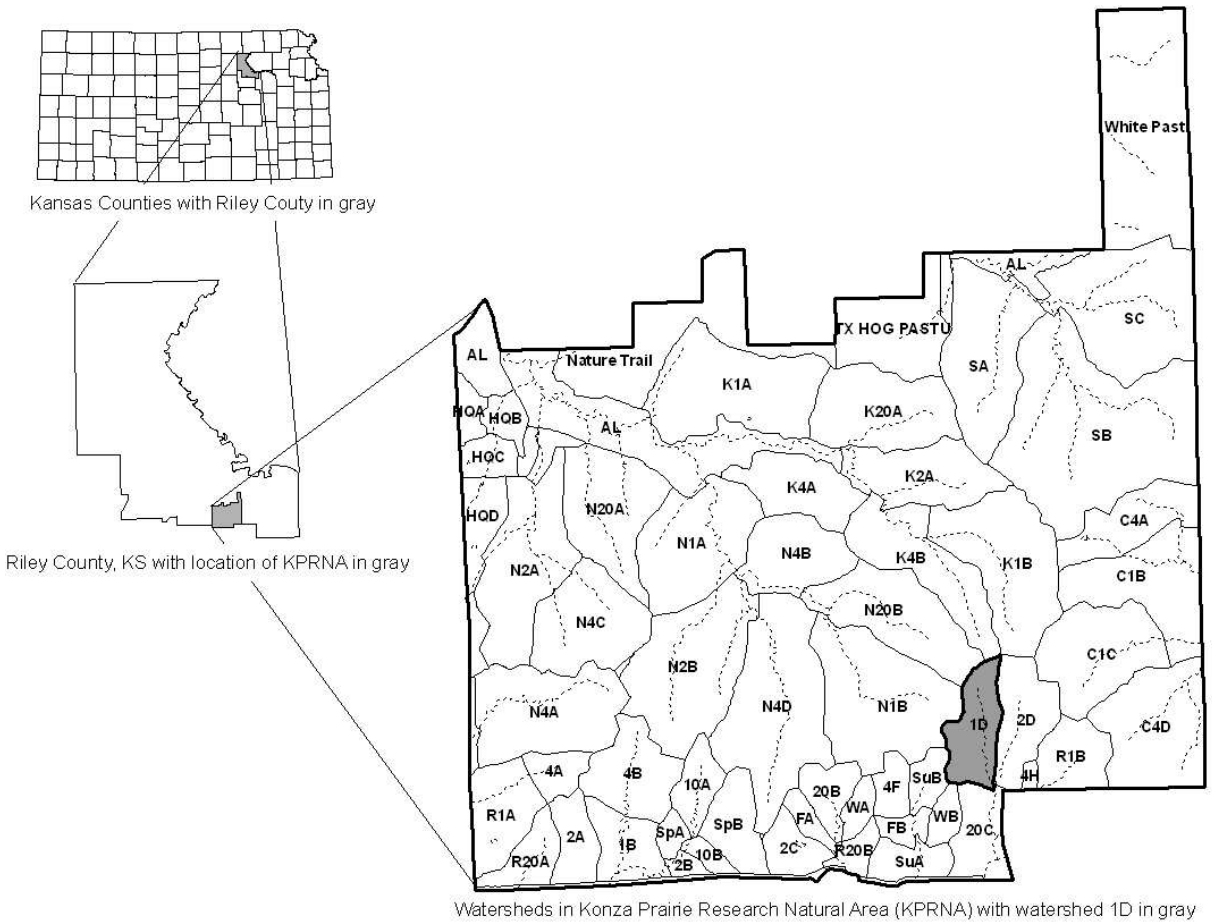

Figure 2.1. Location of Watershed 1D within KPRNA

In watershed 1D, ten sites had previously been established by the Plant Eco-physiology laboratory from the Division of Biology of Kansas State University (Figure 2.2). The ten sites form the sampling strategy for this study. For this study, the sites are classified based on their topographic position with sites 1, 2, 3, and 4 classified as "upland", sites 5, 6, 7, and 8 classified as "slope", and sites 9 and 10 classified as "lowland".

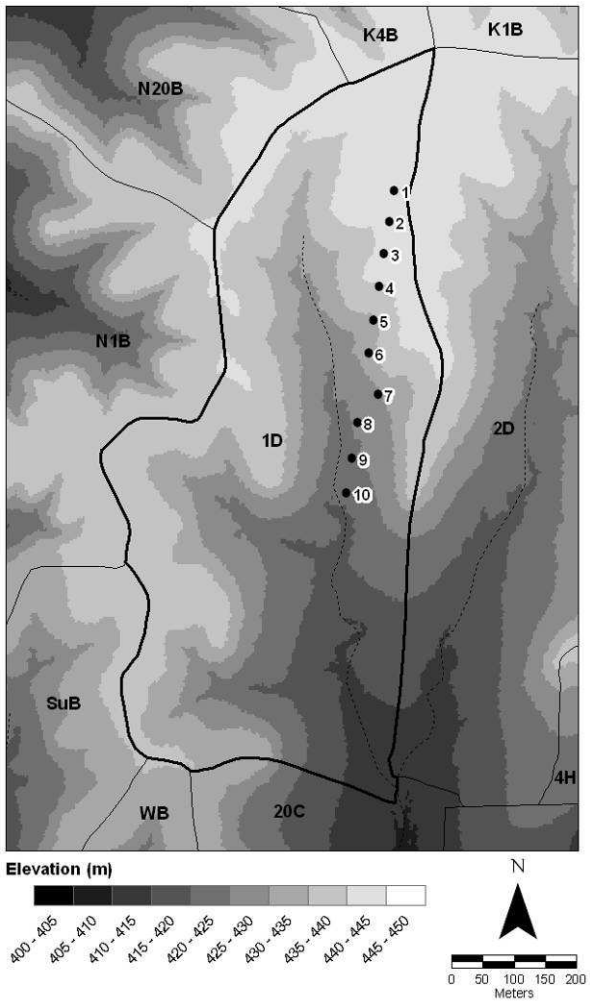

Figure 2.2. Location of reference sites with topography of watershed 1D.

From a previous study of KPRNA watersheds 1D and 1B, 53 total species of plant were encountered with the seven most abundant perennial species being three C4 grasses - Andropogon gerardii (big bluestem), Sorghastrum nutans (Indiangrass), and Schizachyrium scoparium (little bluestem), two C3 forbs - Lespedeza capitata (roundhead lespedeza) and Vernonia baldwinii (Baldwin's ironweed) and two small C3 shrubs - Amorpha canescens (leadplant) and Ceanothus americanus (New Jersey tea) (Nippert and Knapp 2007).

In watershed 1D, the total biomass was dependent on the topographic position. The positions were classified as being upland, break, slope, or lowland. For a model with these four classifications (Model 4), the lowland is defined as sites 9 and 10, the upland is sites 1 and 2, the break is sites 3, 4, and 6, and the slope are sites 5, 7 and 8. Total biomass was highest for the lowland sites and lowest for the break and upland sites. In an alternate model (Model 5), site 5 is classified as a "seep" (Nippert et al 2011).

The geology of KPRNA consists of layers of limestone and shale from the Chase Group and Council Grove Group. A portion of the stratigraphic column applicable to KPRNA is shown in Figure 2.3 (Zeller 1968). The approximate locations for the rock layers are shown in Figure 2.4.

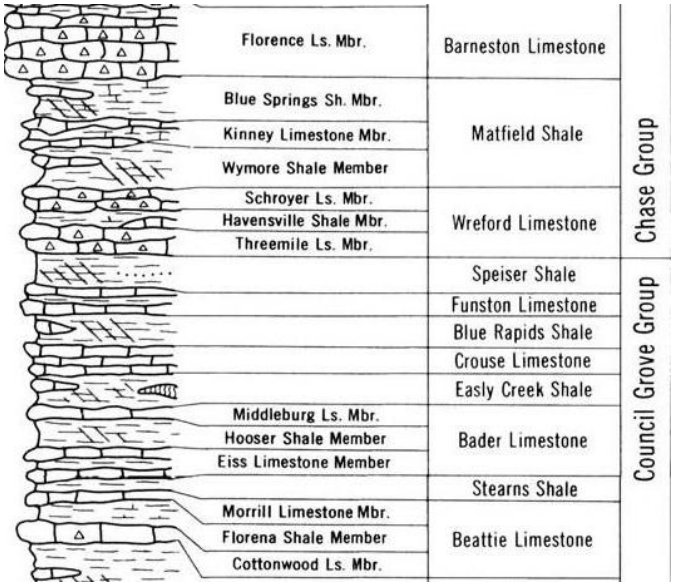

Figure 2.3. Stratigraphic column of Konza Prairie (from Zeller 1968)

The change in elevation of watershed 1D is about 30 m with the sites covering about 20 m of topographic relief (Figure 2.2). The average slope along the transect is 4.8% with the local slopes typically being greater (Figure 2.4). Comparing watershed 1D to adjacent watersheds, the pathway from watershed 1D to the Kansas River via Swede Creek is much longer than the adjacent watersheds (N1B, N20B, K4B) of Kings Creek. The topography of 1D has gentler slopes, less erosion potential, and less exposed rock then the watersheds of Kings Creek.

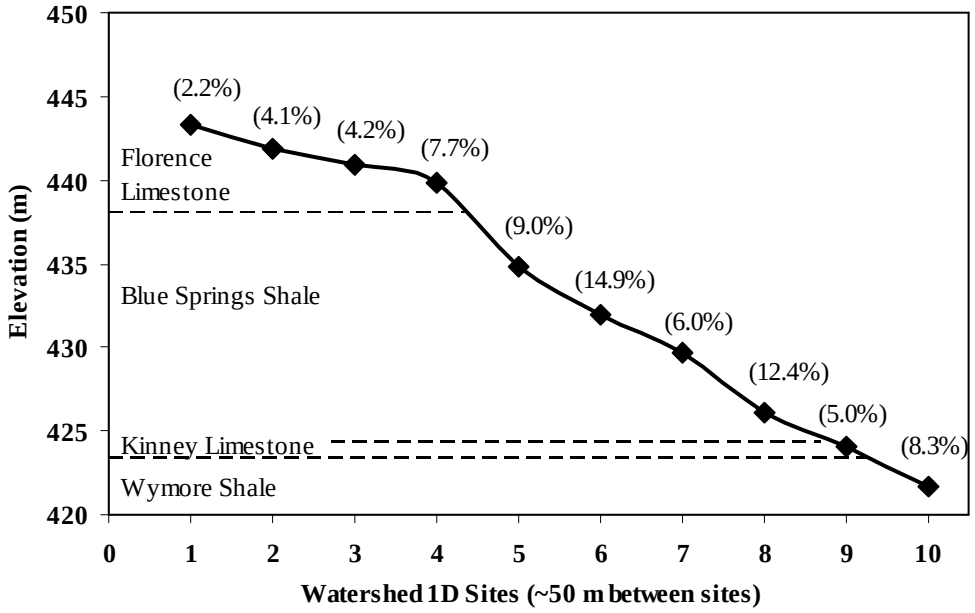

Figure 2.4. Elevations of the 10 sites within watershed 1D showing local slopes (in parentheses) and major rock layers

The thicknesses of each limestone and shale layer were taken from Jewett (1941), and approximated in Figure 2.4 based on field observations of the location of the Florence limestone layer. The Florence limestone layer forms a prominent bench in watershed 1D, and the rock outcropping is observed between sites 4 and 5. From the cross section of the watershed in Figure 2.5, a significant drop in elevation occurs between sites 4 and 5 due to the limestone bench. The local slope at each site is also shown in Figure 2.4. The smallest local gradients are found in the upland area of the watershed and the largest are in the slope.

Soil Descriptions

The soils in the watershed are classified as a silty loam and a silty clay loam. From the county soil survey at scale 1:24,000 (USDA), watershed 1D at KPRNA contains the soil complexes Dwight-Irwin, Benfield-Florence and Tully. The landscape position of these three soil types is consistent with the Benfield-Florence association. From the soil survey, 79% of the watershed is within the Benfield-Florence soil, 16% is within the Tully, and 5% is within the Dwight-Irwin. Of the ten sites in the hillslope, site 1 is within the Dwight-Irwin, and the remaining nine are within the Benfield-Florence. None are located within the Tully (Figure 2.5). The Benfield-Florence complex is a silty clay loam at the surface with an estimated hydraulic conductivity of 3.0 μm/s. The Dwight-Irwin complex is a silty loam at the surface with an estimated hydraulic conductivity of 9.0 μm/s. The Tully is a silty clay loam at the surface with an estimated hydraulic conductivity of 3.0 μm/s.

In the spring of 2011, a soil description was performed at selected sites relating roughly to the uplands, slope, and lowlands of watershed 1D. The following tables (Tables 2.1, 2.2, 2.3 and 2.4) are the results of the soil description investigation with additional details found in Appendix A. In addition to sites 1, 2, 6 and 9, an attempt to describe site 3 was made, but the large amount of stone fragments near the soil surface prevented extraction by the soil probe.

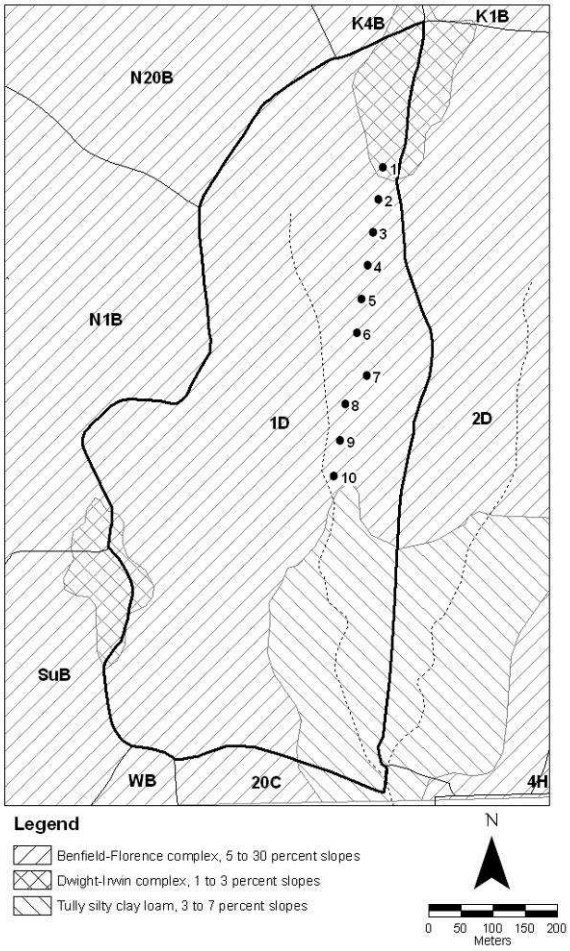

Figure 2.5. Location of reference sites and soil types within watershed 1D

KPRNA Watershed 1D, Site 1 Soil Pedon Properties							
Horizon	Depth	Texture†	% Clay	Structure			Matrix Color
	cm			Grade‡	Size	Type§	Moist
A	0-33	SIL	22	3	Medium	GR	10 YR 3/1
Bt1	33-51	SICL	38	2	Fine	SBK	10 YR 3/3
Bt2	51-66	SICL	38	2	Fine	SBK	7.5 YR 4/3
2Bt3	66-81	SIC	44	2	Fine	PR	5 YR 3/4
2Bt4	81-86+	SIC	44	2	Fine	PR	5 YR 4/4

Table 2.1. Site 1 Soil Pedon Properties.

KPRNA Watershed 1D, Site 2 Soil Pedon Properties							
Horizon	Depth	Texture†	% Clay	Structure			Matrix Color
	cm			Grade‡	Size	Type§	Moist
A1	0-15	SIL	24	3	Fine	GR	10 YR 2/1
A2	15-30	SICL	28	2 Pt 2	Fine Medium	SBK GR	10 YR 3/2
Bt1	30-43	SICL	35	2	Fine	SBK	10 YR 4/3
Bt2	43-53	SICL	39	2	Fine	PR	7.5 YR 4/3
2Bt3	53-66	SIC	42	2	Fine	PR	5 YR 3/3

Table 2.2. Site 2 Soil Pedon Properties.

KPRNA Watershed 1D, Site 6 Soil Pedon Properties							
Horizon	Depth	Texture†	% Clay	Structure			Matrix Color
	cm			Grade‡	Size	Type§	Moist
A	0-20	SIL	20	3	Medium	GR	10 YR 2/1
BA	20-32	SIL	22	2	Fine	SBK	10 YR 2/1
Bt	32-47	SICL	34	2	Fine	PR	10 YR 3/2
2Bt1	47-60	SICL	38	2	Medium	PR	7.5 YR 3/3
2Bt2	60-90	SIC	42	2	Medium	SBK	7.5 YR 3/4
2Bt3	90-110+	SIC	48	2	Medium	PR	5 YR 3/3

Table 2.3. Site 6 Soil Pedon Properties.

KPRNA Watershed 1D, Site 9 Soil Pedon Properties							
Horizon	Depth	Texture†	% Clay	Structure			Matrix Color
	cm			Grade‡	Size	Type§	Moist
A1	0-25	SIL	17	3	Medium	GR	10 YR 2/1
Bt1	25-36	SICL	28	2	Very Fine	SBK	10 YR 3/2
Bt2	36-50	SICL	38	2	Fine	PR	10 YR 3/3
Bt3	50-90+	SIC	44	2	Medium	PR	10 YR 5/4

Table 2.4. Site 9 Soil Pedon Properties.

Notes: † SIL = silt loam, SICL= silty clay loam, SIC = silty clay

‡ 1 = weak, 2= moderate, 3 = strong

§ GR = Granular, SBK = Sub Angular Blocky, PR = Prismatic

¶ Moist colors described in Munsell © notation (Hue, Value, Chroma)

All of the site descriptions have a similar soil texture profile with silt loam on the surface transitioning to a silty clay loam and finally a silty clay. The moist matrix color has a similar consistent transition for three of the four sites described with a black or very dark gray A horizon transition to a brown and to a reddish brown for the B horizon. For site 9, the A horizon moist matrix color is also black but transition to a yellowish brown in the B horizon.

For site 9, the pedon description is similar to the Tully series. For the A1 horizon, the soil survey classifies the soil as a silty clay loam with a moderate structure, but the structure size and type, the moist matrix color, and the depth of horizon are similar to description of the site. The description of the B horizon for site 9 is also similar to the Tully description with slight variations of the color, structure, and horizon depths. Although from the soil map, Site 9 is within the boundaries of the Benfield-Florence series, it is similar to the Tully series and should be considered a Tully soil.

Sites 1, 2, and 6 have a similar pedon description and could be classified as Benfield-Florence soils. With a high prevalence of stone fragments encountered during soil sampling, sites 1 and 2 could also be considered Dwight-Irwin soil.

CHAPTER 3 - Field Measurements with Mini-Disk Infiltrometers

Materials

Automated Mini-disk Infiltrometers (AMDIs) were fabricated in-house with differential pressure transducers and wireless motes to automate data collection. The design is similar to the devices used in Madsen and Chandler (2007) and a version of a product produced by Decagon Devices Inc. (Pullman WA).

Figure 3.1. Automated mini-disk infiltrometers deployed in the field.

The AMDI has a capillary tube to control tension, and from previous laboratory testing that tension was determined to be 3 cm and varying by about ± 0.3 cm. The volume of the reservoir tube for all devices is 96.7 cm^3 with an inside diameter of 2.52 cm and a height of 19 cm. The outside diameter of the tube and the porous disk is 3.16 cm. The differential pressure

transducers (SenSym ASCX01DN, Honeywell, Freeport, IL) have an operating pressure range between 0 and 1 psi equating to a water height range of approximately 70 cm. Each differential pressure transducer was attached to a 3-holed rubber stopper. The two pressure ports occupied two of the holes with port B measuring the base of the water column of the infiltrometer via a tube and port A measuring the top of the water column. The third hole was used for filling the infiltrometer and contained a short tube used to control the maximum height of the water and therefore the volume of water in the infiltrometer. The infiltrometer was filled by aspirating air through a tube attached to a one-way value connected to the third hole in the rubber stopper while the base of the infiltrometer was submerged in water.

AMDIs were connected to wireless miniature data loggers, or "motes" which were housed in solar panel bases with rechargeable batteries. Two motes were employed for the field measurements, and their identifying numbers are 10 and 13. Each mote served a network of seven infiltrometers with six of the seven infiltrometer being used for the measurements. Figure 3.1 shows one network of infiltrometers deployed in the field. The motes excited the pressure transducers on time intervals of approximately five seconds and wirelessly transmitted data to a receiver that was linked to a laptop computer.

Soil moisture was measured with a ThetaProbe (Delta T Devices, Cambridge, England). The device was powered by a 9-volt battery, and a multimeter measured sensor output voltage.

Methods

Unsaturated infiltration tests were performed in the summer of 2009 at ten sites along a diagonal transect from hilltop to stream along the east side of watershed 1D (Figure 2.2). At each site, fine silica sand was placed on the soil surface to ensure proper contact at the disk-soil interface. Two sets of six measurements were collected at a tension of 3 cm. Both sets were taken at the same time under dry initial conditions.

Soil moisture was determined at one measurement location for each site prior to the infiltration test and two measurements for each site following the infiltration test period to determine the change in soil water content. An arbitrary location within 2 m of a set of previously defined observation points was chosen for the initial measurement. The center of one of the six wetted bulbs was chosen for the final measurement after infiltration had ended. The voltage from the ThetaProbe was converted to soil water content.

Data Analysis

Converting Voltage to Soil Moisture

The voltages taken with the Theta Probe were converted into volumetric water content or soil moisture in two steps. First, the voltage, *V*, was converted into real permittivity, ε', from Blonquist et al (2005):

$$\frac{1}{\varepsilon'} = -0.105 + \frac{0.134}{\sqrt{V}} \qquad \textbf{[3-1]}$$

From the user manual of the ThetaProbe Soil Moisture Sensor (ML2x-UM-1.21), the real permittivity term was converted to soil moisture, θ,

$$\theta = \frac{\sqrt{\varepsilon'} - a_0}{a_1} \qquad \textbf{[3-2]}$$

The user manual provides values for the coefficients for mineral soils and organic soils. For mineral soils, the soil type for this study, the coefficients for a_0 and a_1 are 1.6 and 8.4, respectively.

Converting Voltage to Volume

The raw data collected with the AMDIs is in voltages. The voltages relate to the relative height of water in the infiltrometer tube. The following from Madsen and Chandler (2007) converts the voltage to volume:

$$V(t) = V_{tot}\left[1 - \frac{v_0(t) - v_{\min}}{v_{\max} - v_{\min}}\right] \qquad \textbf{[3-3]}$$

Where $v_0(t)$ is the voltage at time t, v_{max} is the maximum voltage, v_{min} is the minimum voltage, V_{tot} is the total volume infiltrated, and $V(t)$ is the volume of water infiltrated at time t. For the mini-disk infiltrometers used in this study, the total volume of water in the reservoir is 96.7 cm^3. Since all infiltration runs ended with the reservoirs being exhausted of water, the total volume of water infiltration is equal to the reservoir volume.

Converting Volume to Infiltration

The collected data was analyzed with the spreadsheet software (Excel, Microsoft Inc, Redmond, WA). Each infiltration test lasted approximately between 15 and 30 minutes. Sequential calculations of time from the start of the test, square root of time from the start of the test, cumulative infiltration, and two terms for the differential linearization analysis were computed to analyze the infiltration data. Cumulative infiltration was computed by taking the volume at time t, $V(t)$, from [3-3] and dividing by the area of the porous disk.

The two terms for the differential linearization (Vandervaere et al 2000) are the differential of the cumulative infiltration versus the square root of time and the geometric mean of the square root of time, where the first term is given by

$$\frac{dI}{d\sqrt{t}} \approx \frac{\Delta I}{\Delta\sqrt{t}} = \frac{I_{i+1} - I_i}{\sqrt{t_{i+1}} - \sqrt{t_i}} \qquad \textbf{[3-4]}$$

The corresponding square root of time term in [3-4] is the geometric mean of the square root of time given by

$$\sqrt{t} = \left[\sqrt{t_i t_{i+1}}\right]^{0.5} \qquad \textbf{[3-5]}$$

Converting Infiltration to Hydraulic Conductivity and Sorptivity

Three graphs were produced for each infiltration measurement. The simple infiltration analysis (Figure 3.2) examines the cumulative infiltration versus time with a linear regression.

The start time for the simple infiltration was modified to remove the early time values dominated by sorptivity. The data series window for the regression analysis was adjusted to optimize the linearity of the sample by adjusting the start time until a maximum R-squared value was found. The cumulative infiltration analysis (Figure 3.3) examines the cumulative infiltration versus the square root of time with a second order polynomial regression with a fixed point at the origin. The differentiated linearization analysis (Figure 3.4) examines the change in infiltration over the change in the square root of time versus the square root of time with a linear regression. The coefficients on the regressed lines are used in the calculations for hydraulic conductivity and sorptivity at the applied tension of -3 cm.

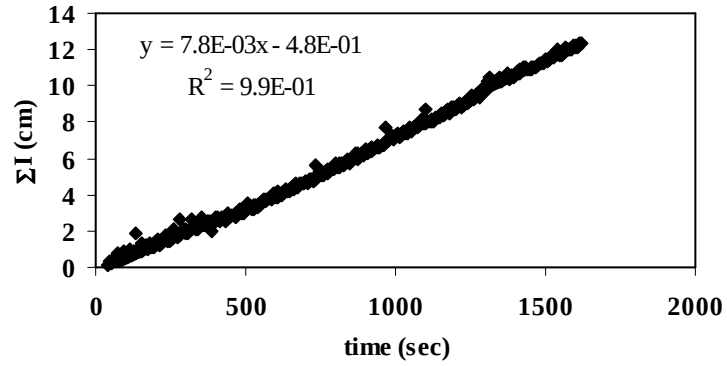

Figure 3.2. Simple infiltration for Site 2, Mote 10, Channel 1

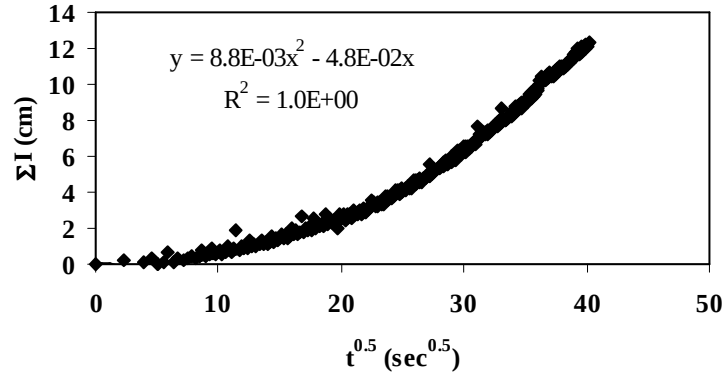

Figure 3.3. Cumulative infiltration for Site 2, Mote 10, Channel 1

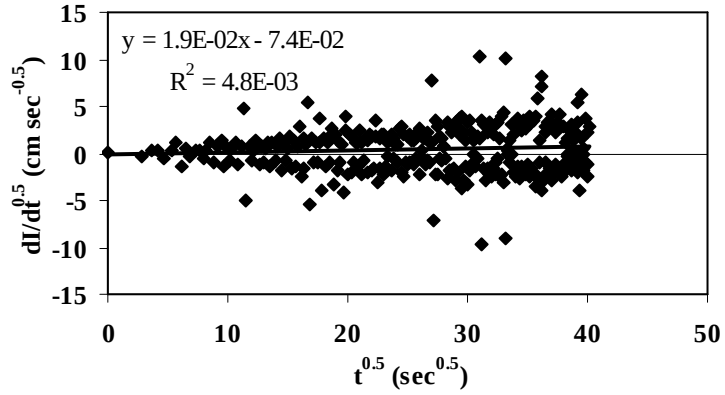

Figure 3.4. Differential linearization for Site 2, Mote 10, Channel 1

The differential linearization consistently produced a very small R^2. This is a result of the electronic noise from the pressure transducer being amplified with the differential linearization analysis. As the volume of water in the reservoir tube decreased, the voltage output from the pressure transducer tended to decrease also. The residual noise produced from the electronics was typically greater than the decease in voltage that was measured at five second intervals. In other words, from one time step to the next, the voltage may increase or decrease, but it tended to decrease. The very small R^2 value shown in Figure 3.4 for the differential linearization process is primarily due to the electronic noise.

In order to utilize the differential linearization technique and have confidence in the results, the data was resampled using the results from the cumulative infiltration analysis as shown in Figure 3.3. Using the data from Site 2, Mote 10, Channel 1 as an example, the equation shown in Figure 3.3 was used to populate the raw cumulative infiltration data, *I*. The resampled cumulative infiltration data is a representation of the original data but without the electronic noise. If the resampled infiltration data is analyzed with the differential linearization analysis, then the results produce a much higher R^2 value as shown in Figure 3.5. The coefficients from the resampled differential linearization and the cumulative infiltration are similar as expected.

Another problem with the differential linearization method is a negative term relating to the sorptivity in the regression equation. This is separate from the small R^2 value that was remedied with resampling, and it is not unique to the differential linearization method because the negative sorptivity term is also seen in the cumulative infiltration method.

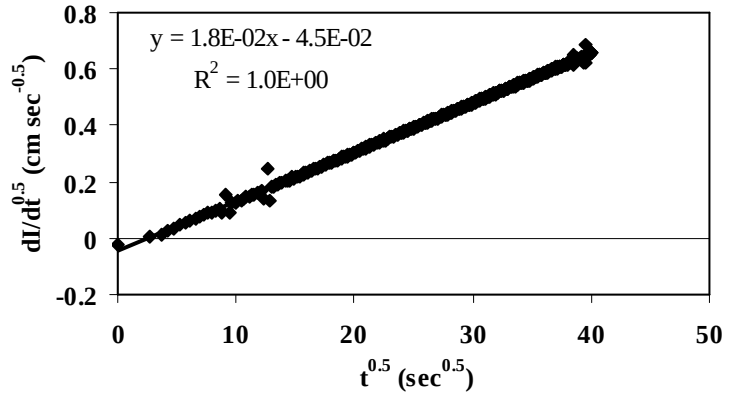

Figure 3.5. Differential linearization with resampled data for Site 2, Mote 10, Channel 1

Sample calculations are shown in Appendix B. The polynomial regression of the cumulative infiltration versus the square root of time for the cumulative infiltration analysis produces an equation of the form

$$I = C_1 t + C_2 \sqrt{t} \qquad \textbf{[3-6]}$$

This is equivalent to the following expression seen in Figure 3.3 with x equal to the square root of time:

$$y = C_1 x^2 + C_2 x \qquad \textbf{[3-7]}$$

where the C_1 term relates to hydraulic conductivity and the C_2 term relates to sorptivity through dimensionless coefficients in the following equations:

$$S(h_0) = C_2 / A_2 \qquad \textbf{[3-8]}$$

$$K(h_0) = C_1 / A_1 \qquad \textbf{[3-9]}$$

From Zhang (1997), the empirically determined sorptivity coefficient for a soil with the van Genuchten (1980) type soil-water retention function is

$$A_2 = \frac{1.4 b^{0.5} (\theta_0 - \theta_i)^{0.25} \exp[3(n-1.9)\alpha h_0]}{(\alpha r_0)^{0.15}} \qquad \textbf{[3-10]}$$

where α and n are the retention parameters identified in van Genuchten (1980) and are based on the soil texture. θ_i and θ_0 are the initial and final soil moistures. The properties of the AMDI have h_0 equal to -3 cm and r_0 equal to 1.58 cm. The b value is in the range of 0 to 1, but often assumed to be 0.55 (Warrick and Broadbridge, 1992). From Zhang (1997), the equation for the empirically determined hydraulic conductivity coefficient for a soil with the van Genuchten

(1980) type soil-water retention function is dependent on the value of *n* and given by the following:

$$A_1 = \frac{11.65(n^{0.1}-1)e\left[2.92(n-1.9)\alpha h_0\right]}{(\alpha r_0)^{0.91}} \quad \text{for } n \geq 1.9 \qquad \textbf{[3-11]}$$

$$A_1 = \frac{11.65(n^{0.1}-1)e\left[7.5(n-1.9)\alpha h_0\right]}{(\alpha r_0)^{0.91}} \quad \text{for } n < 1.9 \qquad \textbf{[3-12]}$$

Soils with high sand content have *n* greater than 1.9 and use equation [3-11], and soils dominated by silts and clays have *n* less than 1.9 and use equation [3-12]. The summary of the sites is in Table 3.2 for the cumulative infiltration analysis from Zhang (1997) with the parameters α and *n* taken from Carsel and Parish (1988).

An alternate method for determining the hydraulic conductivity and sorptivity uses the differentiated linearization analysis proposed by Vandervaere et al (2000). This analysis differentiates [3-6] with respect to the square root of time and arrives at the following:

$$\frac{dI}{d\sqrt{t}} = C_2 + 2C_1\sqrt{t} \qquad \textbf{[3-13]}$$

The sorptivity and hydraulic conductivity are determined from expressions proposed by Haverkamp et al (1994) using coefficients C_1 and C_2.

$$C_2 = S \qquad \textbf{[3-14]}$$

$$C_1 = \frac{2-b}{3}K + \frac{\gamma S^2}{r_0(\theta_0 - \theta_i)} \qquad \textbf{[3-15]}$$

Solving for K yields

$$K = \frac{3}{2-b}\left[C_1 - \frac{\gamma S^2}{r_0(\theta_0 - \theta_i)}\right] \qquad \textbf{[3-16]}$$

where γ is assumed equal to 0.75, but ranges between 0.6 and 0.8 (Haverkamp et al 1994).

A third method for determining the hydraulic conductivity uses the simple infiltration rate and an assumption of the radius of the wetted disk for the dry and wet initial conditions. The radius of the wetted disk, r_{wd}, for the dry initial condition is assumed to be 3.5 cm and for subsequent measurements, the wet condition is 4.5 cm. From a linear infiltration expression

$$I = C_1 t \qquad \textbf{[3-17]}$$

K is found by multiplying C_1 in [3-17] by the ratio of the radii squared.

$$K = C_1\left(\frac{r_0}{r_{wd}}\right)^2 \qquad \textbf{[3-18]}$$

Sample calculations for the three analysis methods are in Appendix B using the data from Site 2, Mote 10, Channel 1 as shown in Figures 3.2, 3.3, and 3.5.

Statistical Analysis

Descriptive statistics were determined for each set of hydraulic conductivity values. The mean, standard deviation, and standard error were calculated for each site. The data passes the Kolmogorov-Smirnov test for normality and therefore data transforms are not needed in order to make data inferences. The size of all sets is 12 data points (n = 12). Paired t-tests were completed for all combinations in order to group the sites into statistically similar groups. To determine the t value for each pair, first the standard deviation of the population (S) is calculated using the standard deviations for each data set (S_1 and S_2) and the number of data points for each data set (n_1 and n_2):

$$S^2 = \frac{(n_1 - 1)S_1^2 + (n_2 - 1)S_2^2}{n_1 + n_2 - 2} \qquad \textbf{[3-19]}$$

with $n_1 = n_2$ for all pairs **[3-19]** reduces to

$$S^2 = \frac{S_1^2 + S_2^2}{2} \qquad \textbf{[3-20]}$$

The calculation for the t value is

$$t = \frac{X_1 - X_2}{S\sqrt{1/n_1 + 1/n_2}} \qquad \textbf{[3-21]}$$

where X_1 and X_2 are the means for each data set. With $n_1 = n_2$ for all pairs, **[3-21]** reduces to

$$t = \frac{X_1 - X_2}{S\sqrt{2/n}} \qquad \textbf{[3-22]}$$

With 12 data points for each site, the degrees of freedom, v, is 22 (v = 2n-2). The level of significance, α, is selected as 0.05. Using a t-distribution table, the critical t-value is 2.07 for a two-sided test. For sites with paired t-values within the critical values ($-t_{a/2} < t < t_{a/2}$), the pair had no evidence of differences and are said to be similar; for the t-values outside the critical values, there is evidence of differences, and the pairs are said to be different. Based on the

similarities and differences of the pairs, the sites fell into one or two of the four groups – a, b, c, and d. Additional similarities exist between sites 5 and 8 and between sites 4, 7 and 9.

Results

Site	θ_i	θ_{f1}	θ_{f2}	θ_f	$\Delta\theta$
1	0.34	0.41	0.43	0.42	26%
2	0.37	0.46	0.45	0.45	22%
3	0.34	0.43	0.42	0.42	24%
4	0.33	0.38	0.38	0.38	16%
5	0.40	0.47	0.46	0.47	16%
6	0.35	0.43	0.45	0.44	25%
7	0.37	0.46	0.46	0.46	23%
8	0.35	0.43	0.44	0.44	26%
9	0.37	0.46	0.46	0.46	23%
10	0.37	0.43	0.45	0.44	21%

Table 3.1. Initial moisture content, θ_i, and final moisture contents, θ_{f1} and $\theta_{f2,}$ with the average final moisture content, θ_f, and percent change in soil moisture content, $\Delta\theta$, for the ten sites at KPRNA watershed 1D.

The soil moisture increases between 16% and 26% among all ten sites during the infiltration tests. The average initial moisture content of the ten sites is 0.36, and the average final moisture content is 0.44. On average, the volume of the soil that is occupied by water was initially 36% before the infiltration test and 44% at the end of the infiltration tests.

Using the method from Zhang (1997) with the parameters from Carsel and Parish (1988) for a silt loam, the results of all 120 measurements are presented in Table 3.2. K(h) for all ten sites along the hillslope of watershed 1D at KPRNA ranges from a low of 0.23 cm-$s^{-1}x10^{-3}$ at site 7 to a high of 1.6 cm-$s^{-1}x10^{-3}$ at site 6. The mean values range from 0.44 cm-$s^{-1}x10^{-3}$ at site 10 to 1.18 cm-$s^{-1}x10^{-3}$ at site 6 (Table 3.3).

Site	1	2	3	4	5	6	7	8	9	10
K	0.68	0.75	0.58	0.85	0.92	1.47	1.03	0.71	0.60	0.38
	0.59	0.62	0.72	0.59	1.03	1.29	0.51	1.00	0.36	0.33
	0.64	0.87	0.77	0.69	0.77	1.57	0.85	0.70	0.47	0.82
	0.64	0.63	0.70	0.61	0.86	1.40	0.61	1.26	0.36	0.27
	0.66	0.67	0.61	0.54	0.77	0.76	0.84	0.55	0.49	0.37
	0.83	0.66	0.72	0.49	0.83	1.31	0.90	0.57	0.48	0.37
	0.62	0.68	0.89	0.51	1.31	0.90	0.53	0.87	0.44	0.47
	0.70	1.04	0.61	0.44	0.98	1.20	0.60	0.88	0.45	0.48
	0.91	0.81	0.80	0.53	0.82	1.17	0.37	0.66	0.47	0.41
	0.55	0.92	0.69	0.95	1.56	1.01	0.78	0.95	0.72	0.46
	0.98	0.67	0.75	0.44	1.02	0.89	0.23	0.82	0.46	0.40
	0.97	0.87	0.85	0.61	0.92	1.17	0.66	0.91	0.78	0.52

Table 3.2. Unsaturated hydraulic conductivity, K(h=-3cm) (cm s^{-1} x 10^{-3}) using the method from Zhang (1997) with parameters from Carsel and Parish (1988)

Site	X	SD	SE
1	0.73	0.15	0.043
2	0.77	0.13	0.039
3	0.72	0.093	0.027
4	0.61	0.16	0.045
5	0.98	0.24	0.068
6	1.18	0.25	0.072
7	0.66	0.23	0.067
8	0.82	0.20	0.058
9	0.51	0.13	0.037
10	0.44	0.14	0.040

Table 3.3. Statistical summary of the hydraulic conductivity, K(h=-3cm) (cm s^{-1} x 10^{-3}) values in table 3.1 showing the mean (X), standard deviation (SD), and standard error (SE).

The results of the paired t-tests show the differences and similarities between the sites (Table 3.4) and allow for the sites to be organized into groups (Figure 3.6).

Site	2	3	4	5	6	7	8	9	10
1	-0.62	0.10	1.97	**-3.15**	**-5.34**	0.87	-1.30	**3.91**	**4.89**
2	-	0.88	**2.68**	**-2.79**	**-5.06**	1.37	-0.84	**4.84**	**5.84**
3	-	-	1.99	**-3.31**	**-5.56**	0.83	-1.43	**4.07**	**5.10**
4	-	-	-	**-4.62**	**-6.73**	-0.68	**-2.96**	1.70	**2.73**
5	-	-	-	-	-1.98	**3.40**	1.78	**6.17**	**6.89**
6	-	-	-	-	-	**5.29**	**3.83**	**8.31**	**8.96**
7	-	-	-	-	-	-	-1.85	2.02	**2.83**
8	-	-	-	-	-	-	-	**4.61**	**5.43**
9	-	-	-	-	-	-	-	-	1.21

Table 3.4. Paired t-values for sites 1 through 10. Bold indicates evidence of a difference between paired sites (α=0.05).

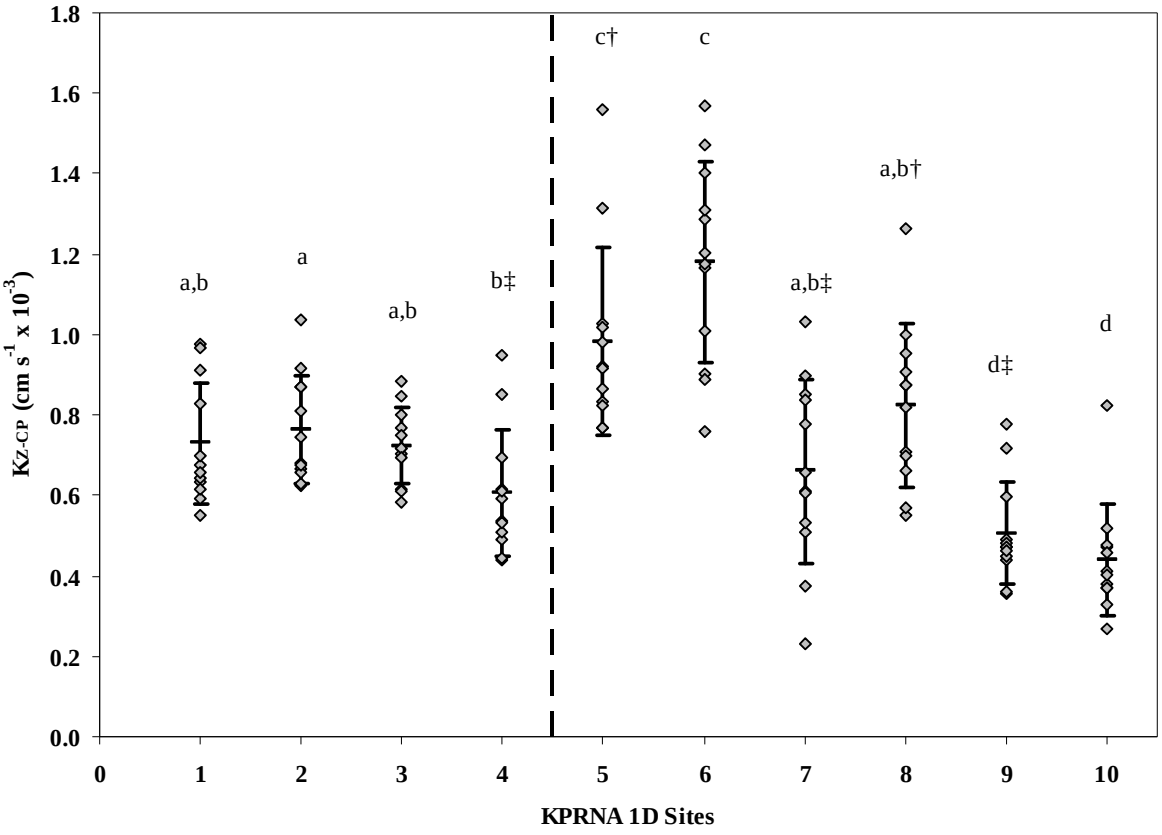

Figure 3.6. Unsaturated hydraulic conductivity, K(h=-3cm) using the method from Zhang (1997) with parameters from Carsel and Parish (1988).

Notes: One standard deviation from the group mean is shown by the vertical bars and significant differences (α=0.05) among groups are identified by letters a, b, c, and d. Additional similarities between sites are shown with ‡ and †. Approximate location of the limestone bench is shown as a dashed line between sites 4 and 5.

The results of analysis using the simple linear method and the Vandervaere et al (2000) methods to determine K(h) are shown in Figures 3.7 and 3.8. Sorptivity values using the Zhang (1997) with parameters from Carsel and Parish (1988) are shown in Figure 3.9, and Figure 3.10 shows the sorptivity using the Vandervaere et al (2000) method.

Additional data, analysis, and comparisons of the mini-disk infiltrometers are found in Appendix C.

.

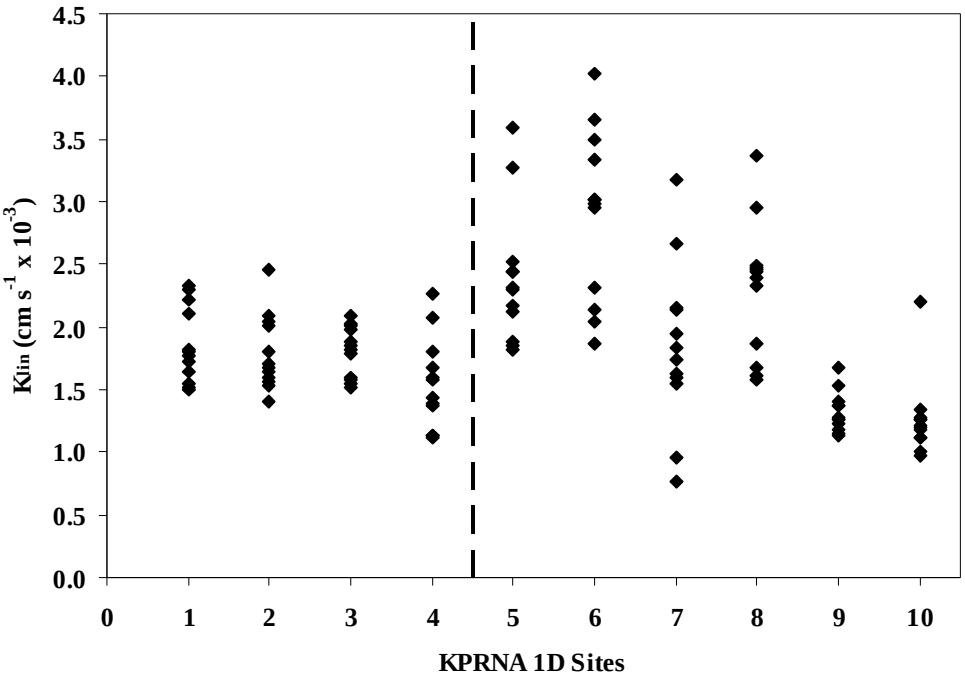

Figure 3.7. Unsaturated hydraulic conductivity K(h=-3cm) using the simple linear method.

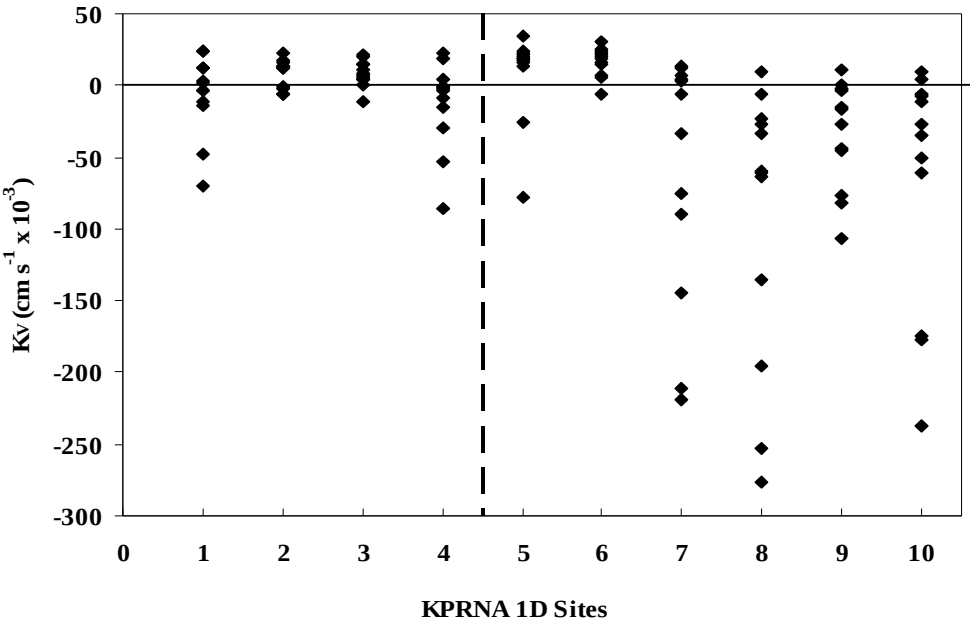

Figure 3.8. Unsaturated hydraulic conductivity K(h=-3cm) using resampled data and the method from Vandervaere et al (2000).

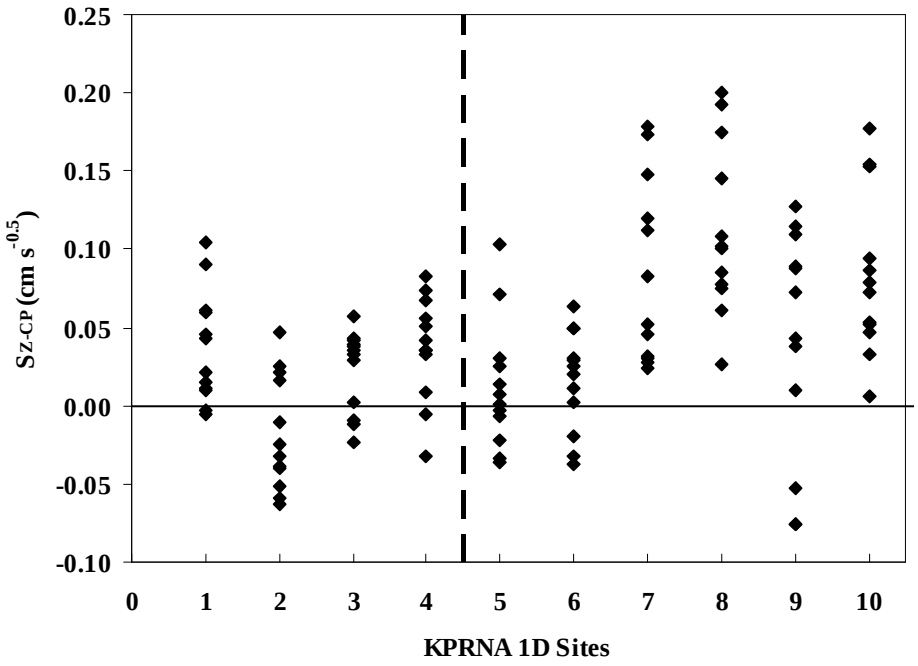

Figure 3.9. Sorptivity using the method from Zhang (1997) with parameters from Carsel and Parish (1988).

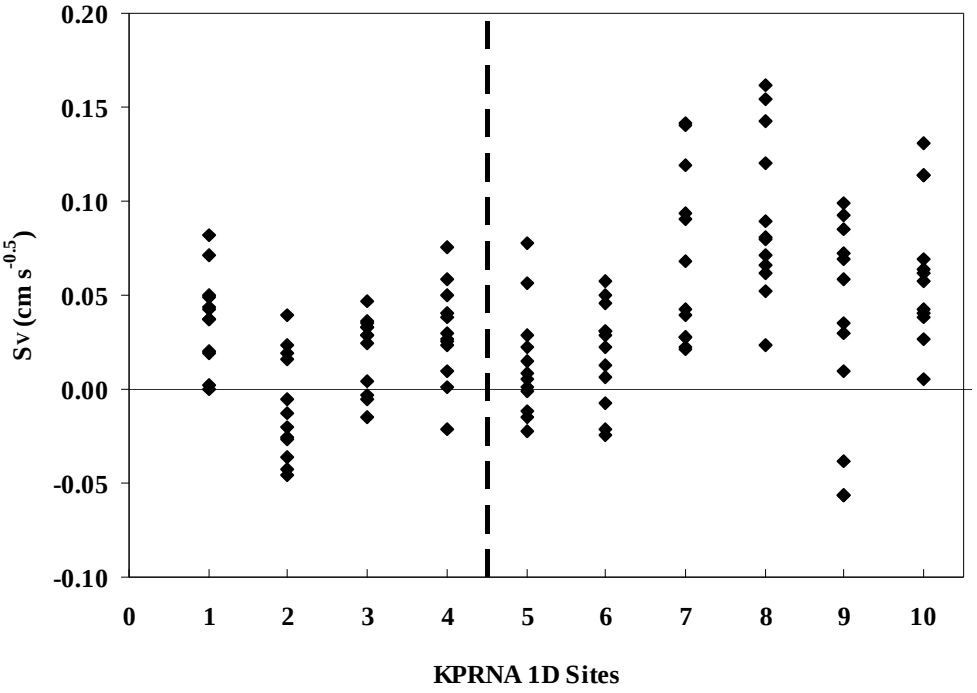

Figure 3.10. Sorptivity using resampled data and the method from Vandervaere et al (2000).

Discussion

Considering K(h) using the Zhang (1997) method with Carsel and Parish (1988) parameters, there are significant differences among the ten sites in watershed 1D of KPRNA. The hypothesis of a spatial variability of infiltration over an assumed homogeneous landscape is confirmed.

Analysis Methods

Using the mean value of K(h) for each site, the results of the linear analysis (Figure 3.7) are 2 to 3 times higher than what the Zhang (1997) methodology produces. The assumed radius of the wetted disk may be underestimated.

The Zhang (1997) and the linear methods produced the most consistently reliable results for hydraulic conductivity while the Vandervaere et al (2000) method does not produce reliable results for hydraulic conductivity. From [3-16], K is dependent on S, and for a large values of S (C_2 in [3-14]) or a small value of C_1 (in [3-15]) the resulting K is negative. In the Zhang (1997) and linear methods, hydraulic conductivity is not dependent on sorptivity.

For sorptivity, the Zhang (1997) analysis produces both positive and negative values. For negative results, this is due to the second term of the polynomial regression of the cumulative infiltration (Figure 3.2) being negative. A negative sorptivity would indicate a negative infiltration for very early times, but this is not physically possible. A negative value could be a result of a lower infiltration rate for early times as compared to the later, near steady-state, infiltration. It is expected that the infiltration would be higher at early times due to the combination of the transmission of water through the soil and the increasing water content of the soil. Rather than accepting a physically impossible result, a negative value of sorptivity will be considered negligible or effectively zero.

One explanation for the negative values for sorptivity, negative values for C_1 in [3-6] and [3-13], could be the change in soil moisture. From Table 3.1, the soil moisture increases on average about 22% for all sites with site 4 and 5 having the least change and sties 1 and 8 having the greatest change in measured soil moisture with the ThetaProbe. Sorptivity is dependent on the change in soil moisture. The initial soil moisture content is relatively high and increases slightly during the infiltration experiment. It is possible that the initial water content of the soil was too high to measure significant sorptivity effects for the applied tension. The change in soil moisture might be too small for the adequate determination of sorptivity. Further test that control for the initial soil moisture content are needed to better understand the relationship between sorptivity and soil moisture of heavy textured soils representative of the soils in KPRNA.

An alternate analysis for determining the sorptivity while still using the Zhang method is to segment the cumulative infiltration into the linear and nonlinear pieces where sorptivity dominates the nonlinear portion and hydraulic conductivity dominates the linear, steady-state portion. The combined approach was shown to produce more consistent results than the partitioned (Madsen and Chandler, 2007). Alternative analyses similar to this approach are shown in Appendix D.

The sorptivity, S, and hydraulic conductivity, K, produced from the Vandervaere et al (2000) analysis and shown in Figures 3.10 and 3.8 respectively are not realistic. The negative values for K and S are not physically possible. The positive values computed for K and S are outside the range of what is expected and quite different from the results of the simple linear

analysis or the Zhang (1997) analysis. Any spatial inference of K or S from the Vandervaere method is inappropriate.

The initial R^2 values were consistently low for all linear regressions of the differential linearization method. While this does not produce confidence in the results of this method, it could be a consequence of electronic noise from the automation which seems to be amplified by this approach. Resampling the infiltration data from the cumulative infiltration regression equation as seen for example in Figure 3.3, results in better R^2 values for the differential linearization method. Both the linear and the two-term polynomial approach have consistently high R^2 values (near or above 0.99).

By resampling the differential linearization data from the cumulative infiltration, the regression fitness improves, but the results with the Vandervaere analysis remain unrealistic. In Figure 3.8, K(h) ranges from -280 cm s^{-1} x 10^{-3} to 34 cm s^{-1} x 10^{-3}. From Vandervaere (2000), gravity is the dominant force when

$$\frac{\gamma C_1^2}{r_0(\theta_0 - \theta_i)} < \frac{C_2}{2} \qquad \textbf{[3-23]}$$

and lateral capillarity dominates when

$$\frac{\gamma C_1^2}{r_0(\theta_0 - \theta_i)} > \frac{C_2}{2} \qquad \textbf{[3-24]}$$

When flow is driven by the lateral capillary forces, then [3-16] may produce unreliable results. The large values of C_1 versus C_2, small disk radius, or small change in soil moisture could produce a flow dominated by lateral capillary forces. The radius of the disk on the AMDIs is smaller than the disk radii shown in the examples in Vandervaere et al (2000). The AMDIs have a disk radius of 15.8 mm, and the smallest radius in Vandervaere et al (2000) is 24.25 mm.

For the Vandervaere analysis, the hydraulic conductivity is dependent on sorptivity. From the regression analysis of the cumulative infiltration and the differential linearization equations, the value of sorptivity is sometimes negative. A negative value for sorptivity is not physically possible for an infiltration test. Either sorptivity from the infiltration runs is negligible and therefore can be considered zero, or the proposed methods for determining sorptivity are invalid for the experimental conditions. If the value for sorptivity is invalid, then the sorptivity dependent value for hydraulic conductivity from the Vandervaere analysis would also be invalid.

The analysis of the infiltration using the differential linearization method proposed by Vandervaere et al (2000) is either not appropriate for the AMDIs due to the small disk radius or not appropriate for the soils in KPRNA due to their high clay content and initial soil moisture. The cumulative infiltration method with the empirical analysis proposed by Zhang (1997) is a much more robust process to determine hydraulic conductivity using the AMDIs. The determination of sorptivity from the cumulative infiltration equation is as reliable as the differential linearization equation due to the negative sorptivity coefficients produced. The linear method from the simple infiltration analysis produces realistic, quantitative values for hydraulic conductivity but overestimates hydraulic conductivity compared to the cumulative infiltration analysis. The linear method is not capable of determining sorptivity since it only examines the steady infiltration rate.

Spatial Controls

From Figure 3.6, the ten sites can be organized into four main groups. Groups a and b with sites 1, 2, 3, 4, 7, an 8 have mid-range values for K(h) between about 0.6 cm s^{-1} x 10^{-3} to 0.8 cm s^{-1} x 10^{-3}. Group c with sites 5 and 6 has the highest mean value for K(h) with values near 1.0 cm s^{-1} x 10^{-3}, and group d with sites 9 and 10 has the lowest mean value for K(h) with values near 0.45 cm s^{-1} x 10^{-3}. Group c has a mean K(h) more than twice that of group d.

The sites are spatially arranged in a line from the top of watershed 1D to the bottom with a spacing of 50 m between sites. From the soil survey, three soil units are defined over a watershed of length of about 1,200 m with the soil units separated by about 500 m measured along the transect. From the statistical analysis of the AMDI measurements, the significance differences between sites occur at about 100 m spacing. To put it another way, two adjacent sites within 100 m of each other are likely to be similar but not three adjacent sites that are farther than 100 m apart. The length scale of the watershed with respect to K(h) is about 100 m or about 5 times smaller than the scale of information given in the soil survey. Measuring K(h) at a length scale less than 100 m would produce only marginally better results, and it is expected that the variability within a 100 m area can be adequately represented either stochastically or homogeneously (Seyfried and Wilcox 1995).

The length scale of 100 m applies to watershed 1D, and it is expected that similar watershed would have a similar length scale. The watershed 2D directly to the east has a similar

topography, and it is expected that a length scale of 100 m would adequately represent this watershed. In contrast, the watersheds to the north that are part of the Kings Creek system may be adequately represented by a length scale that is smaller than 100 m. It is expected that a smaller length scale would be more appropriate for the Kings Creek watersheds since the topographic change is much greater, and topography has some influence on K(h).

Topographic Controls

Sites 1 through 4 are at the top of the hillslope and classified as upland. The top of the slope has limestone fragments near the surface and could be associated with either the Dwight-Irwin complex or the Benfield-Florence complex.

Sites 5 through 8 are located in the middle of the hillslope, are associated with the Benfield-Florence complex, and are classified as slope. Sites 5 and 6 are near a "slip" where a mass of soil has broken free from the surrounding material and is being eroded and transported down slope. From the soil investigation and the results of the laboratory measurements in the following sections, the mass movement could be a result of soil piping or an increase in pore water pressures. In the area near sites 5 and 6, the surface infiltration is high relative to the surrounding area and compared to the hydraulic conductivity below the surface as the soil transitions from a silty loam to a clay loam. Water infiltrates the surface readily, but encounters resistance to downward flow less than a meter below the surface. Since downward flow is impaired, the water seeps laterally. The increased water content and pore water pressure decreases the strength of the soil. Subsurface erosion in the form of soil piping may form if the subsurface lateral flow becomes concentrated by preferential flow paths. The subsurface flow could be eroding the soil near the boundary of lower permeability. Mass movement in the form of a "slip" occurs.

Sites 7 and 8 are similar in infiltration to sites 1 through 4, but the relationship could be coincidental rather than evidence of similarities of soil type or texture. Sites 7 and 8 can be considered a transition section from the higher infiltration of sites 5 and 6 to the lower infiltration of sties 9 and 10.

The slope position of the site could contribute to the soil hydraulic properties. Slopes susceptible to overland tended to have lower macropore flow and therefore lower K_{sat} (Holden 2009). Areas at the bottom of the slope are more likely to be saturated than along the slope or on the top of the watershed. This higher degree of saturation at the bottom of the watershed could

result in a greater occurrence of the saturation-excess overland flow and therefore lower K_{sat}. The gradual decrease in K(h) from the high near 1.0 cm s^{-1} x 10^{-3} at sites 5 and 6 to the lows near 0.45 cm s^{-1} x 10^{-3} at sites 9 and 10 may be partially explained by the degree of saturation and the frequency of overland flow.

The lowland area of sites 9 and 10 has the lowest infiltration as well as the lowest elevation of all the sites. The erosion processes of the hillslope could explain the low infiltration rate at the bottom of the hill. The upland area at the top of the watershed is a source of erodible material, although with the small gradients of the local slope, the process to drive erosion is comparatively smaller than the slope area of sites 5 through 8. The slope could experience erosion, deposition, or transmission of sediment. The mass of soil from the "slip" that was observed near sites 5 and 6 is a source for erodible material. The lowland area could also experience erosion, deposition, or transmission. The lowland area of sites 9 and 10 has less topographic relief compared to the slope resulting in a greater probability of deposition. The sediment particles transported from the slope areas to the lowland areas of sites 9 and 10 may be clogging the macropores at the surface further decreasing K_{sat} (Holden 2009).

The local slopes as shown in Figure 2.4 may have some impact on K(h). Site 6 has the greatest value for K(h) and the greatest local slope at 14.9%. The slopes at the bottom of the watershed are 5.0% for site 9 and 8.3% for site 10, and sites 9 and 10 also have considerably lower K(h). While K(h) tends to decrease from site 5 to site 10, the local slopes vary. The local slope at site 5 at 9.0% is just slightly more than the local slope at site 10 at 8.3%, but the difference in K(h) is much greater (0.98 cm s^{-1} x 10^{-3} for site 5 compared to 0.44 cm s^{-1} x 10^{-3} for site 10).

From Nippert et al (2011), total biomass was largest in the lowlands, negating the idea of plant biomass being directly related to K(h) (Thompson et al 2010). Further investigations between K(h) and biological activity are needed to determine if biomass or other biological variables could be used as a predictor for K(h).

Geologic Controls

The Florence limestone bench divides the upland area from the slope area. The upland area has a relatively constant K(h) for sites 1 through 4 (about 0.7 cm s^{-1} x 10^{-3}). Below the limestone bench, K(h) is significantly higher at sites 5 and 6 (about 1.0 cm s^{-1} x 10^{-3}) but tends to decrease as the elevation decreases. The lowland area of sites 9 and 10 has the lowest values for

K(h). The lower layers of shale and limestone shown in Figure 2.4 do not appear to influence K(h) as much as the Florence limestone located at the top of the watershed.

In Nippert et al (2011) an alternate classification of site 5 was "seep". Site 5 was nearest to the outcropping of the limestone bench with sites 1 through 4 perched on top of the Florence limestone layer. The interface of the Florence limestone and the Blue Springs Shale may be creating a perched groundwater layer. The hydraulic conductivity of the limestone is assumed to be much greater than the shale. Any water that has infiltrated at the top of the watershed and into the limestone layer might be transported laterally once it reached the less permeable shale layer. For these assumptions, some groundwater is expected to discharge near site 5 rather than percolate though the shale layer. The addition of the groundwater seeps to the hydrology at site 5 might explain the subsurface erosion processes and could also be related to the jump in K(h) relative to site 4. The mechanics relating the subsurface flows to K(h) are unclear and require further study.

Statistical Variability

The computed values of K(h) from the Zhang (1997) method produced a set of values that are normally distributed based on the Kolmogorov -Smirnov test for normality. The normal distribution of K(h) is in contrast to the assumption of a logarithmic distribution of hydraulic conductivity (Freeze 1975). A normal distribution of hydraulic conductivity would have implications for a stochastic model of the watershed.

Conclusion

Using topography, geology, soil maps, or plant biomass may help to explain the mechanisms resulting in the spatial variability of K(h), but the relationship is unclear. It does not appear that one variable can be used to predict the value of K(h), and K(h) may be dependent on all of these factors plus additional inputs that were not considered in this study.

For the determination of K(h) from the infiltration measurements, the Zhang (1997) analysis method and the linear method produced reasonable values for K(h) while the Vandervaere (2000) method did not. The root of the problem lies with sorptivity. The change in soil moisture for the field measurements was quite low due to the high initial moisture content in the silty loam soils. Since sorptivity is greatly dependent on the change in soil moisture, the small changes in soil moisture produced unreliable or inaccurate values for sorptivity. While the

Zhang (1997) method produces reliable values for K(h), it does not produce reliable values for sorptivity. The values for sorptivity produced by the Vandervaere (2000) method are equally as unreliable as the Zhang (1997) approach. The Vandervaere (2000) method produces unreliable values for hydraulic conductivity since the model links sorptivity to hydraulic conductivity. According to Vandervaere et al (2000), hydraulic conductivity is dependent on sorptivity, and since the values for sorptivity are unreliable, the values for hydraulic conductivity are equally unreliable.

CHAPTER 4 - Laboratory Measurements of Extracted Soil Cores

Introduction

In order to determine the variability of hydraulic conductivity with depth and with tension, large soil cores were extracted from the field and tested in the laboratory. By extracting soil from the field and taking measurements in the laboratory, more tests can be performed in a controlled environment. By measuring the infiltration rates at several tensions, the saturated and unsaturated hydraulic conductivity can be determined providing inference on soil structure. By measuring the infiltration rates at several depths, the relationship between depth and hydraulic conductivity can be determined. The saturated hydraulic conductivity is a constant soil parameter, and unsaturated hydraulic conductivity is a function of soil moisture and tension.

The diameter of the soil core is about the same diameter as the large disk on the SMS infiltrometer. It is expected that the infiltration will be one-dimensional for the large disk infiltrometers. For the AMDIs, it is assumed that the diameter of the soil cores is large enough for the same three-dimensional infiltration analyses used for the field measurements. The length of the soil core at 60 cm long enough to capture the variability in the A horizon and part of the B horizon while still being small enough to manage the sample in the laboratory.

Collection and Preparation of the Soil Samples

The ten stations in watershed 1D at KPNRA were divided into four groups based on the statistical analysis of the field measurements of hydraulic conductivity (Figure 3.6). Large soil cores, 60 cm in length and 9 cm in diameter, were extracted for three of the ten sites corresponding to middle-range values of hydraulic conductivity (group a), high values (group c) and low values (group d). One sample was extracted from sites 2, 6, and 9. An attempt was made to extract a sample from site 4, corresponding to group b, but large rock fragments near the surface would have prevented sampling of an intact core.

Samples from sites 6 and 9 were collected in the fall of 2009 and were stored in a 4 inch PVC pipe with expandable urethane foam sealant. The urethane foam sealant would bond to both the soil and the PVC pipe providing an air and water tight seal around the soil without compressing the soil. The sample from site 2 was collected in the spring of 2010 and was contained in a plastic soil tube liner. The plastic soil tube liner is a clear plastic liner provided

with the core sampling equipment. The primary purpose of the plastic soil tube liner is to contain the soil to prevent soil and soil moisture loss.

The initial plan for the two samples collected in the fall of 2009 was a saturated hydraulic conductivity test. The samples were sealed with silicone caulk to a porous base plate. Tubes with porous cups to act as piezometers were inserted into the side of the soil sample at 10 cm depth intervals. The samples were then filled from the bottom with a deaired $CaSO_4$ solution.

The soil cores in the PVC pipes could not be completely sealed to prevent external leakage; therefore the measured discharge values were not reliable. The head measurements of the piezometers indicated significant bypass flow where water would flow around the soil and not through the soil. The bypass flow resulted in unexpected measurements of little to no head difference within the soil core between depths. In addition to the head measurements of the piezometers, the response time for the piezometers to reach equilibrium also indicated bypass flow. For example, after adjusting the head gradient, the piezometer at depth 40 cm would reach a constant value after 15 minutes while the piezometers at shallower depth would take several hours. In addition, the head at 40 cm would be higher than the shallower depth by a few centimeters even though it was expected to be lower. With the leakage and bypass flow, the results were determined to be unreliable, and the saturated hydraulic conductivity tests were abandoned and replaced by unsaturated hydraulic conductivity tests with tension infiltrometers.

For the tension infiltrometer tests, another error occurred in the experimental set-up. The plastic soil tube liner for the extracted soil core for site 2 limited the flow of air out of the soil resulting in air entrapment and inaccurate measurements. In unsaturated flow, water flows into and through the soil, but air also flows through and out of the soil. After administering the unsaturated test at several tensions to the surface of sample from site 2, no significant change in the flow rate was observed, but air bubbles exiting at the top of the sample were observed. This indicated that the flow rate was not determined by the soil properties or the tension of the infiltrometer, but the ability of air to exit the system. By puncturing several holes in the plastic soil tube liner, the air pressure inside the tube was able to equilibrate with the air pressure outside. The PVC pipe with expandable urethane foam sealant did not create the same air entrapment conditions as the plastic soil tube liner, thus no alterations were needed to equalize the pressures when conducting infiltration on the samples for sites 6 and 9. The inability to

completely seal the PVC system in the attempted saturated tests was beneficial for the two phase flow in the unsaturated tests.

The soil samples were placed on an outflow base plate with a porous disk and filter paper. The base was sealed by either a rubber gasket or silicone sealant to prevent leakage. Steel plates were attached to threaded rods to stabilize the soil column.

Any vegetation on the top end of the soil core was trimmed, and soil was removed up to a depth of 1 cm to provide a flat, level surface. Contact material of moist silica sand was placed on the soil to provide a smooth surface and good contact between the soil and the infiltrometer disk.

In order to produce consistent results between the samples, and following the instruction in the SMS infiltrometer user manual, the top of the soil sample was positioned level with the bottom of the infiltrometer. For field measurements, the infiltrometer would be placed on the soil surface, level with the soil to be tested. In the laboratory, the top of the laboratory table was used as the common elevation. The infiltrometer was placed directly on the table top with the top of the soil sample adjusted to also be level with the table top.

The soil sample was divided into 6 segments each of approximately 10 cm in depth. When segmenting the sample, care was taken not to smear the soil and to instead break the soil along the aggregate boundaries in order to preserve the existing soil structure. For the large disk infiltrometer tests, the segments were divided sequentially, that is the surface segment was tested, then 10 cm of soil would be removed, and the soil at depth of 10 cm would be tested. For the mini-disk infiltrometer tests, the soil core was already segmented, and all six segments were tested simultaneously.

The soil cores were segmented at 10 cm because of the expected length scale at depth for the soils in the watershed. From the soil survey (USDA), the soils found in the watershed have horizons about every 15 to 20 cm. By sampling at every 10 cm, the soil horizons should be represented with additional detail within the horizons.

Large Disk Infiltration

Preparation of the Large Disk Infiltrometer

The large disk infiltrometer was manufactured by Soil Moisture Systems, LLC in Tucson, AZ. The original 20 cm disk head infiltrometer was replaced by an 8 cm disk head to match the diameter of soil cores which were approximately 9 cm in diameter. The procedure for using the device follows the manufacture's Users Manual.

Filling of the Infiltrometer

The reservoir was filled with tap water at room temperature. The disk was submerged in a pan of water in order to completely wet the nylon membrane and to eliminate air bubbles within the disk head.

Automated Data Collection

The automation components of the AMDIs used in the field measurements were adapted for the large disk infiltrometers. A pressure transducer from Mote 8 was used to monitor volumetric changes in the infiltrometer reservoir. Port A of the differential pressure transducer was connected to the top of the reservoir tower, and port B was connected with a T-connection to the bubbling tube at the bottom of the reservoir tower.

Measurement

The 8 cm diameter disk was placed on the soil sample with moist silica sand acting as the contact material to ensure good contact. The tube in the bubble tower was positioned at the lowest level for maximum tension. The bubble tower tube was incrementally raised by 1 cm until air was pulled into the bubble tower and infiltration began. This tension was identified as the bubble point, the highest tension the soil will pull.

Tension was typically set sequentially at -6 cm, -3 cm, -2 cm, -1 cm, and 0 cm. The first applied tension was the -6 cm with the subsequent tensions decreasing in magnitude. This allowed for efficient testing of the soil core. If the tensions were to have been applied in increasing magnitude, then the soil would require extra time to drain to match the corresponding moisture content. Altering the sequence of the applied tensions could possibly produce hysteresis effects depending of if the soil was wetting or drying during the infiltration test. By

conducting the sequence of experiments in this particular order, the infiltrometer would always be imbibing the soil.

For the site 9 core, the highest tension was -3 cm. On occasions when the soil would not pull -6 cm of tension, the maximum tension was reset to -5 cm or lower as was the case for site 9. The time and reservoir water level were recorded at the start of each infiltration test.

The infiltration test was ended after steady state was achieved. The target time for each infiltration run was 15 minutes with two exceptions: Due to the "noise" of the pressure transducer, a minimum of 0.5 cm of height in the change in water level in the reservoir is necessary to fit a regressed line on the charted data with confidence. This required a run time longer than 15 minutes in some infiltration tests particularly at greater tensions. At lesser tensions, the run time would be shorter due to the limitations of the pressure transducers. Due to the limitations of the 5 volt power supply, the pressure transducer would only register values under the 45 cm mark or roughly half of the capacity of the reservoir. 45 cm of water in the reservoir corresponds to 11 cm of cumulative infiltration. A reservoir change in storage height greater than 45 cm often occurred in less than 15 minutes for tensions of -1 cm and 0 cm. Since steady state infiltration was achieved before reservoir exhaustion, this was not a critical issue. A 100-year one-hour rainfall event produces less than 10 cm of precipitation in Riley County, Kansas. Cumulative infiltration of 11 cm in less than 15 minutes is not a probably occurrence with the soils being tested.

Analysis of the Large Disk Data

The infiltration of the large soil cores with the large disk infiltrometer is assumed to be one-dimensional. In order to test the assumption, three different analysis methods are used. The one-dimensional analysis assumes that the infiltration rate at an applied tension, h, is equal to the unsaturated hydraulic conductivity at the applied tension, K(h). A three-dimensional analysis from Reynolds and Elrick (1991) uses the Wooding-Gardner equation in a piecewise manner to determine K(h). The third method is the Zhang (1997) method that was employed to analyze the field infiltration measurements in the previous section.

The data output for the pressure transducer measurements is voltage and time. The beginning and ending values of the voltage are related to the beginning and ending values of the height of water in the reservoir. Similar to the procedure for the AMDIs, the voltage at $t = 0$ is

set equal to 0 cm of infiltration, and the voltage at the end of the infiltration run is set equal to the change in reservoir storage. With the beginning and ending conditions known, the relationship between the change in reservoir storage and time can be determined. The change in reservoir storage can be converted to the infiltration of water into the soil by multiplying by the ratio of the radii squared:

$$I_S = \frac{r_R^2}{r_S^2} I_R \qquad \textbf{[4-1]}$$

where I_S is the infiltration rate into the soil, I_R is the rate in change of reservoir height, r_S is the radius of the soil column, and r_R is the inside radius of the reservoir. For one-dimensional infiltration, the infiltration rate into the soil is also taken to be the unsaturated hydraulic conductivity, K(h) at the applied tension, h.

Using Excel, a graph of infiltration versus time can be plotted. A linear regression of the data provides a slope, intercept and R^2 value. The start time was adjusted to eliminate the initial sorptivity phase. The start time was increased until R^2 reached its maximum value. In Figure 4.1 the slope of the line is the unsaturated hydraulic conductivity at -2 cm tension, K(h=-2 cm), for site 2 at 1 cm depth.

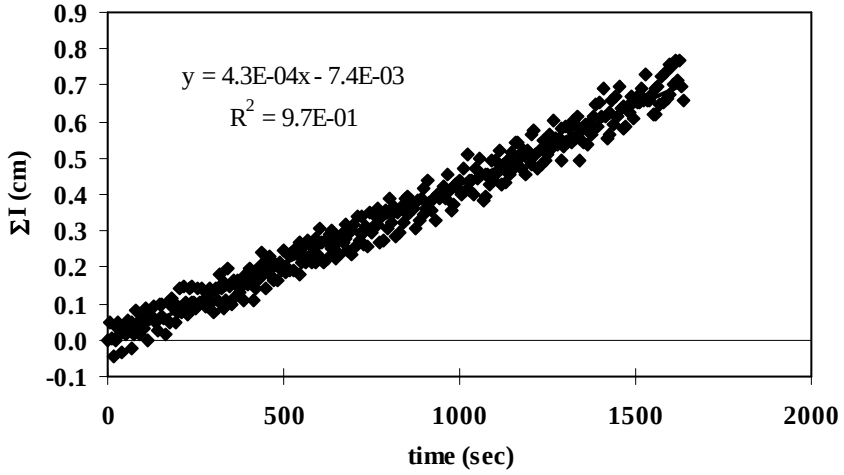

Figure 4.1. Simple infiltration of Site 2, Depth 1 cm, Tension -2 cm

The cumulative infiltration uses the square root of time as the x-axis, the cumulative infiltration on the y-axis with a two-term polynomial regression to fit the data. The analysis is similar to the cumulative infiltration method from the field measurements. The resulting graph

and regression equation for K(h=-2 cm), for site 2 at 1 cm depth is shown in **Figure 4.2** as an example.

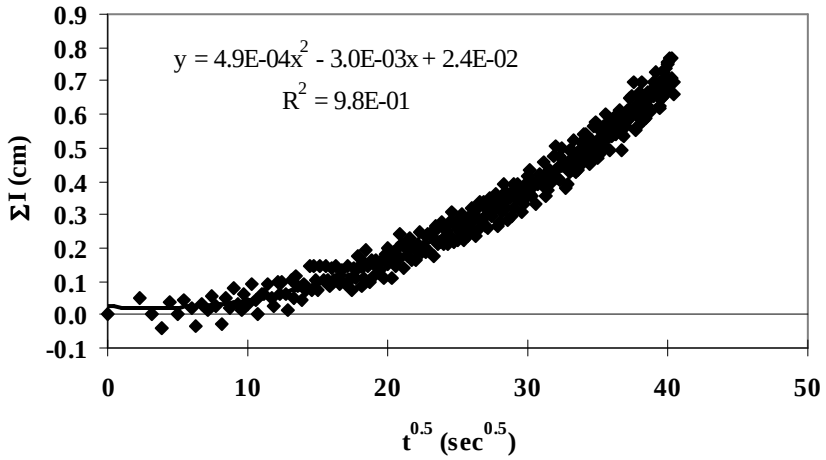

Figure 4.2. Cumulative infiltration of Site 2, Depth 1 cm, Tension -2 cm

Calculating α and K_{sat}

Gardner's (1958) equation relating unsaturated hydraulic conductivity to tension is given as

$$K(h) = K_{sat} e^{\alpha h} \qquad \textbf{[4-2]}$$

Using the Gardner format, an exponential equation was fit to a graph of tension versus unsaturated hydraulic conductivity. Figure 4.3 shows the resulting equation for Site 2, Depth 1 cm. By setting the y-axis as the natural log of K(h), or ln K(h), the resulting regression equation is linear, although the best fit for the data from Site 2, Depth 1 cm may not be linear.

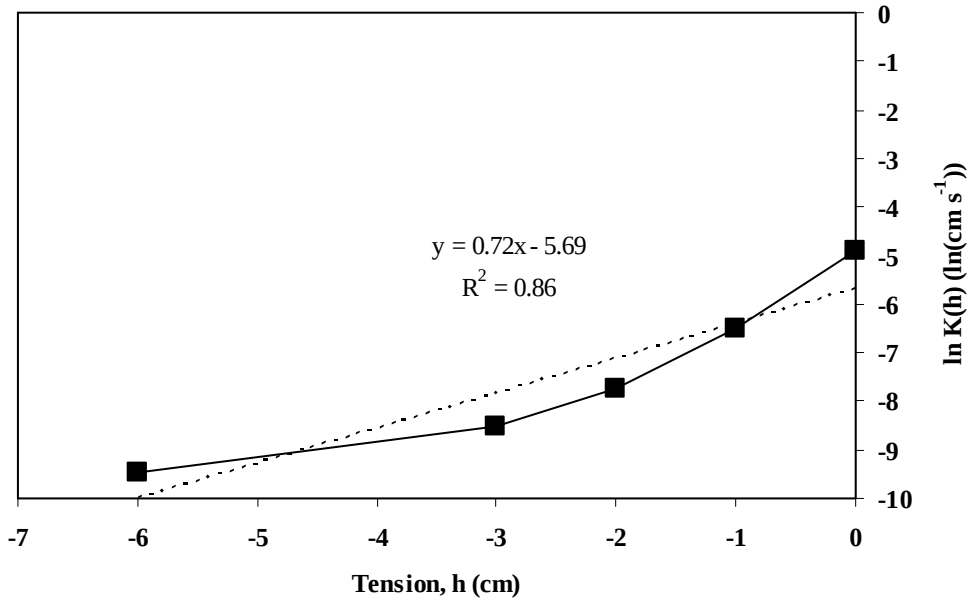

Figure 4.3. Exponential regression of Site 2, Depth 1 cm

The α and K_{sat} values were determined from the unsaturated hydraulic conductivity at the applied tensions and fitting a regressed line to equation [4-2] (Figure 4.3). Since the relationship between hydraulic conductivity and applied tension can be non-linear on a natural log scale, the range of applied tensions was reduced to between -1 cm and -3 cm (Figure 4.4). The reduced range would represent the influence of the macropores contribution to the flow. The macropores are the larger pores in the soil structure that range from 75 μm to larger than 5000 μm (Brewer 1964). The flow through the macropore is much faster than through the smaller micropores. The larger pore diameters create preferential flow paths for water and solute movement for saturated and near saturated soil conditions.

By only examining this smaller region, the regression has a better fit, but the regression model would only apply to this region. Values can be interpolated within -1 cm and -3 cm, but extrapolation much beyond the region is inappropriate.

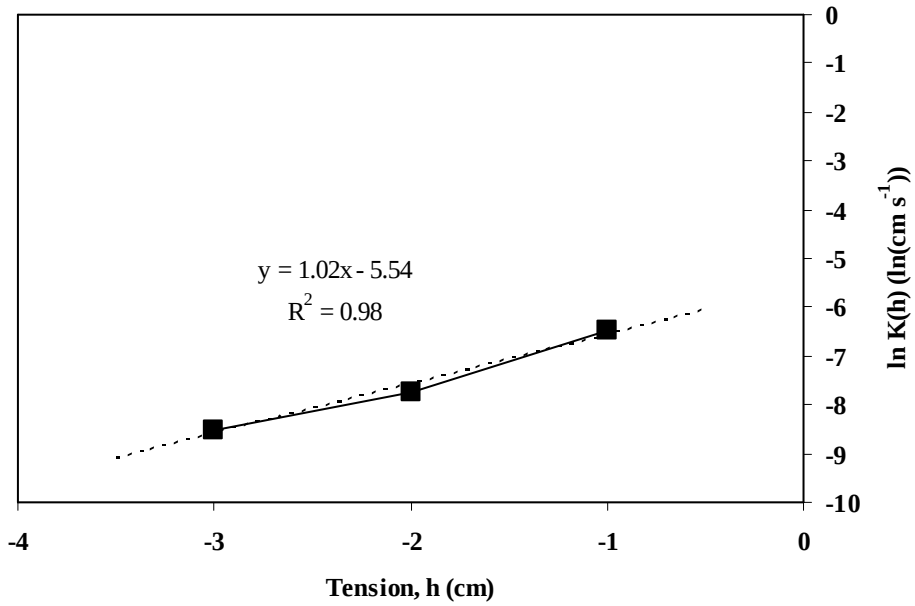

Figure 4.4. Exponential regression of the reduced region of Site 2, Depth 1 cm

For three-dimensional infiltration, the Wooding solution is used with the Gardner equation. From the Wooding solution for homogenous, isotropic soil, the steady-state flow rate, Q_S, is given by

$$Q_S = \left(\frac{r}{G_d} + \pi r^2 \alpha \right) \phi_0 \qquad \textbf{[4-3]}$$

where ϕ_0 is the matrix flux potential, α is the soil texture parameter, r is the radius of the disk, and G_d is a dimensionless shape factor equal to 0.25. The matrix flux potential can be approximated by

$$\phi_0 = \frac{K(h)}{\alpha} \qquad \textbf{[4-4]}$$

Combining the Wooding solution, the matrix flux potential and the Gardner equation, the resulting equation, the Wooding-Gardner equation, is in the form

$$Q_S = \left(\frac{r}{G_d \alpha} + \pi r^2 \right) K_{sat} e^{\alpha h} \qquad \textbf{[4-5]}$$

With a minimum of two measurements of Q_S at differing tensions, the K_{sat} and α can be calculated by first solving for α

$$\alpha = \frac{\ln\left[\frac{Q(h_2)}{Q(h_1)}\right]}{h_2 - h_1} \qquad \textbf{[4-6]}$$

and then using [4-5] to determine K_{sat}. With multiple measurements at varying tensions, a modified approach to the Wooding-Gardner solution is proposed by Reynolds and Elrick (1991). Since K(h) can be non-linear with unique values for K_{sat} and α for pair of tensions, a segmented approach to determine K_{sat} and α is followed. The following equations and procedure are taken from Reynolds and Elrick (1991).

$$K(h) = \overline{K}_{x,y} \exp\left(\overline{\alpha}_{x,y} h\right) \qquad \textbf{[4-7]}$$

$$\overline{K}_{x,y} = \frac{G_d \overline{\alpha}_{x,y} Q_x}{r\left(1 + G_d \overline{\alpha}_{x,y} \pi r\right)\left(Q_x / Q_y\right)^P} \qquad \textbf{[4-8]}$$

Where x = 1,2,3,… and y = x+1, and

$$P = \frac{h_x}{h_x - h_y} \qquad \textbf{[4-9]}$$

And

$$\overline{\alpha}_{x,y} = \frac{\ln\left(Q_x / Q_y\right)}{h_x - h_y} \qquad \textbf{[4-10]}$$

First $\overline{\alpha}_{x,y}$ is calculated from a sequence of *Q* and *h* values from **[4-10],** then with **[4-8]** $\overline{K}_{x,y}$ is determined. With $\overline{\alpha}_{x,y}$ and $\overline{K}_{x,y}$ known, equation [4-7] can be used to determine K(h) for a given tension within the applicable range.

Another option for three-dimensional infiltration analysis is the Zhang (1997) method that was employed for the previous section for the field measurements. The method follows the same procedure as the field measurement analysis. The difference between the field analysis and the laboratory analysis are the device parameters. The large disk infiltrometer has a larger disk radius than the AMDI and has the ability to vary the applied tension. Example calculations for these two analyses are found in Appendix E.

Results

One-Dimensional Infiltration

For one-dimensional infiltration, the unsaturated hydraulic conductivity is equal to the infiltration rate into the soil. Equation [4-1] was applied to the results of the simple infiltration analysis (Figure 4.1). The results of the infiltration are shown in Figures 4.5, 4.6, and 4.7 for sites 2, 6 and 9.

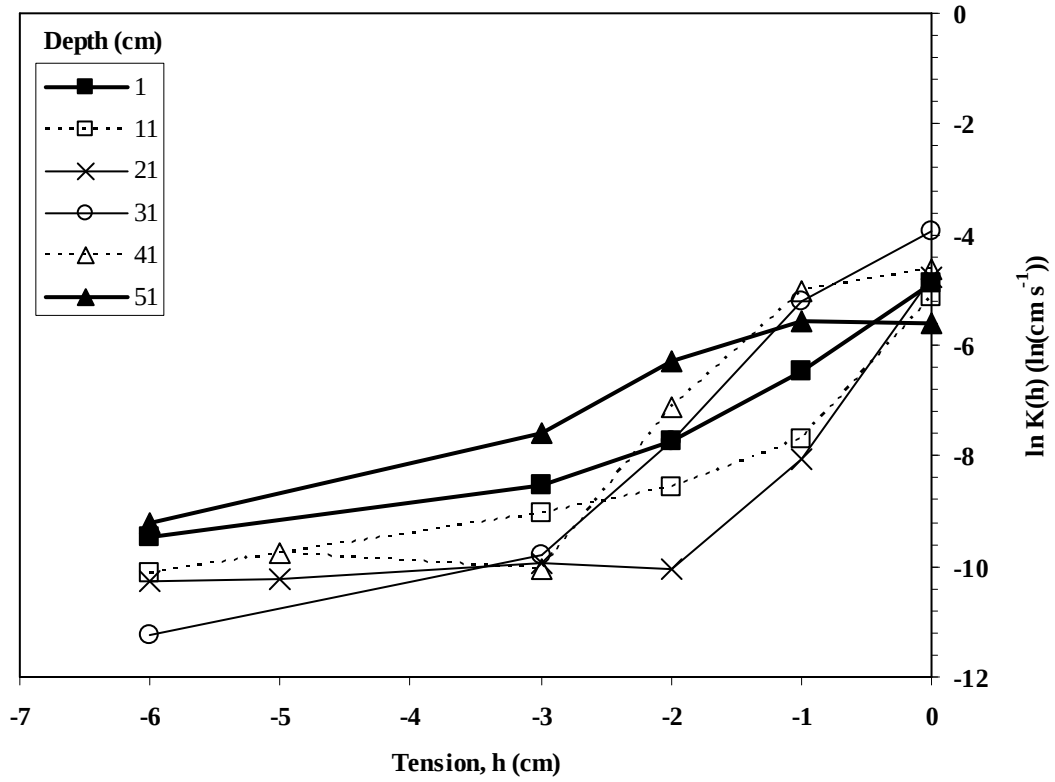

Figure 4.5. Unsaturated hydraulic conductivity, K(h), for the large disk at varying depths and tensions for Site 2.

The relationship between K(h) and depth is dependent on the tension for site 2 as seen in **Figure 4.5**. The soil at depth 51 cm has the highest K(h) at -6 cm tension, but its ranking among other depths is reversed between -2 cm and 0 cm tension. At 0 cm tension, the soil at depth 51 cm has the lowest K(h). Conversely, the soil at depth 31 cm has the lowest K(h) at -6 cm tension and the highest at 0 cm. The reorganization of rank for K(h) occurs between -3 cm and 0 cm of

tension. All depths exhibit a highly non-linear relationship between tension and the natural log of K(h).

From the regression of the data series shown in Table 4.1, the values for K_{sat} and α vary greatly for both the full range of tensions and the reduced range. Generally, the soil parameters, K_{sat} and α, increase as the range of data is reduced, but there is no apparent relationship between the parameters and depth.

	-6 cm to 0 cm		-3 cm to -1 cm	
Depth (cm)	K_{sat} (cm s^{-1} x 10^{-3})	α (cm^{-1})	K_{sat} (cm s^{-1} x 10^{-3})	α (cm^{-1})
1	3.4	0.72	3.4	1.0
11	1.7	0.72	0.84	0.67
21	1.1	0.74	2.3	2.0
31	10.3	1.3	50	2.3
41	9.4	1.2	94	2.5
51	5.1	0.66	12	1.0

Table 4.1. K_{sat} and α for Site 2 at various depths

The reorganization of the rankings of K(h) with respect to depth is less extreme for site 6 than for site 2 as seen in Figure 4.6. While site 6 still exhibits a switching of ranks, the shifts are more gradual from -6 cm to 0 cm of tension. Examining the soil at depth 53 cm, K(h) is the lowest among all depths for the range of applied tensions. The midrange of soil depths has the highest K(h) near 0 cm tension.

Similar to site 2, the results of the regression analysis for site 6 shown in Table 4.2 vary greatly for both the full range of tensions and the reduced range. The soil parameters, K_{sat} and α, increase as the range of data is reduced. The soil parameters in the midrange depths have the highest values.

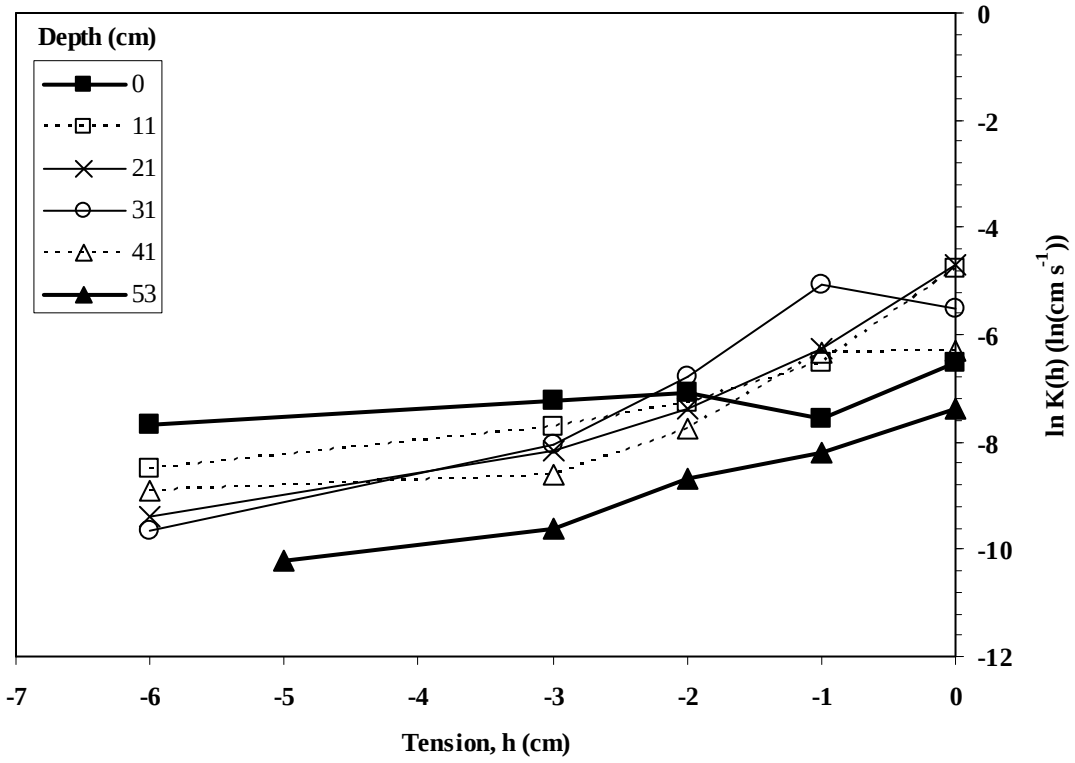

Figure 4.6. Unsaturated hydraulic conductivity, K(h), for the large disk at varying depths and tensions for Site 6.

	-6 cm to 0 cm		-3 cm to -1 cm	
Depth (cm)	K_{sat} (cm s^{-1} x 10^{-3})	α (cm^{-1})	K_{sat} (cm s-1 x 10^{-3})	α (cm^{-1})
0	1.0	0.14	1.2	0.16
11	3.7	0.56	2.6	0.61
21	4.5	0.74	4.6	0.94
31	5.9	0.78	26	1.5
41	1.6	0.48	5.0	1.1
53	0.52	0.58	0.60	0.70

Table 4.2. K_{sat} and α for Site 6 at various depths

Infiltration for site 9 was only measured between -3 cm and 0 cm. With less data than sites 2 and 6, contrasts can still be seen between the sites and depths as shown in Figure 4.7. Site 9 follows the expected trend with respect to K(h), tension and depth. The soil at the surface has the highest K(h) for all tensions, and the soil at the deepest measurement of 51 cm depth has the

lowest K(h) for almost all tensions. The midrange depths fall between the two extremes with the exception of depth 31 cm at 0 cm tension.

Since the two ranges of data are similar, the soil parameters for site 9 are do not vary greatly as shown in Table 4.2. Although there is no apparent relationship between the soil parameters and depth, the values are closer in scale. For example, K_{sat} varies by a factor of 20 from 0.36 to 6.6 cm/s x 10^{-3} for site 9 while the range of K_{sat} for site 2 varies by a factor of 100 from 0.84 to 94 cm/s x 10^{-3}.

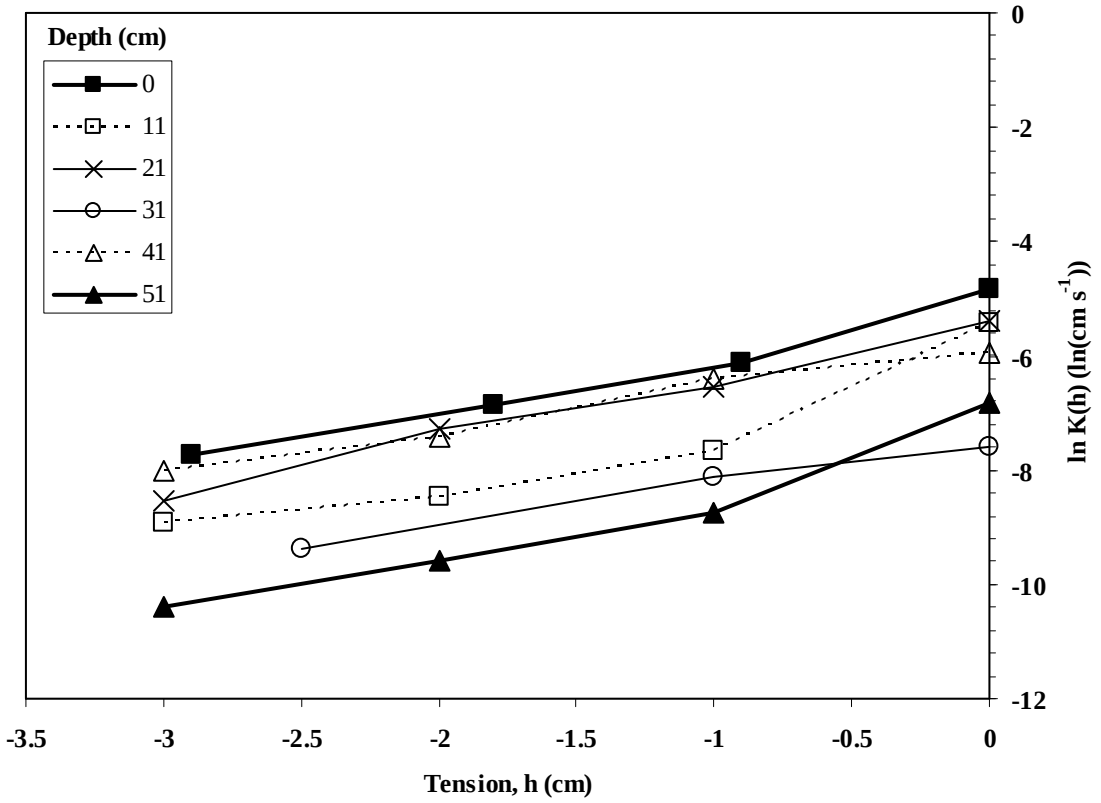

Figure 4.7. Unsaturated hydraulic conductivity, K(h), for the large disk at varying depths and tensions for Site 9.

	-3 cm to 0 cm		-3 cm to -1 cm	
Depth (cm)	K_{sat} (cm s^{-1} x 10^{-3})	α (cm^{-1})	K_{sat} (cm s^{-1} x 10^{-3})	α (cm^{-1})
0	6.6	0.97	4.5	0.80
11	2.6	1.1	0.82	0.63
21	4.5	1.0	4.3	1.0
31	0.55	0.72	0.69	0.83
41	2.9	0.73	3.5	0.81
51	0.78	1.2	0.36	0.82

Table 4.3. K_{sat} and α for Site 9 at various depths

A comparison of K(h) verses depth for the three sites at -3 cm tension is shown in Figure 4.8. The values of K(h=-3cm) were calculated from the exponential regression equations for the range of tensions from -3 cm to -1 cm. The tension was chosen to be -3 cm because the AMDIs have a nominal tension of -3 cm, and later comparisons will be made between the large disk and the mini-disks. Site 6 has the highest K(h = -3 cm) between the surface and depths up to 30 cm and generally decreases with depth. Site 2 has the lowest K(h = -3 cm) for all depths except for an unexpectedly high value for the depth near 50 cm. The site 9 K(h = -3 cm) fluctuates with depth but falls between site 2 and 6 for most depths.

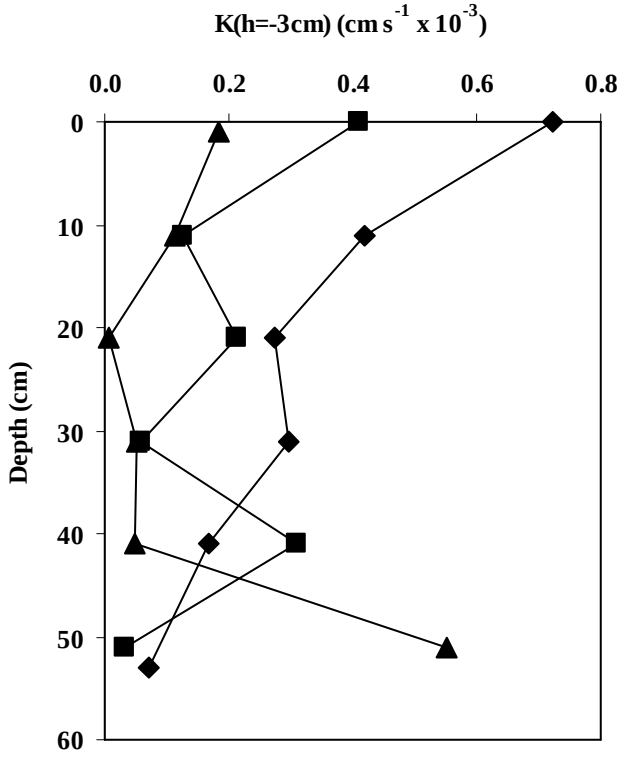

Figure 4.8. K(h=-3cm) for sites 2 (triangles), 6 (diamonds), and 9 (boxes) using the large disk infiltrometer calculated by exponential regression.

Another comparison of K(h) verses depth for the three sites is shown for -1 cm tension in Figure 4.9. Similar to Figure 4.8, the values of K(h=-1cm) were calculated from the exponential regression equations for the range of tensions from -3 cm to -1 cm. By changing the tension by 2 cm, the resulting figure is vastly different. First, the magnitude of the unsaturated hydraulic conductivity values for -1 cm tension is one order larger than -3 cm tension. Second, the values at and near the surface are close for all three sites, but they diverge from 30 cm depth and deeper. Evidence of a high hydraulic conductivity for site 2 at depths 30 cm and deeper can be seen for -1 cm tension, but the increase in hydraulic conductivity does not appear for the -3 cm tension until 50 cm depth. Site 6 and site 9 have values for K(h=-1cm) that are quite comparable except for the 30 cm depth. At 30 cm, K(h=-1cm) is about 20 times more at site 6 than at site 9.

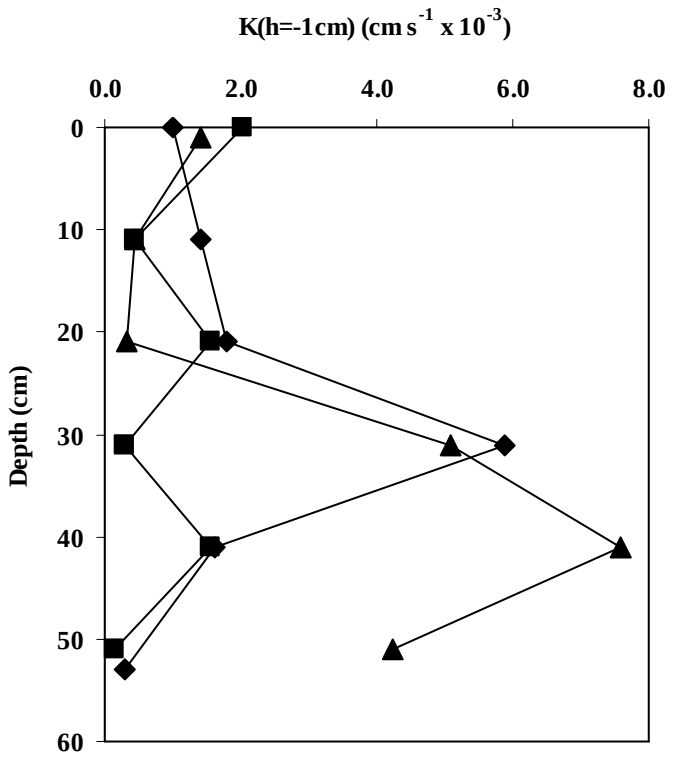

Figure 4.9. K(h=-1cm) for sites 2 (triangles), 6 (diamonds), and 9 (boxes) using the large disk infiltrometer calculated by exponential regression.

Three-Dimensional Infiltration

The three-dimensional infiltration was determined with two methods. The Reynolds and Elrick (1991) method is a piecewise application of the Wooding-Gardner equation. The Zhang (1997) method is the same empirically derived formulas for the cumulative infiltration equations that were used in the analysis of the field measurements. With the Zhang (1997) method, the value for α has been assumed based on the soil texture, and neither α nor K_{sat} are calculated with this analysis method. It is assumed that the flow is one-dimensional, and the purpose of using a three-dimensional analysis is to test this assumption. In addition, by using the same method of analysis for both the field and the laboratory measurements, the results may be more easily compared.

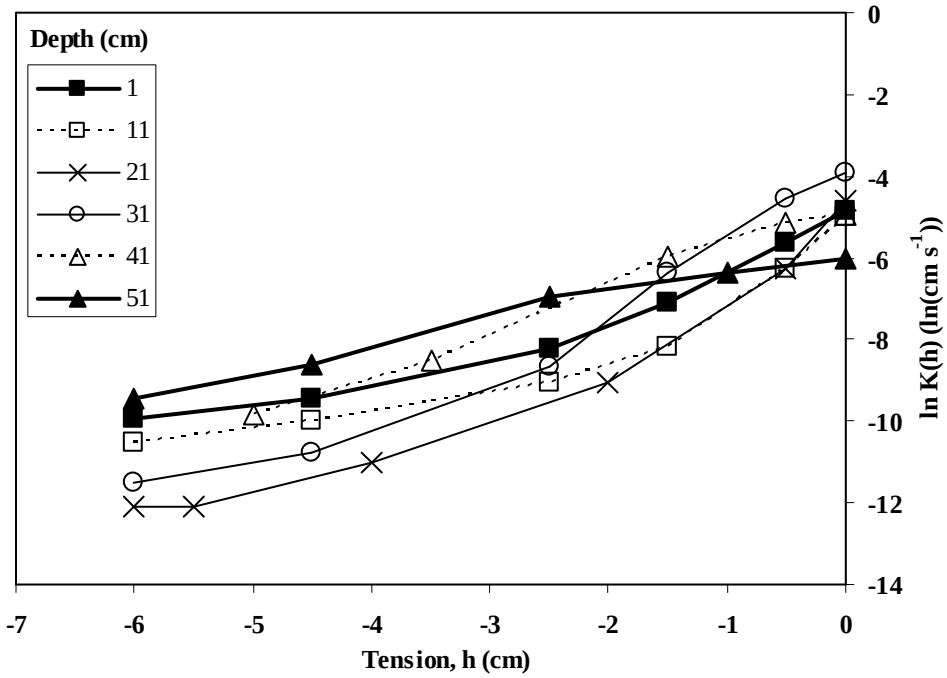

Figure 4.10. Unsaturated hydraulic conductivity, K(h), for the large disk at varying depths and tensions for Site 2 using the method from Reynolds and Elrick (1991).

The results of the Reynolds and Elrick (1991) analysis (Figure 4.10) method show similarities to the one-dimensional results for site 2. The values of K(h) for the depths are dependent on the tension. The ranks of the depths based on K(h) changes with tension similar to the one-dimensional analysis, but the shifts are more gradual.

The values for K_{sat} and α from the Reynolds and Elrick (1991) analysis for site 2 (Table 4.4) show their variability with respect to tension and depth. In Table 4.4, K_{sat} is represented by $\overline{K}_{x,y}$ and α is represented by $\overline{\alpha}_{x,y}$ for the tension pair h_x and h_y. The K_{sat} values in Table 4.4 are the intercept of the K(h)-axis when tension is equal to zero, and therefore does not have a practical interpretation for tension ranges outside of 0 cm. The values for K_{sat} and α in Table 4.4 are used in equations [4-5] and [4-7]. There does not appear to be a consistent trend in the values for K_{sat} or α with respect to tension or depth.

Depth (cm)	h_x, h_y (cm)	$\overline{\alpha}_{x,y}$ (cm^{-1})	$\overline{K}_{x,y}$ (cm s^{-1} x 10^{-3})
1	-6, -3	0.31	0.31
	-3, -2	0.78	1.88
	-2, -1	1.26	5.45
	-1, 0	1.60	7.98
11	-6, -3	0.36	0.24
	-3, -2	0.48	0.38
	-2, -1	0.86	1.01
	-1, 0	2.56	6.68
21	-6, -5	0.05	0.01
	-5, -3	0.14	0.03
	-3, -1	0.94	0.77
	-1, 0	3.30	9.89
31	-6, -3	0.48	0.18
	-3, -2	2.03	27.7
	-2, -1	2.55	79.5
	-1, 0	1.26	19.8
41	-5, -2	0.88	4.41
	-2, -1	2.09	58.5
	-1, 0	0.41	7.12
51	-6, -3	0.54	2.04
	-3, -2	1.29	24.4
	-2, 0	0.35	2.43

Table 4.4. K_{sat} and α for Site 2 at various depths and tension pairs using the method from Reynolds and Elrick (1991)

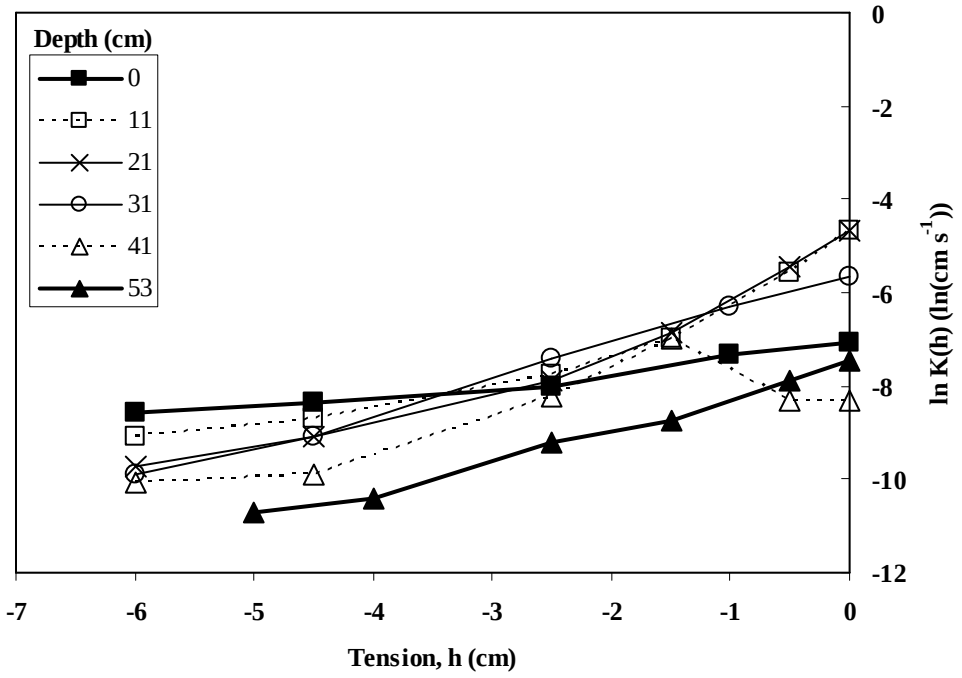

Figure 4.11. Unsaturated hydraulic conductivity, K(h), for the large disk at varying depths and tensions for Site 6 using the method from Reynolds and Elrick (1991).

The results for site 6 using the Reynolds and Elrick (1991) analysis method as shown in Figure 4.11 are similar to the one-dimensional analysis. The same types of shifts in order appear, but there appears to be an aberrant result for 41 cm depth at and near 0 cm tension. The values are much lower than expected and do not follow the same pattern as the one-dimensional analysis. This aberrant result in the piecewise analysis is the result of the near constant value of K(h) at -1 cm and 0 cm for the 41 cm depth. This results in an α value that is near zero as seen in Table 4.5.

Depth (cm)	h_x, h_y (cm)	$\overline{\alpha}_{x,y}$ (cm^{-1})	$\overline{K}_{x,y}$ (cm s^{-1} x 10^{-3})
0	-6, -3	0.15	0.46
	-3, -2	0.16	0.49
	-2, 0	0.27	0.84
11	-6, -3	0.26	0.54
	-3, -2	0.47	1.38
	-2, -1	0.75	2.80
	-1, 0	1.75	9.21
21	-6, -3	0.42	0.72
	-3, -2	0.76	2.55
	-2, -1	1.12	5.69
	-1, 0	1.56	9.50
31	-6, -3	0.54	1.27
	-3, -2	1.28	15.13
	-2, 0	0.63	3.42
41	-6, -3	0.11	0.08
	-3, -2	0.86	2.26
	-2, -1	1.40	7.37
	-1, 0	0.04	0.25
53	-5, -3	0.30	0.10
	-3, -2	0.95	1.10
	-2, -1	0.45	0.32
	-1, 0	0.84	0.58

Table 4.5. K_{sat} and α for Site 6 at various depths and tension pairs using the method from Reynolds and Elrick (1991).

The values for K_{sat} and α from the Reynolds and Elrick (1991) analysis for site 6 (Table 4.5) show their variability with respect to tension and depth. K_{sat} and α increase as the tension increase (becomes less negative), but that trend does not always hold true for the tension pairs of -1 and 0 cm.

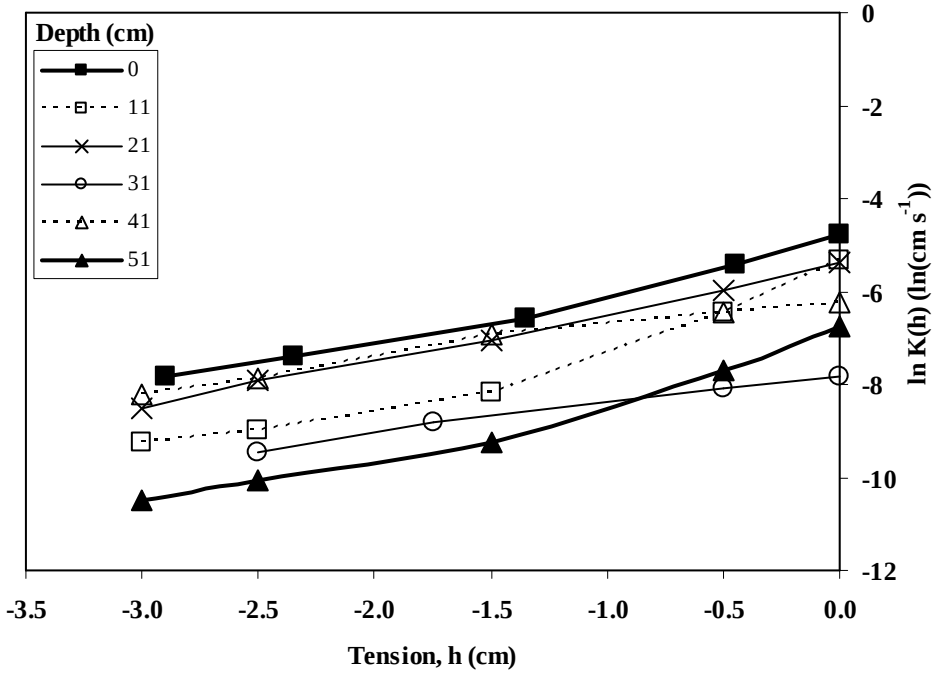

Figure 4.12. Unsaturated hydraulic conductivity, K(h), for the large disk at varying depths and tensions for Site 9 using the method from Reynolds and Elrick (1991).

The results for site 9 using the Reynolds and Elrick (1991) analysis (Figure 4.11) method are very similar to the one-dimensional analysis. The shape and position of the K(h) for each depth are the same in Figure 4.12 as in Figure 4.7. The only difference is the additional points along the line from the piecewise analysis.

Depth (cm)	h_x, h_y (cm)	$\overline{\alpha}_{x,y}$ (cm^{-1})	$\overline{K}_{x,y}$ (cm s^{-1} x 10^{-3})
0	-2.9, -1.8	0.80	4.02
	-1.8, -0.9	0.80	4.08
	-0.9, 0	1.44	8.33
11	-3, -2	0.46	0.39
	-2, -1	0.80	0.93
	-1, 0	2.25	4.84
21	-3, -2	1.26	8.69
	-2, -1	0.74	2.69
	-1, 0	1.17	4.62
31	-2.5, -1	0.83	0.63
	-1, 0	0.53	0.40
41	-3, -2	0.62	1.75
	-2, -1	1.00	4.29
	-1, 0	0.47	2.00
51	-3, -2	0.80	0.31
	-2, -1	0.85	0.34
	-1, 0	1.91	1.17

Table 4.6. K_{sat} and α for Site 9 at various depths and tension pairs using the method from Reynolds and Elrick (1991).

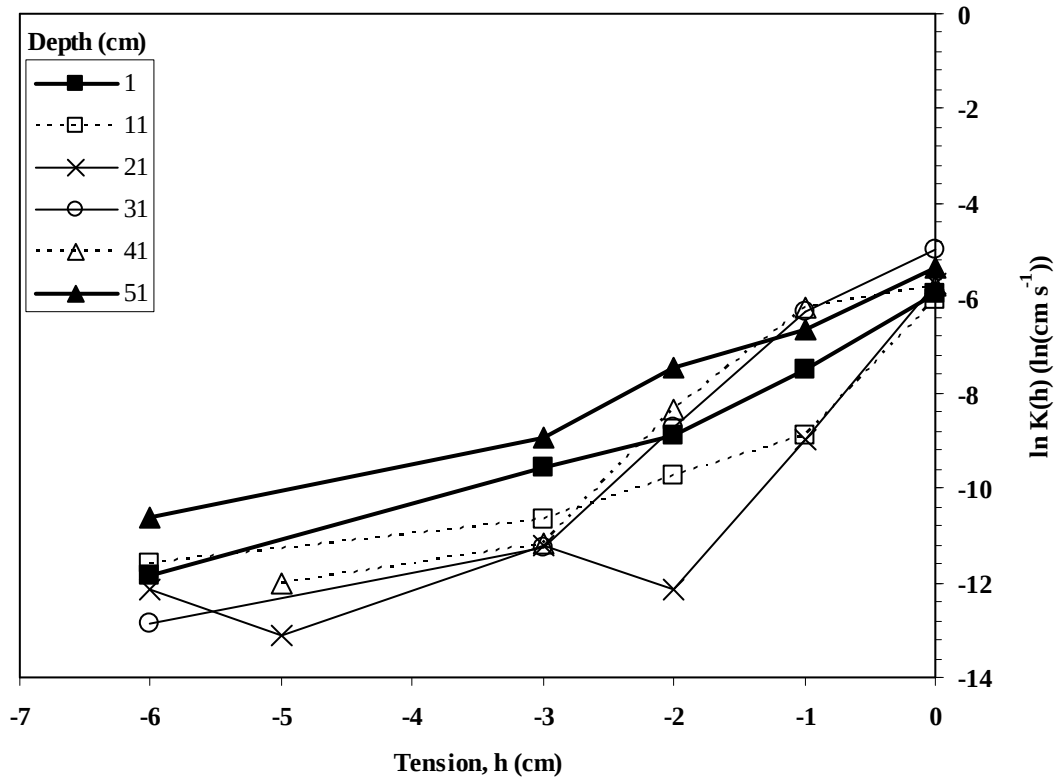

Figure 4.13. Unsaturated hydraulic conductivity, K(h), for the large disk at varying depths and tensions for Site 2 using the method from Zhang (1997).

The results from the Zhang (1997) analysis (Figure 4.13) are different from the one-dimensional and the Reynolds and Elrick (1991) method. There appears to be aberrant data points for 31 cm depth at tensions -5 and -2 cm. The midrange depths still appear highly non-linear, while the near surface and deepest measurement appear quite linear. All depths at 0 cm tension seem to converge near a common K(h) value.

The results from the Zhang (1997) analysis (Figure 4.14) are similar to the one-dimensional method for site 6 (Figure 4.6). The simple infiltration and the cumulative infiltration analysis produce similar results for site 6. The magnitude of K(h) from the Zhang (1997) analysis is less than both the one-dimensional method and the Reynolds and Elrick (1991) methods.

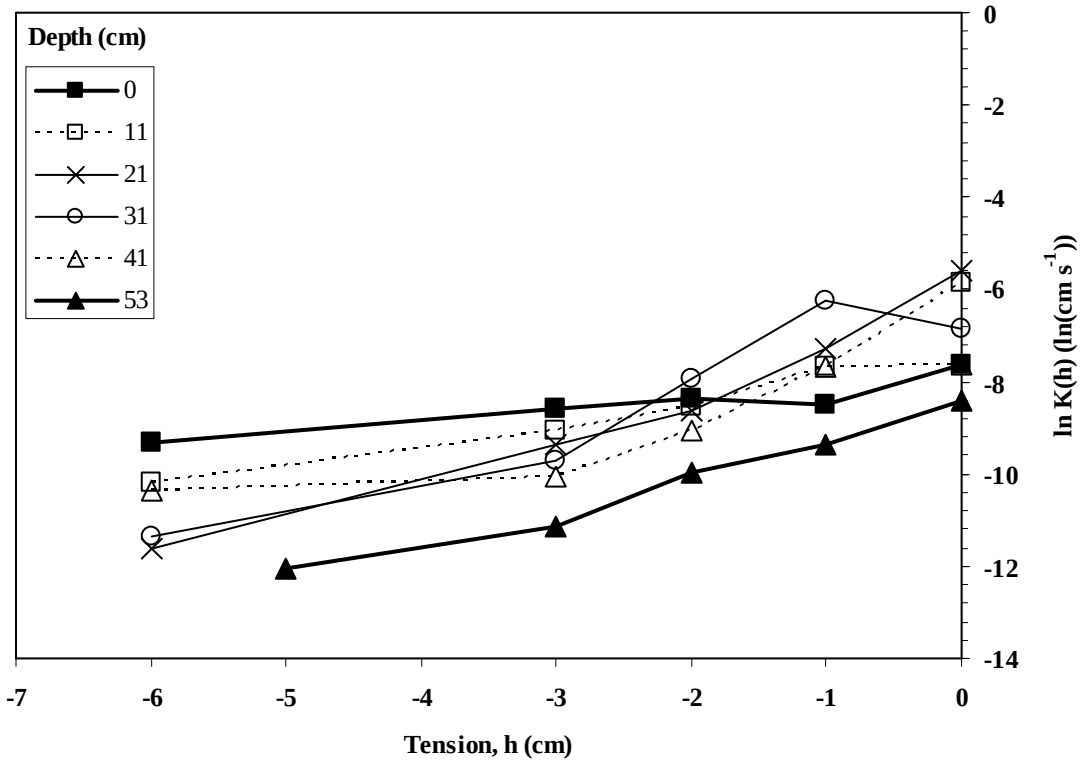

Figure 4.14. Unsaturated hydraulic conductivity, K(h), for the large disk at varying depths and tensions for Site 6 using the method from Zhang (1997).

For site 9 with the Zhang (1997) analysis (Figure 4.15), the value at 51 cm depth for -3 cm tension is much lower than expected compared with previous results and the other values for site 9. The aberrant results form 51 cm depth at site 2 were also much lower than expected. For the heavier textured soils at the bottom of the soil column, the Zhang (1997) underestimates K(h) rather than overestimates. Both the Reynolds and Elrick (1991) and the one-dimensional linear analysis methods use the same source for the infiltration rate (Figure 4.1), while the Zhang (1997) uses a different method to obtain K(h) (Figure 4.2). The remainder of the graph appears similar to the one-dimensional and the previous three-dimensional analysis except that the values of K(h) are slightly lower.

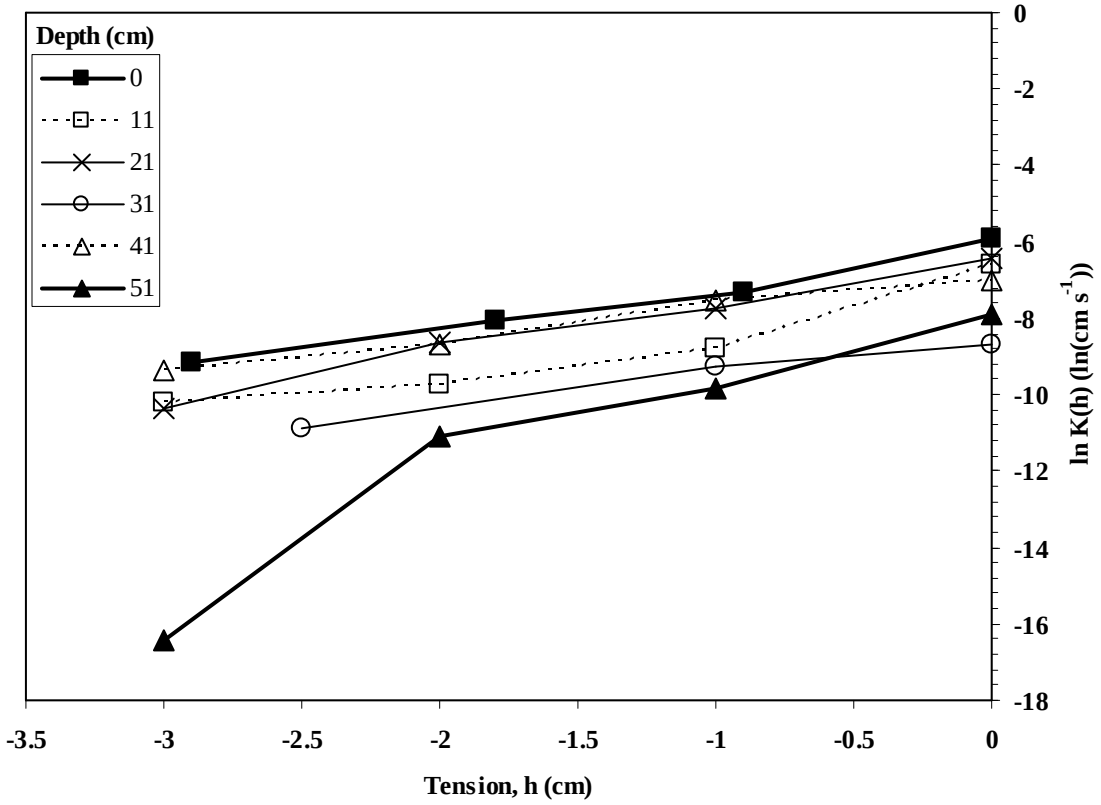

Figure 4.15. Unsaturated hydraulic conductivity, K(h), for the large disk at varying depths and tensions for Site 9 using the method from Zhang (1997).

Discussion

One-dimensional infiltration

For site 2, the shifts in the K(h) ranking of the depths around -3 and -2 cm tension indicates a varying influence of macropores and micropores on the flow rate. At tensions near 0 cm, macropore flow would dominate, and at tensions near 6 cm micropore flow would dominate. This indicates a bimodal distribution of macropores and micropores. For the soil at 51 cm depth, micropore flow dominates the infiltration rates as can be seen when the tension increases (becomes less negative), K(h) does not increase compared to the other depths. For the other depths, macropore flow dominates. K(h) is low for -6 cm tension and increases dramatically as tension increases.

K(h) is expected to increase as tension increases, but the relationship shown in Figure 4.5 for the one-dimensional analysis of site 2 indicates a non-linear relationship between the natural

log of K(h) and tension. K(h) increases at a greater rate then the Gardner (1958) model would permit for the series of data requiring the piecewise segmentation proposed by Reynolds and Elrick (1991) in order to properly model the data.

For site 6, the data does not exhibit the same type of shifts as sites 2 indicating a more unimodal pore distribution. The influence of macropores is less for site 6 indicating that the flux through the soil is dominated by matrix flow through micropores.

For site 9, while there are a few shifts in the order of the depths with respect to tension, the data follows a linear relationship for all depths. The Gardner (1958) model without adjustment could adequately describe the data, although the data is limited to the measured tension range between -3 and 0 cm.

K(h) should increase as tension becomes less negative, and it generally does. A few infiltration runs are in opposition to this assumption. Site 2 at depth 21 cm and tension -2 cm, depth 41 cm and tension -3 cm and depth 51 cm and tension 0 cm seem like aberrant results. For site 6, depth 0 cm at tension -1 cm and depth 31 cm at tension -1 cm are also seem in error. The sources of the error may be the result of the measurement techniques or operator error. Either the applied tension or the volume of water infiltrated may have been misapplied or recorded incorrectly. In addition, the regression analysis used to determine the infiltration rates may need additional adjustments to better capture the steady-state flow rate. Also the infiltrometer may lack the precision to differentiate between the various applied tensions and the volume of water infiltrated.

Aside from some apparent errors seen in the results of site 6 as discussed above, the exponential regression seems adequate for sites 6 and 9 for the range of tensions measured. Plotted on a log-normal scale, the data points appear linear. If the exponentially regressed line is adequate to describe the relationship between hydraulic conductivity and tension, then a piecewise analysis as proposed by Reynolds and Erick (1991) is unnecessary.

For site 2, the exponential regression does not seem to be as good of a fit for the entire range of data points as compared to sites 6 and 9. The non-linearity of the relationship between tension and hydraulic conductivity on a log-normal scale implies the unsuitability of the Gardner (1958) equation for Site 2 for the entire range of applied tensions.

Comparison between one- and three-dimensional infiltration analyses

The values of K(h) are higher in the one-dimensional analysis than in the Zhang (1997) analysis but comparable to the Reynolds and Elrick (1991) method. It would be expected that the two methods that utilized a three-dimensional analysis would produce results similar in magnitude. The three-dimensional method of Reynolds and Elrick (1991) more closely aligns with the one-dimensional than the other three-dimensional method of Zhang (1997).

The Wooding-Gardner equation, **[4-5],** used in the Reynolds and Elrick (1991) analysis has a shape parameter, G_d, that can be modified to match the shape of the assumed dispersion of water in the soil. For large values of G_d, the assumed dispersion decreases as the influence of the term $r/G_d\alpha$ decreases. The value of G_d was chosen to be 0.25, and this value seems to approximate the one-dimensional analysis more closely than the Zhang (1997) method does. The Zhang (1997) method does not have fitting parameters and cannot be adjusted to more closely match the values from the one-dimensional analysis.

Compared to the one-dimensional analysis, the three-dimensional analyses had some aberrant results. The differences seen with the Zhang (1997) method can be explained by the graphical analysis of the data. Both the one-dimensional and the Reynolds and Elrick (1991) methods use the data from the simple linear infiltration analysis, while Zhang (1997) uses the cumulative infiltration with the two term polynomial. Slightly different results from the two regression analyses are one explanation for the dissimilar results between Zhang (1997) and the other methods. The aberrant results from the Zhang (1997) method are lower than expected and are for the soil segments with already low K(h).

Comparison to field measurements

Figure 4.8 and Figure 4.9 show how depth influences K(h) for the sites at two different tensions. For the -3 cm tensions, the values obtained from the large disk with one-dimensional analysis are in a different order compared to the field measurements. While site 6 has the highest K(h=-3 cm) from both the laboratory measurements and the field measurements, sites 2 and 9 are in different positions. Site 2 has a greater K(h) than site 9 based on the field measurements, but the laboratory measurements show site 9 having the greater K(h) than site 2.

The differences could be due to the when the large cores were sampled or how the large cores were extracted and stored. While the field measurements were all conducted during the

summer time, the extraction of the soil cores occurred over two time periods. Site 6 and 9 were collected in the fall of the same year the field measurements were collected, and site 2 was collected in the spring of the following year shortly after the annual burn treatment. The differences in the season during extraction, the conditions in the field during extraction, and the amount of time the cores spent stored in the laboratory may have resulted in seasonal or temporal effects (Heddadj and Gascuel-Odoux 1999) or additional disturbances to the extracted soil column.

Comparison to soil information and landform

The information on the soil from the soil survey and the soil descriptions at the selected sites indicates that the hydraulic conductivity should decrease with depth as the soil transitions from a silty loam to a clay loam. The heavier texture of the clay loam is expected to be less permeable than the silty loam. During the field investigation for the soil descriptions, the size and prevalence of the roots and pores decreases with depth further suggesting that the infiltration rates would decrease with depth.

From the results of the large soil core data, the relationship between infiltration and depth is not as clear as the soil descriptions would indicate. The assumed exponential relationship (Beven 1997) between hydraulic conductivity and depth was not observed. The variations in the soil textural and structural properties are not represented in a simple exponential relationship with depth similar to how the Gardner equation is not adequate in representing unsaturated hydraulic conductivity over a large range of tensions.

As the soil was extracted from the site, it expands because it is no longer contained in the radial direction. As the soil was tested, 10 cm was sequentially removed and eliminated an additional source of compression, the overburden, but in the vertical direction. It is assumed that the overburden increases as depth increases because at greater depths, the mass of soil above increases (Rose 1965). As loads are removed, the soil expands, and the porosity increases. As the porosity increases, the volume available to hold and transport water increases. The sampling strategy to reduce disturbance may inadvertently introduced another source of error.

The soil descriptions are a systematic way to qualitatively identify soils, but the soil descriptions cannot capture the complex way the soil structure influences infiltration and unsaturated flow through the soil.

The influence of the limestone bench or the large fragments of fractured limestone originating from the Florence limestone layer may be seen in the site 2 at depth near 50cm. For site 2, the soil has a higher than expected unsaturated hydraulic conductivity for the 51 cm depth. It is expected that K(h) would decrease with depth, but the depth at 51 cm is the deepest measured depth and it is also the highest measured K(h) for tensions -2 cm to -6 cm.

Mini-Disk Infiltration

Preparation

Using the segmented soil columns from the large disk tension infiltrometer, the hydraulic conductivity was determined using the AMDIs. Between the large disk infiltration tests and AMDI tests, the soil samples were wrapped in foil to prevent drying and stored at room temperature. To reduce physical disturbance, the segments remained in either the segmented PVC tubes (for sites 6 and 9) or soil liners (for site 2) during storage and AMDI testing.

The segmented soil columns were placed in a tray of silica sand. Tripod stands fabricated for use with the mini-disk infiltrometers were attached to the outer shell of the soil segments. Pre-moistened sand was applied to the top of the soil samples in order to create a uniform contact surface. Figure 4.16 shows the arrangement of the materials prior to an infiltration run.

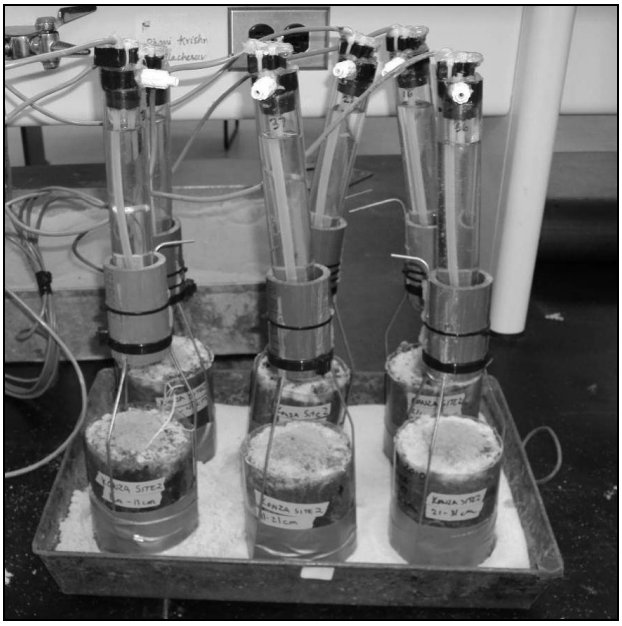

Figure 4.16. Experimental set-up of the automated mini-disk infiltrometers for laboratory testing. Site 2 is shown.

Measurement

The same procedure from the field measurement section is repeated again for the laboratory measurements of the AMDIs with a few exceptions. Soil moisture was determined gravimetrically by measuring the mass, m_w of the samples before and after the infiltrations. After all the infiltration measurements were taken the samples were dried in an oven to determine the dry mass, m_d.

$$\theta = \frac{m_w - m_d}{m_d} \qquad \textbf{[4-11]}$$

With the measurements of mass and an approximated volume for each soil segment, an approximate dry density, ρ_d, can be computed using the following equation

$$\rho_d = \frac{m_d}{V_T} \qquad \textbf{[4-12]}$$

where V_t is the total volume of the soil. The volume of the soil is a cylinder with an approximated height of 10 cm for most soil segments and a diameter of 9 cm.

In a second deviation from the field measurements, the laboratory infiltration measurements did not always exhaust all water from the reservoir tube; some water in the reservoir tube remained at the conclusion of the test. Additionally if infiltration was extremely slow, the test was terminated after one hour and the height of the water remaining in the tube was recorded. Calculations were then adjusted based on the volume of infiltrated water.

Analysis of the mini-disk data

The analysis for the laboratory AMDIs followed the same procedure as the field measurements with the exception of the statistical analysis. The simple infiltration, cumulative infiltration, and the differential linearization graphs for the AMDI measurement at site 2 depth 1 cm are shown in Figures 4.17 – 4.19. With only one measurement per site and depth, a statistical analysis was not performed.

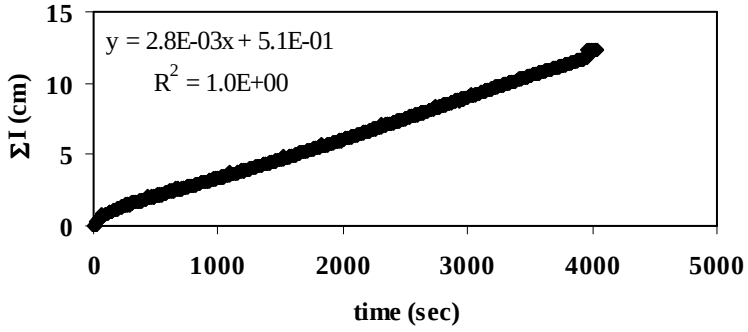

Figure 4.17. Simple infiltration for site 2 depth 1 cm.

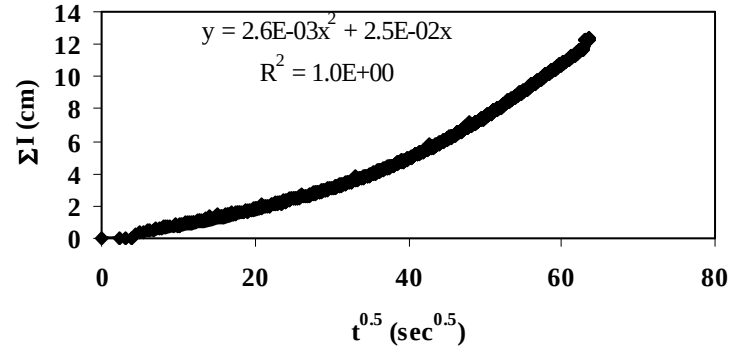

Figure 4.18. Cumulative infiltration for site 2, depth 1 cm.

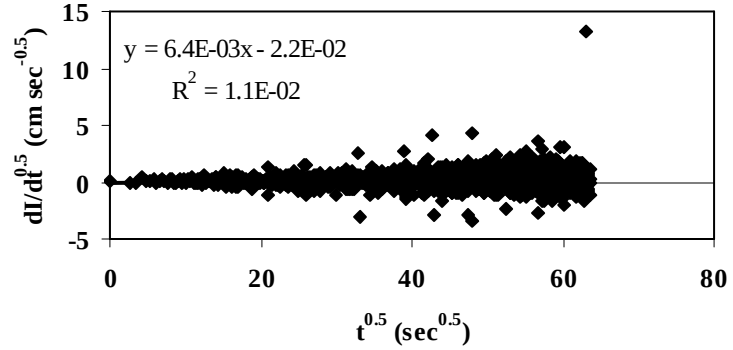

Figure 4.19. Differential linearization for site 2, depth 1 cm.

A resampling strategy using the results of the cumulative infiltration for the differential linearization analysis was not performed for AMDI laboratory measurements. The analysis of the field measurements showed that the resampling technique was successful in reducing the R-

squared values an improving the regression fitness from the differential linearization, but the method still produced values for hydraulic conductivity and sorptivity that were outside the range of expected values. Vandervaere et al (2000) analysis using differential linearization is inappropriate for the mini-disk infiltrometers.

Results of mini-disk tests

The results of the AMDI tests in the laboratory on the segmented soil columns are shown in Figure 4.20 and 4.21. The simple linear method is shown along with the cumulative infiltration method for the three sites at the various depths in Figure 4.20, and Figure 4.21 shows the relationship between the linear method and the cumulative infiltration method.

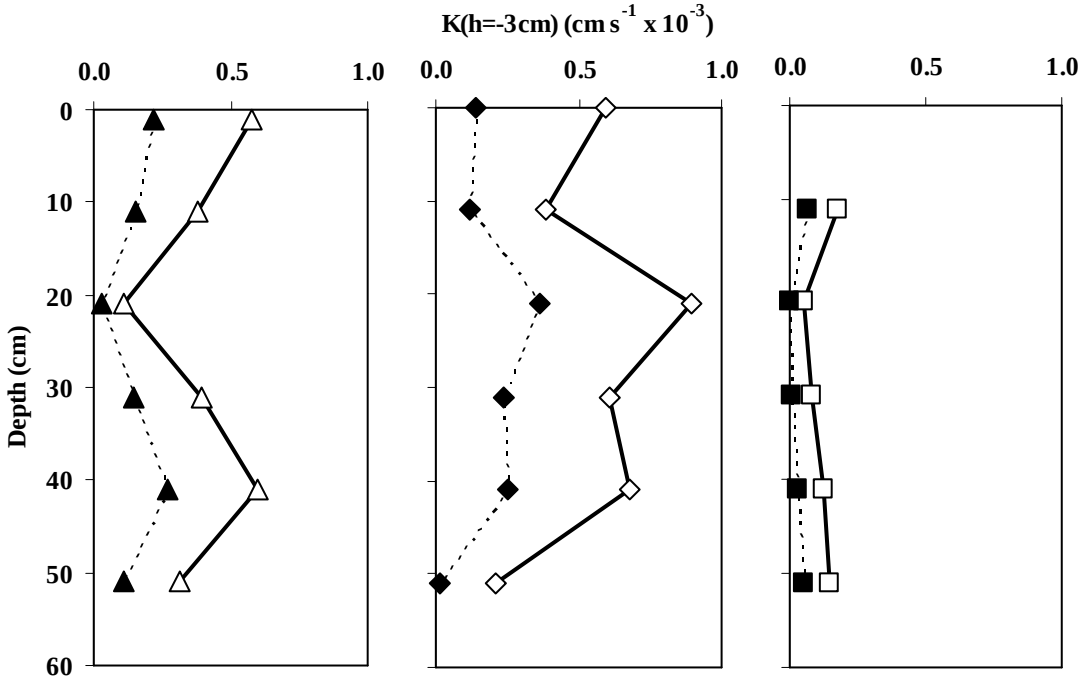

Figure 4.20. K(h=-3 cm) for sites 2,6 and 9 from the mini-disk measurement in the laboratory.

Notes: Points are shown for site 2 (triangles), 6 (diamonds), and 9 (boxes), for the Zhang (1997) method with parameters from Carsel and Parish (1988) (filled markers) and from the simple linear method (open markers).

From Figure 4.20, the results of the simple linear method are consistently higher than the Zhang (1997) method. The relationship between the simple linear method and the Zhang (1997)

method are the same as in the field study. Hydraulic conductivity with respect to depth fluctuates for sites 2 and 6, but seems consistently low for site 9.

Examining the same data in a different format, Figure 4.21 also shows that the results of the simple linear method are consistently higher than the results obtained from the Zhang (1997) method.

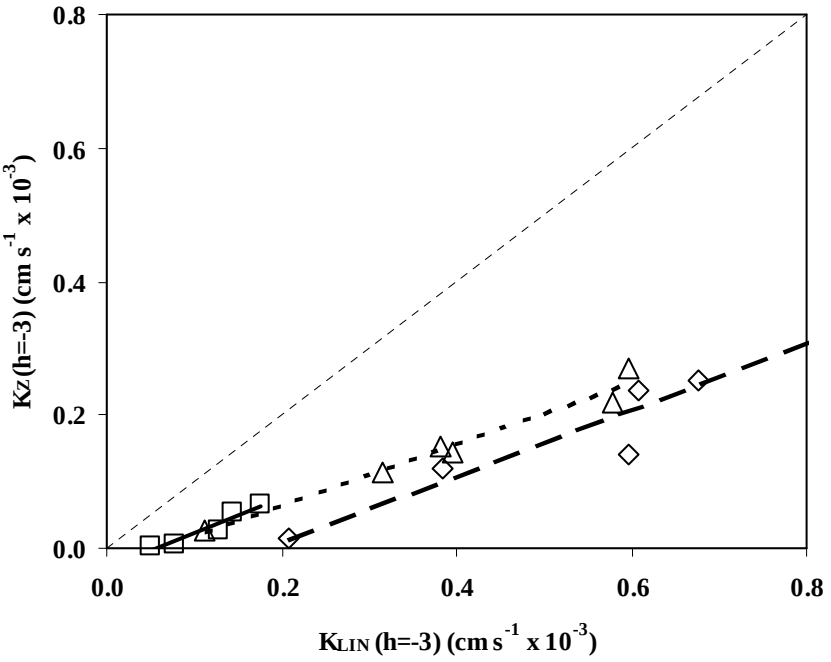

Figure 4.21. Comparison of Zhang (1997) method to linear method in determining K(h=-3) with Mini-Disk infiltrometers for sites 2, 6, and 9.

Notes: Points are shown for site 2 (triangles), 6 (diamonds), and 9 (boxes), and regressed lines are shown for sites 2 (dot), 6 (dash) and 9 (solid). Unity line is shown as thin dashed.

The results of the dry density, ρ_d, analysis are shown in Table 4.7. For all sites, the dry density is the lowest at the surface and tends to increase as the depth increases. For site 2, the dry density increases from 0.83 g cm^{-3} at the surface to 1.24 g cm^{-3} at depth of 21 cm and then decreases to 1.10 g cm^{-3} at 51 cm depth. For site 6, the soil at the surface has a dry density of 1.01 g cm^{-3}, increases up to 1.26 g cm^{-3} at 41 cm depth, and decreases to 1.09 g cm^{-3} at 53 cm depth. For site 9, the soil near the surface has a dry density of 1.23 g cm^{-3} and gradually increases to 1.38 g cm^{-3} at 51 cm depth. The dry density at site 9 is greater than both sites 2 and 6 and continues to increase for all measured values.

Site	Depth (cm)	Volume (cm^3)	Mass (g)	ρ_d ($g\ cm^{-3}$)
2	1	636	528	0.83
	11	636	684	1.08
	21	636	730	1.15
	31	636	786	1.24
	41	636	755	1.19
	51	763	842	1.10
6	0	700	710	1.01
	11	636	720	1.13
	21	636	770	1.21
	31	636	706	1.11
	41	636	802	1.26
	53	636	697	1.09
9	11	636	781	1.23
	21	636	834	1.31
	31	636	838	1.32
	41	636	860	1.35
	51	763	1051	1.38

Table 4.7. Approximate dry densities, ρ_d, for the three sites at the six segmented depths for the mini-disk infiltrations.

The soil moisture shown in Table 4.8 is the gravimetric water content from equation [4-11]. The percent change in soil moisture ranges from 4% to 30%. The change in soil moisture is seen in the soil segments from site 9, and this is like due to the relatively low initial soil moisture. There does not appear to be a pattern relating soil moisture, either initial or final, to depth.

Site	Depth (cm)	θ_i	θ_f	$\Delta\theta$
2	1	0.59	0.63	5%
	11	0.38	0.44	18%
	21	0.40	0.43	7%
	31	0.37	0.42	13%
	41	0.39	0.41	4%
	51	0.37	0.40	8%
6	0	0.39	0.45	14%
	11	0.44	0.47	5%
	21	0.41	0.43	6%
	31	0.44	0.45	4%
	41	0.39	0.43	11%
	53	0.42	0.45	6%
9	11	0.21	0.27	30%
	21	0.29	0.32	9%
	31	0.26	0.29	14%
	41	0.26	0.30	14%
	51	0.23	0.26	11%

Table 4.8. Initial moisture content, θ_i, and final moisture content, θ_f, for the three sites at the six segmented depths for the mini-disk infiltrations.

Discussion of Mini-Disk Results

The simple linear method over estimates K(h) compared to the cumulative infiltration method of Zhang (1997). This is the same conclusion made regarding the field measurements. The simple linear method assumes a wetted disk radius of 3.5 cm for initially dry conditions and 4.5 cm for wet initial conditions. Figure 4.22 shows the theoretically wetting front for the two methods. The simple linear method assumes a one-dimensional wetting front where the wetting front has a constant depth that increases with time. The Zhang (1997) assumes a three-dimensional wetting front in the shape of a bulb that increases in size with time.

In order for the results of the simple linear method to better correlate with the Zhang method, the assumed wetted disk radius could be increased. A wetted disk radius of 6.5 cm would produce an estimate of K(h) that is comparable to the Zhang method, although the larger radius may not have any basis in reality. The size of wetted disk radius could also be site

specific depending on the soil type, and one value may not be adequate for the range of soil types encountered in the field.

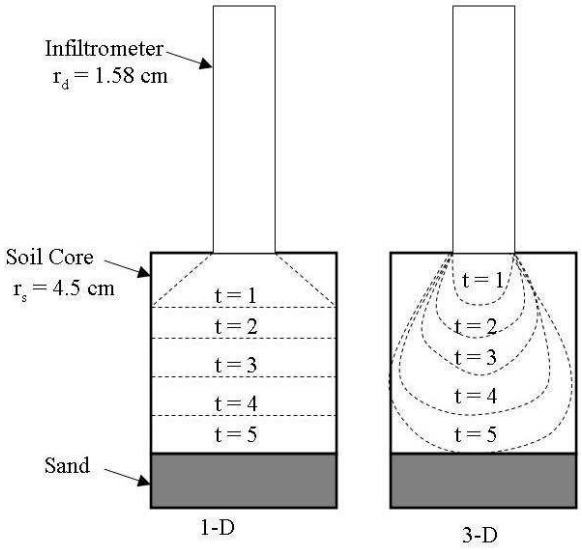

Figure 4.22. One-dimensional versus three-dimensional infiltration for the AMDIs

The average values of K(h=-3cm) for all depths using the Zhang method are $1.6x10^{-4}$ cm/s, $1.9x10^{-4}$ cm/s, and $3.1x10^{-5}$ cm/s for sites 2, 6, and 9 respectively. The difference between sites is not apparent with sites 2 and 6, but K(h) for site 9 is less.

A decrease in K(h) with depth is expected, but any relationship between K(h) and depth is not evident with the mini-disk measurements. For site 9, the values below depth 11 cm increase slightly. For sites 2 and 6, the relationship between depth and K(h) appears random with the values at depth 20 cm being especially aberrant. The values for sites 2 and 6 near depth 20 cm are either much lower (site 2) or much higher (site 6) than would be expected.

One reason for the unexpected relationship between K(h) and depth is the relief of the overburden. The soil column samples were extracted and kept intact before testing, and they were maintained intact with the exception of the segmentation process. When the samples were extracted, the soil expanded because it was not bound laterally. Although the lateral expansion would affect the overall K(h) of the soil column, the relative relationship with depth would not be affected. As the samples were segmented, and the overburden removed, the soil could expand vertically, and the relative relationship of K(h) with depth would be affected.

Perhaps the biggest factor that explains the variability of the AMDI measurements is the lack of precision of the devices. In the field measurements, the standard deviation of the sites is

about 0.2 x 10^{-3} cm s^{-1}. The variations in the measurement are a combination of the statistical distribution of the hydraulic conductivity values and of the residual error.

Since the surface segment of site 9 was destroyed prior to the laboratory experiments with the AMDIs, it is difficult to compare the field measurements (which were taken only at the surface) to the laboratory measurements. Based on the consistency of values for K(h) at depths for site 9, it is assumed that the value near the surface is similar to the value at 11 cm depth.

Overall the results of the laboratory measurements using the AMDIs are considerably lower then the field measurements. This could be due to the seasonal variability of hydraulic conductivity. The field measurements were collected in the summer, while the soil was extracted in the fall and spring. Another source of variation could be the temperature. The field measurements were collected outside in August with high temperatures near 40° C, while the laboratory measurements were collected in a controlled environment with a temperature near 20° C.

The dynamic viscosity of water at T_2 = 20° C is μ_2 = 1.004 m^2 s^{-1} x 10^{-6}. Assuming the effective temperature for the field measurements is T_1 = 40° C, μ_1 is 0.658 m^2 s^{-1} x 10^{-6}. The equation for converting hydraulic conductivity at T_1 to hydraulic conductivity at T_2 is

$$K_2 = K_1 \frac{\mu_1}{\mu_2} \qquad \textbf{[4-13]}$$

With this conversion, the average values of K(h) from the field measurements using the Zhang (1997) method is 0.50 cm s^{-1} x 10^{-3} for site 2, 0.77 cm s^{-1} x 10^{-3} for site 6, and 0.33 cm s^{-1} x 10^{-3} for site 9.

Device:		Mini-disk	
Location:	Field	Laboratory	
Site	(cm s^{-1} x 10^{-3})	(cm s^{-1} x 10^{-3})	% Change
2	0.50	0.22	-57%
6	0.77	0.14	-82%
9	0.33	0.07	-80%

Table 4.9. Summary of the hydraulic conductivity, K(h=-3cm) (cm s^{-1} x 10^{-3}) values for the three sites

Notes: The mini-disk values for both the field and laboratory measurements are from the Zhang (1997) method. The value for site 9 is taken at 11 cm depth. The values for K(h = -3cm) from the field measurements have been adjusted for temperature.

Adjusting for temperature, the laboratory measurements are still lower than the field measurements. This indicates a possible seasonal influence in the soil since the field measurements were taken in the summer and the soil cores were extracted in the fall (sites 6 and 9) or spring (site 2). Another explanation for the variation is the disturbance in the soil cores. Even though the soil cores were intact, they could still have been disturbed by the extraction process, transport, and storage. For sites 6 and 9, the cores were subjected to saturated hydraulic conductivity tests prior to the infiltration tests which would be another source of disturbance. The extent of the effects of disturbance or seasonal variation have not been quantified in this study.

CHAPTER 5 - Conclusions

Comparisons between Methods

Extracted Soil Core

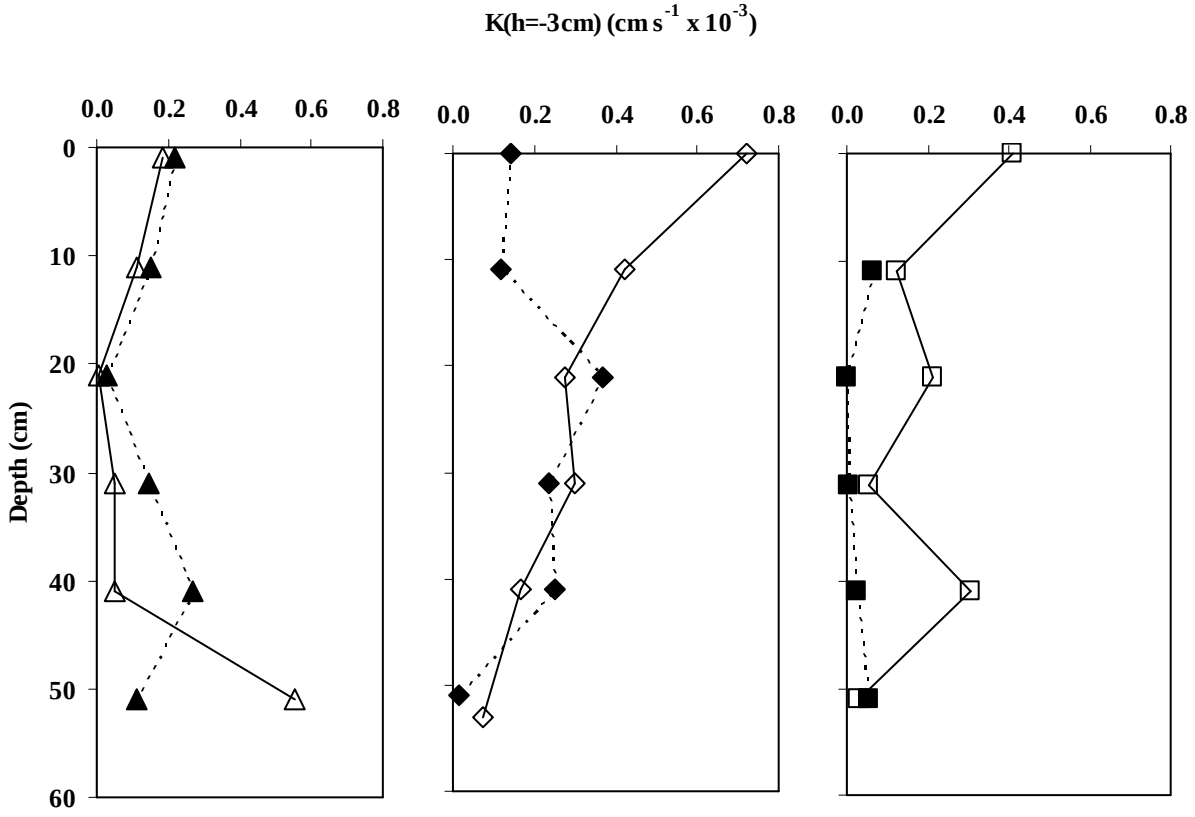

Figure 5.1. K(h=-3 cm) for sites 2, 6, and 9 comparing the mini-disk values against the large disk values at various depths.

Notes: Points are shown for site 2 (triangles), 6 (diamonds), and 9 (boxes), and), and for the mini-disk measurements using the Zhang (1997) method with parameters from Carsel and Parish (1988) (filled markers) and for the large disk using the one-dimensional analysis method (open markers).

The results of both the large disk and the mini-disk infiltrometers (Figure 5.1) do not show a strong relationship between hydraulic conductivity and depth. The unsaturated hydraulic conductivity values for site 2 near the surface are close between the mini-disk and the large disk but diverge unpredictably as depth increases. Near 40 cm depth, the value from the large disk is smaller than the mini-disk, but near 50 cm depth, the values switch and the large disk produces a

much greater value of K(h) than the mini-disk. Site 2 is on the Florence limestone layer, and the soil depth is at least 60 cm based on the findings during soil core extraction and soil descriptions visits. Limestone rock fragments are present at the surface with increasing prevalence as depth increases. The relatively high value of K(h) near 50 cm depth may be related to the course limestone fragments or the underlying limestone layer.

The larger diameter disk is able to detect the influence of the rock fragments but the smaller diameter cannot. With the large disk, the diameter is approximately the same diameter of the soil core, and therefore the large disk is able to measure the infiltration of the entire surface and near surface of the soil. The mini-disk covers a much smaller surface area of the soil core, and therefore cannot measure the infiltration from the entire surface of the soil core.

In contrast the values for site 6 are quite comparable at depths 20 cm and deeper, but the values near the surface are not. The large disk results follow the expected trend of a declining hydraulic conductivity with respect to depth. The mini-disk results are lower than what is expected for the surface and near surface values but follow the expected trend similar to the large disk results for depths 20 cm and deeper.

Site 9 has consistently low results from the mini-disk, and the large disk produce varying results. Depths near 20 cm and 40 cm are greater than would be expected compared to the mini-disk results and the results from the adjacent depths.

Although it is expected that the hydraulic conductivity would decrease with depth, the K(h) varies greatly as depth increases. Any regression analysis of the data would not be reliable. The assumption that measurements of the surface could be used to predict a vertical profile of K(h) is not valid based on these results.

All of the methods of analysis used in the laboratory measurements of the extracted soil core produced realistic results that were within range of expected values. Although there were some aberrant results, none of the values for K(h) were orders of magnitude greater than or less than the expected values.

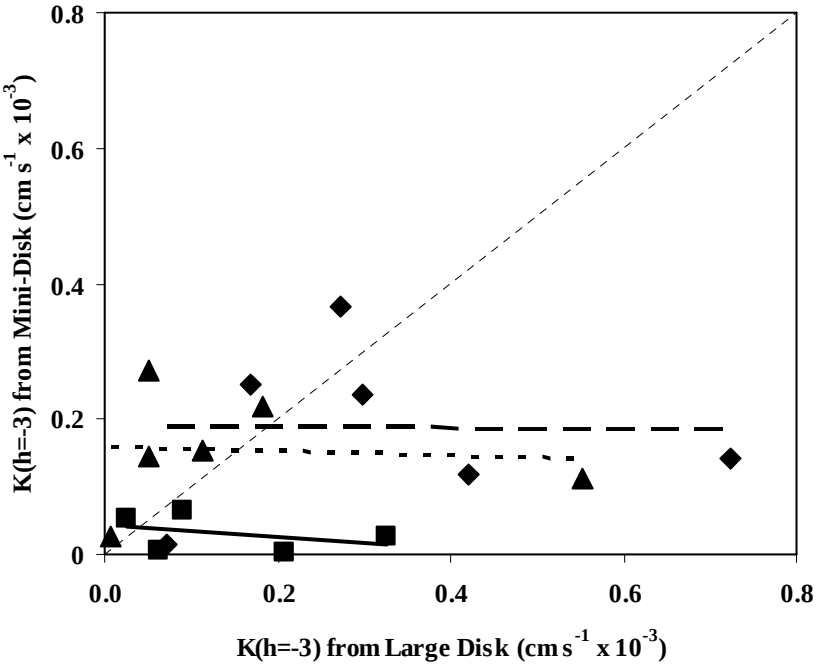

Figure 5.2. Comparison of one-dimensional large disk infiltration to three-dimensional mini-disk value of K(h=-3 cm) for sites 2, 6, and 9.

Notes: Points are shown for sites 2 (triangles), 6 (diamonds), and 9 (boxes). Mini-disk values are according to Zhang (1997) and Carsel and Parish (1988). Large Disk values were calculated by exponential regression for the tension region of -1 cm to -3 cm. Regressed lines are shown for sites 2 (dot), 6 (dash) and 9 (solid). Unity line is shown as thin dashed.

The results of the AMDIs in the laboratory are quite variable. They do not correlate well with the results from the large disk (Figures 5.2 and 5.3). Possible explanations involve the method of analysis, the variation of precision of the mini-disk devices, experimental error, or the inherent differences between the devices. Sources of experimental error separate from the mini-disk devices are smearing of the soil sample, inaccurate time or volume measurements, and uncorrected temperature effects.

The AMDIs can produce a measurement error with the bubbling tube, porous disk, and quantity and quality of contact sand as possible sources of variation. The mini-disk infiltrometers, unlike the large disk infiltrometer, lacks a method for easy calibration of the applied tension. The errors in the AMDI measurements in the field investigation are averaged over the 12 measurements. Using a single measurement for the laboratory analysis does not

provide any statistical averaging. A single measurement at each depth is insufficient to conduct any type of statistical analysis.

Figure 5.2 shows the results of the one-dimensional infiltration from the large disk versus three-dimensional infiltration from the AMDIs. Examining a three-dimensional infiltration for the large disk infiltrometer on the extracted soil core results in an underestimation of K(h) with respect to the AMDI values (Figure 5.3). The assumption of one-dimensional infiltration for the large disk appears to be more accurate than the three-dimensional assumption.

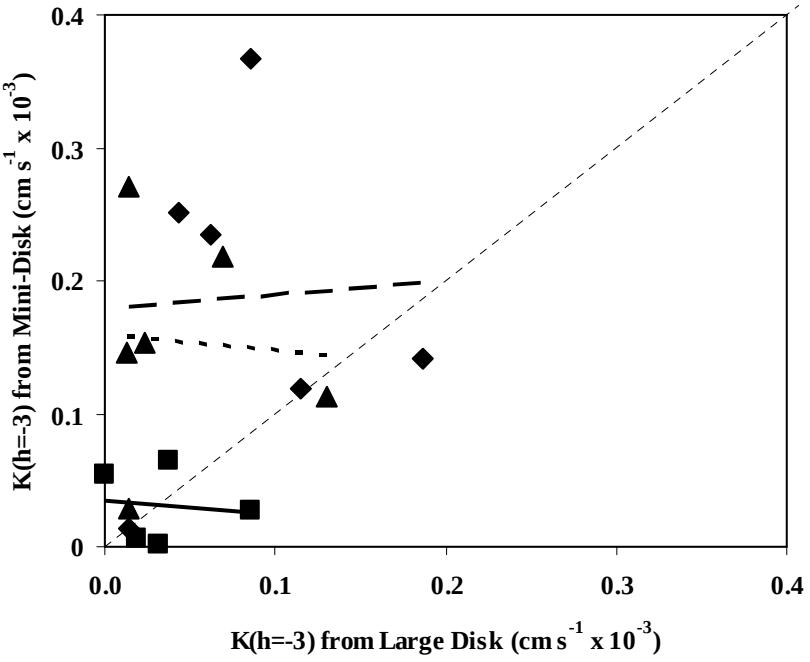

Figure 5.3. Comparison of three-dimensional large disk infiltration to three-dimensional mini-disk value of K(h=-3 cm) for sites 2 (triangles), 6 (diamonds), and 9 (boxes).

Notes: Mini-disk values and large disk values are both according to Zhang (1997) and Carsel and Parish (1988). Regressed lines are shown for sites 2 (dot), 6 (dash) and 9 (solid). Unity line is shown as thin dashed.

Segmentation Analysis

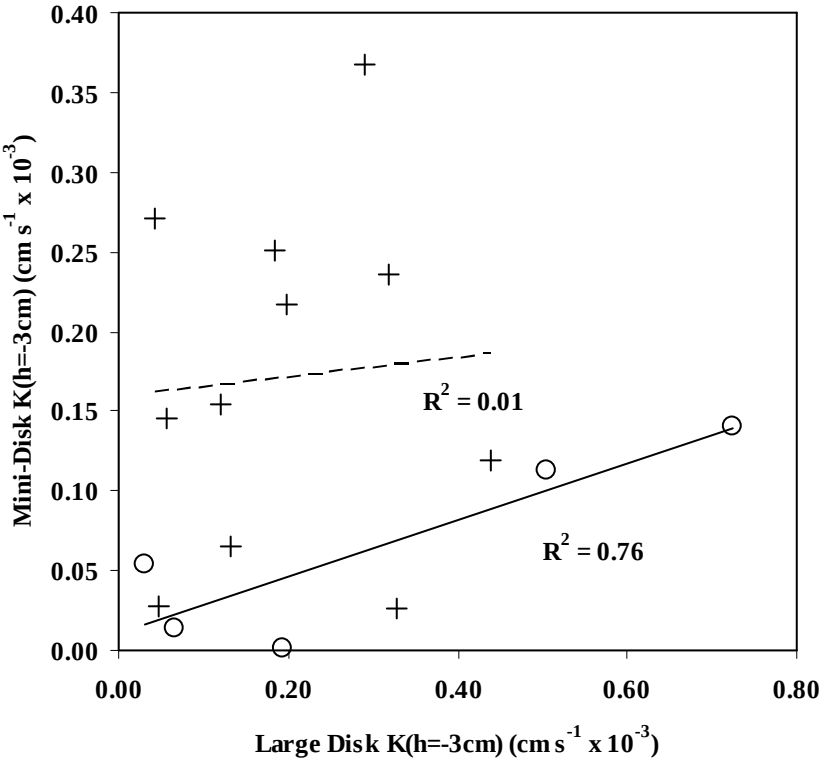

Figure 5.4. Comparison of large disk versus mini-disk for segmentation effects.

Notes: Circles with solid regressed line are in the segment group; plus signs with dashed regressed line are in the column group.

The soil samples were segmented as the infiltration tests with the large disk infiltrometer progressed, but for the mini-disk, the soil column was already segmented. Prior to this analysis, it was unclear what affect the soil 10 cm below the measured surface had on the infiltration at the surface.

To determine the effects of segmentation, the results of both the mini-disk and the large disk were compared and separated into two groups based on the large disk infiltration analysis. The values for the unsaturated hydraulic conductivity at -3 cm tension using the Zhang (1997) analysis were used in the comparison representing the mini-disk values. For the large disk, the one-dimensional simple infiltration results were used.

The first group, which will be called the column group, are the soil samples that were measured with the large disk infiltrometer and would eventually be further segmented. The

second group, which will be called the segment group, did not require any further segmentation of the soil column after the large disk infiltration. The second group typically consists of segmented soils of approximately 10 cm in depth. They are the bottom most segments in the three columns and two segments that were retested after segmentation due to irregular or incomplete initial results. Three segments were retested: site 9 at 21 cm depth, site 6 at 0 cm depth, and site 2 at 31 cm depth. At site 9, the results of the infiltration analysis were greater than expected, plus data failed to be collected properly at tensions -1 cm and 0 cm. At site 6, the data from the results was not recorded property and need to be reproduced. At site 2, the results from the retesting produced similar values of infiltration as the initial testing, and the results from the initial tests were used. The retesting of site 2 was not used in the segmentation analysis or in the final results.

Comparing the two groups from the large disk analysis to their counterparts in the mini-disk analysis (Figure 5.4), there is no significant difference. The correlation between the two infiltrometer methods is poor (R^2=0.01) for the column group and moderate (R^2=0.76) for the segment group. If the segmentation has an effect on the infiltration, it is not evident in the analysis.

CHAPTER 6 - Summary

In this study, the goal was to identify the suitability of a soil survey for characterizing the lateral and vertical distribution of hydraulic conductivity in a tall grass prairie. To accomplish this, multiple field measurements of infiltration were taken and three soil cores were extracted and subjected to additional infiltration tests. The infiltration measured in the field was analyzed with several methods to determine the lateral variability of hydraulic conductivity and sorptivity and to determine the suitability of each analysis method. The infiltration measured in the laboratory was analyzed to determine the vertical distribution of hydraulic conductivity, to infer soil structure, and to compare to the field measurements.

It was found that soil properties vary in an assumed homogeneous landscape, and landscape position does affect the soil hydraulic properties. Compared to the information from the soil survey, the measured values are within range of what is expected, but the spatial distribution pattern of permeability from the soil survey does not match what was measured in the field. Sites 5 and 6 within the Benfield-Florence complex have the greatest hydraulic conductivity while sites 9 and 10 have the lowest hydraulic conductivity and is significantly lower. Sites 9 and 10 may be considered to be within either the Benfield-Florence complex or the Tully, but both have the same estimated hydraulic conductivity at 3.0 $\mu m\ s^{-1}$.

When determining hydraulic conductivity from infiltration measurements taken either in the field or in the laboratory, several analysis methods are available and produce various results. The soil hydraulic properties, K and S, are dependent on which analysis method is selected. The empirically based analysis method proposed by Zhang (1997) provides robust results that are based on soil texture, soil retention function, and device parameters. In contrast, the Vandervaere et al (2000) approach is a physically based approach that links hydraulic conductivity to sorptivity, but the results are erratic.

From the mini-disk data, having only one applied tension for the infiltration measurements limits the types of analysis available and the type of information that can be extracted from the measurements. With the Zhang (1997) analysis, assumptions were made regarding the type of soil-water retention function and the parameters of the soil-water retention function dependent on the soil type. It was assumed and confirmed from the soil descriptions

that the soil texture was the same, silty loam, for all sites and therefore used the same parameters for the soil-water retention function.

The simple linear infiltration method of analysis assumes a radius for the wetted disk based on initially wet or dry conditions. The simple linear infiltration method produces results similar to the Zhang (1997) method but about 2 to 3 times higher. The differential linearization (Vandervaere et al 2000) does not provide reasonable or reliable results from the mini-disk data. The inappropriateness of the Vandervaere analysis could be related to the mini-disk devices or the type and condition of the soil being tested. The electronic noise produced by the automation of the mini-disk infiltrometers is amplified by the Vandervaere analysis method. Correcting for the noise by resampling the data does not improve the reliability of the results.

The second part of the study was to extract soil cores from the same areas as the field study and perform infiltration measurements in the laboratory. This would allow the comparisons of two types of infiltrometers in a controlled environment and to collect more detailed information on the structure and permeability of the soil at various depths. The results of the laboratory measurements using the large disk infiltrometer showed complex soil structure for the soils that was not seen with the mini-disks or the soil descriptions.

The large disk tension infiltrometer has the advantage of being able to apply multiple pressure heads with the adjustable tube in the bubble chamber. The major advantage of the mini-disk tension infiltrometer is its small size and portability allowing multiple measurement to be collected with ease in the field. The automation with the motes allows for many simultaneous measurements in any type of spatial sampling strategy desired.

Consistency in measurement and analysis method is necessary for proper spatial characterization of soil hydraulic properties. Conclusions were able to be made within measurement types. The data from the field measurements that was analyzed using the cumulative infiltration with the equations from Zhang (1997) was able to show the spatial variability of hydraulic conductivity. The laboratory measurements of the extracted soil core using the large disk infiltrometer at varying tensions showed the complex soil structure between sites and depths. The comparisons between the large disk and the mini-disk measurements or between the field and the laboratory measurements were less successful.

References

Ahuja, L., J. Naney, R. Green and D. Nielsen. 1984. Macroporosity to characterize spatial variability of hydraulic conductivity and effects of land management. Soil Sci. Soc. Am. J. 48:699-702.

Beven, K. 1997. TOPMODEL: A Critique. Hydrol. Process. 11: 1069-1085.

Blonquist, J.M., S.B. Jones and D.A. Robinson. 2005. Standardizing characterization of electromagnetic water content sensors: Part 2. evaluation of seven sensing systems. Vadose Zone Journal 4:1059-1069.

Brewer R. 1964. Fabric and mineral analysis of soils, John Wiley and Sons, New York (1964).

Bronstert, A. 1999. Capabilities and limitations of detailed hillslope hydrological modelling. Hydrol. Process. 13:21-48.

Carsel, R.F. and R.S. Parrish. 1988. Developing joint probability-distributions of soil-water retention characteristics. Water Resour. Res. 24:755-769.

Casanova, M., I. Messing and A. Joel. 2000. Influence of aspect and slope gradient on hydraulic conductivity measured by tension infiltrometer. Hydrol. Process. 14:155-164.

Dohnal, M., J. Dusek and T. Vogel. 2010. Improving hydraulic conductivity estimates from minidisk infiltrometer measurements for soils with wide pore-size distributions RID A-1233-2009 RID A-6972-2009 RID A-2515-2009. Soil Sci. Soc. Am. J. 74:804-811.

Duell, A.B. 1990. Effects of burning on infiltration, overland flow, and sediment loss on tallgrass prairie. Master of Science. Kansas State University.

Elsenbeer, H., K. Cassel, and J. Castro. 1992. Spatial Analysis of Soil Hydraulic Conductivity in a Tropical Rain Forest Catchment. Water Resour. Res. 28: 3201-3214.

Freeze, R.A. 1975. A Stochastic-Conceptual Analysis of One-Dimensional Groundwater Flow in Nonuniform Homogeneous Media. Water Resour. Res. 11:725-741.

Gardner, W.R. 1958. Some steady-state solutions of the unsaturated moisture flow equation with application to evaporation from a water table. Soil Sci. 85:228.

Geroy IJ, Gribb MM, Marshall HP, Chandler DG, Benner SG, and McNamara JP, in press. Aspect influences on soil water retention and storage. Hydrological Processes.

Gribb, M., R. Kodesova and S. Ordway. 2004. Comparison of soil hydraulic property measurement methods. J. Geotech. Geoenviron. Eng. 130:1084-1095.

Haverkamp, R., P. Ross, K. Smetten and J. Parlange. 1994. 3-dimensional analysis of infiltration from the disc infiltrometer .2. physically-based infiltration equation. Water Resour. Res. 30:2931-2935.

Heddadj, D. and C. Gascuel-Odoux. 1999. Topographic and seasonal variations of unsaturated hydraulic conductivity as measured by tension disc infiltrometers at the field scale. Eur. J. Soil Sci. 50:275-283.

Holden, J. 2009. Topographic controls upon soil macropore flow. Earth Surf. Process. Landforms 34:345-351.

Jewett, J.M. 1941. The geology of Riley and Geary counties, Kansas. Kansas Geological Survey, Bulletin, no. 39, 164 pages.

Kechavarzi, C., K. Spongrova, M. Dresser, S. Matula and R.J. Godwin. 2009. Laboratory and field testing of an automated tension infiltrometer RID A-4736-2011. Biosystems Engineering 104:266-277.

Madsen, M.D., D.G. Chandler and J. Belnap. 2008. Spatial gradients in ecohydrologic properties within a pinyon-juniper ecosystem. Ecohydrology 1:349-360.

Madsen, M.D. and D.G. Chandler. 2007. Automation and use of mini disk infiltrometers. Soil Sci. Soc. Am. J. 71:1469-1472.

Mohanty, B.P., M.D. Ankeny, R. Horton and R.S. Kanwar. 1994. Spatial-analysis of hydraulic conductivity measured using disc infiltrometers. Water Resour. Res. 30:2489-2498.

Mohanty, B.P. and Z Mousli. 2000. Saturated hydraulic conductivity and soil water retention properties across a soil-slope transition. Water Resour. Res. 36: 3311-3324.

Mualem, Y. 1986. “Hydraulic Conductivity of Unsaturated Soils: Prediction and Formulas.” Methods of Soil Analysis, Part 1: Physical and Mineralogical Methods. ASA-SSSA, Madison, WI. 799-823

Nippert, J.B. and A.K. Knapp. 2007. Linking water uptake with rooting patterns in grassland species RID A-2931-2008. Oecologia 153:261-272.

Nippert, J.B., T.W. Ocheltree, A.M. Skibbe, L.C. Kangas, J.M. Ham, K.B.S. Arnold and N.A. Brunsell. 2011. Linking plant growth responses across topographic gradients in tallgrass prairie. Oecologia 166:1131-1142.

Perroux, K. and I. White. 1988. Designs for disk permeameters. Soil Sci. Soc. Am. J. 52:1205-1215.

Reynolds, W.D. and D.E. Elrick. 1991. Determination of hydraulic conductivity using a tension infiltrometer. Soil Sci. Soc. Am. J. 55:633-639.

Rose, C.W., W.R. Stern and J.E. Drummond. 1965. Determination of hydraulic conductivity as a function of depth and water content for soil in situ. Aust. J. Soil. Res. 3: 1-9.

Russo, D. 1988. Determining soil hydraulic-properties by parameter estimation: on the selection of a model for the hydraulic-properties. Water Resour. Res. 24:453-459.

Schaap, M.G. and F.J. Leij. 1998. Database-related accuracy and uncertainty of pedotransfer functions. Soil Sci. 163:765-779.

Seyfried, M.S. and B.P. Wilcox. 1995. Scale and the nature of spatial variability: Field examples having implications for hydrologic modeling. Water Resour. Res. 31: 173-184.

Sobieraj, J. A., H. Elsenbeer, R.M. Coelho, and B. Newton. 2002. Spatial variability of soil hydraulic conductivity along a tropical rainforest catena. Geoderma, 108: 79-90.

Thompson S.E., C.J. Harman, P. Heine, and G.G Katul. 2010. Vegetation-infiltration relationships across climatic and soil type gradients. J. Geophys. Res., 115: G02023.

USDA- Natural Resources Conservation Service. August 27, 2007 (spatial data), November 22, 2001 (tabular data). *Web Soil Survey*. Retrieved May 25, 2011. http://websoilsurvey.nrcs.usda.gov

USDA-Soil Conservation Service. 1975. Soil Survey of Riley County and Part of Geary County, Kansas.

Vandervaere, J.P., M. Vauclin and D.E. Elrick. 2000. Transient flow from tension infiltrometers: I. the two-parameter equation. Soil Sci. Soc. Am. J. 64:1263-1272.

Van Genuchten, M.T. 1980. A closed-form equation for predicting the hydraulic conductivity of unsaturated soils. Soil Sci. Soc. Am. J. 44:892-898.

Warrick, A. and P. Broadbridge. 1992. Sorptivity and macroscopic capillary length relationships. Water Resour. Res. 28:427-431.

Wooding, R.A. 1968. Steady infiltration from a shallow circular pond. Water Resour. Res. 4:1259-1273.

Zeleke, T.B. and B.G. Si. 2005. Scaling relationships between saturated hydraulic conductivity and soil physical properties. Soil Sci. Soc. Am. J. 69: 1691-1702.

Zeller, D.E. (editor) 1968. The stratigraphic succession in Kansas. Kansas Geological Survey, Bulletin 189, 81 p.

Zhang, R.D. 1997. Infiltration models for the disk infiltrometer. Soil Sci. Soc. Am. J. 61:1597-1603.

Appendix A - Additional Soil Description Details

Site 1 Soil Description

A – 0 to 33 cm; Very dark gray (10 YR 3/1) silt loam moist; strong medium granular structure; friable moist; slightly sticky; slightly plastic; many fine roots throughout; many fine dendritic tubular pores; clear boundary.

Bt1 -- 33 to 51 cm; Dark brown (10 YR 3/3) silty clay loam moist; moderate fine sub angular blocky structure; firm moist; moderately sticky; moderately plastic; many fine roots throughout; many fine dendritic tubular pores; clear boundary.

Bt2 -- 51 to 66 cm; Brown (7.5 YR 4/3) silty clay loam moist; moderate fine sub angular blocky structure; firm moist; moderately sticky; moderately plastic; many fine roots throughout; many fine dendritic tubular pores; clear boundary.

2Bt3 -- 66 to 81 cm; Dark reddish brown (5 YR 3/4) silty clay moist; moderate fine prismatic structure; firm moist; very sticky; very plastic; common fine roots throughout; common fine dendritic tubular pores; clear boundary.

2Bt4 – 81 to 86+ cm; Reddish brown (5 YR 4/4) silty clay moist; moderate fine prismatic structure; very firm moist; very sticky; very plastic; few fine roots throughout; few fine dendritic tubular pores.

Site 2 Soil Description

A1 – 0 to 15 cm; Black (10 YR 2/1) silt loam moist; strong fine granular structure; friable moist; slightly sticky; slightly plastic; many fine roots throughout; many fine dendritic tubular pores; clear boundary.

A2 – 15 to 30 cm; Very dark grayish brown (10 YR 3/2) silty clay loam moist; moderate fine subangular blocky structure parting to moderate medium granular; friable moist; slightly sticky; slightly plastic; many fine roots throughout; many fine dendritic tubular pores; clear boundary.

Bt1 -- 30 to 43 cm; Brown (10 YR 4/3) silty clay loam moist; moderate fine subangular blocky structure; friable moist; moderately sticky; moderately plastic; many fine roots throughout; many fine dendritic tubular pores; clear boundary.

Bt2 -- 43 to 53 cm; Brown (7.5 YR 4/3) silty clay loam moist; moderate fine prismatic structure; firm moist; moderately sticky; moderately plastic; common fine roots throughout; common fine dendritic tubular pores; clear boundary.

2Bt3 -- 53 to 66 cm; Dark reddish brown (5 YR 3/3) silty clay moist; moderate fine prismatic structure; firm moist; very sticky; very plastic; few fine roots throughout; few fine dendritic tubular pores.

Site 6 Soil Description

A1 – 0 to 20 cm; Black (10 YR 2/1) silt loam moist; 15 mm chert fragments; strong medium granular structure; very friable moist; slightly sticky; slightly plastic; many fine roots throughout; many fine dendritic tubular pores; abrupt boundary.

BA – 20 to 32 cm; Black (10 YR 2/1) silt loam moist; 10 mm reddish sandstone fragments; moderate fine subangular blocky structure; friable moist; moderately sticky; moderately plastic; many fine roots throughout; many fine dendritic tubular pores; clear boundary.

Bt – 32 to 47 cm; Very dark grayish brown (10 YR 3/2) silty clay loam moist; 2 to 5 mm chert fragments; moderate fine prismatic structure; friable moist; very sticky; very plastic; common fine roots throughout; many fine dendritic tubular pores; abrupt boundary.

2Bt1 -- 47 to 60 cm; Dark brown (7.5 YR 3/3) silty clay loam moist; moderate medium prismatic structure; friable moist; moderately sticky; moderately plastic; common fine roots throughout; many fine dendritic tubular pores; gradual boundary.

2Bt2 -- 60 to 90 cm; Dark brown (7.5 YR 3/4) silty clay moist; moderate medium subangular blocky structure; firm moist; very sticky; very plastic; few fine roots throughout; common fine dendritic tubular pores; gradual boundary.

3Bt3 -- 90 to 110 cm; Dark reddish brown (5 YR 3/3) silty clay moist; 5 mm chert fragments; moderate medium prismatic structure; firm moist; very sticky; very plastic; few fine roots throughout; common fine dendritic tubular pores;.

Site 9 Soil Description

A1 – 0 to 25 cm; Black (10 YR 2/1) silt loam; strong medium granular structure; very friable moist; slightly sticky; slightly plastic; many fine roots throughout; many fine dendritic tubular pores; clear smooth boundary.

Bt1 – 25 to 36 cm; Very dark grayish brown (10 YR 3/2) silty clay loam; moderate very fine subangular blocky structure; friable moist; moderately sticky; moderately plastic; common fine roots throughout; many fine dendritic tubular pores; clear smooth boundary.

Bt2 – 36 to 50 cm; Dark brown (10 YR 3/3) silty clay loam; 2% 5 mm chert fragments; moderate fine prismatic structure; friable moist; moderately sticky; moderately plastic; common fine roots throughout; many fine dendritic tubular pores; clear smooth boundary.

Bt3 – 50 to 90+ cm; Yellowish brown (10 YR 5/4) silty clay; moderate medium prismatic structure; friable moist; very sticky; very plastic; few fine roots throughout; common fine dendritic tubular pores;.

Appendix B - Sample Calculations for the Mini-Disk

Zhang (1997) Methodology

Using Site 2, Mote 10, channel 1 as an example, hydraulic conductivity and sorptivity are calculated using the method from Zhang (1997) for the cumulative infiltration.

The polynomial regression of the cumulative infiltration versus the square root of time produces and equation of the form $y = C_1 x^2 + C_2 x$, where the C_1 term relates to hydraulic conductivity and the C_2 term relates to sorptivity through dimensionless coefficients with the following

$$K(h_0) = C_1 / A_1 \qquad \textbf{[B-1]}$$

$$S(h_0) = C_2 / A_2 \qquad \textbf{[B-2]}$$

with coefficients, A1 and A2 defined by Zhang (1997) based on soil-water retention function, soil texture, and infiltrometer properties. The sorptivity coefficient, A_2 is given by

$$A_2 = \frac{1.4 b^{0.5} (\theta_0 - \theta_i)^{0.25} \exp[3(n-1.9)\alpha h_0]}{(\alpha r_0)^{0.15}} \qquad \textbf{[B-3]}$$

where α and n are the retention parameters of the van Genuchten (1980) soil-water retention curve. From Carsel and Parish (1988), the α value for a silt loam is 0.02 cm^{-1} with n equal to 1.41. The properties of the mini-disk infiltrometer have h_0 equal to -3 cm, and r_0 equal to 1.58 cm. The b value is assumed to be 0.55 (Warrick and Broadbridge, 1992). The initial water content and the water content at h_0 were measured with the Theta Probe and determined to be 0.37 and 0.46, respectively. Solving for the sorptivity coefficient:

$$A_2 = \frac{1.4(0.55)^{0.5} (0.46-0.37)^{0.25} \exp[3((1.41)-1.9)(0.02)(-3)]}{[(0.02)(1.58)]^{0.15}} = 0.76$$

From the graphical analysis, C_2 is -0.048, and then sorptivity is computed thusly,

$$S(h_0) = C_2 / A_2 \qquad \textbf{[B-4]}$$

$$S(h_0) = -0.048 / 0.76 = -0.063 \frac{cm}{\sqrt{s}}$$

With n less than 1.9 for a silt loam, the equation to determine the dimensionless coefficient for hydraulic conductivity is

$$A_1 = \frac{11.65(n^{0.1} - 1)e[7.5(n - 1.9)\alpha h_0]}{(\alpha r_0)^{0.91}} \quad \textbf{[B-5]}$$

Using the same parameters for the sorptivity calculations,

$$A_1 = \frac{11.65((1.41)^{0.1} - 1)\exp[7.5((1.41) - 1.9)(0.02)(-3)]}{[(0.02)(1.58)]^{0.91}} = 11.8$$

From the graphical analysis, C_1 is 0.008780, and then hydraulic conductivity is computed thusly,

$$K(h_0) = C_1 / A_1 \quad \textbf{[B-6]}$$

$$K(h_0) = 0.0088/11.8 = 0.00075\frac{cm}{s} = 0.75\times10^{-3}\frac{cm}{s}$$

Vandervaere et al (2000) Methodology

Again, using Site 2, Mote 10, channel 1 as an example, hydraulic conductivity and sorptivity are calculated using the method from Vandervaere et al (2000) for the differential linearization equation. The differential linearization equation takes the form

$$\frac{dI}{d\sqrt{t}} = C_2 + 2C_1\sqrt{t} \quad \textbf{[B-7]}$$

Using Excel, the linearly regressed line takes the form $y = mx + b$ where m is equal to $2C_1$, b is C_2, y is $\frac{dI}{d\sqrt{t}}$, and x is the square root of time. For Site 2, Mote 10, channel 1, the infiltration equation is $y = 0.018x - 0.045$. C_1 is equal to half of 0.018 or 0.0090.

The sorptivity and hydraulic conductivity are determined from expressions proposed by Haverkamp et al (1994) using coefficients C_1 and C_2.

$$C_2 = S \quad \textbf{[B-8]}$$

Sorptivity is equal to $-0.045\frac{cm}{\sqrt{s}}$.

$$C_1 = \frac{2-b}{3}K + \frac{\gamma S^2}{r_0(\theta_0 - \theta_i)} \quad \textbf{[B-9]}$$

Solving for K yields

$$K = \frac{3}{2-b}\left[C_1 - \frac{\gamma S^2}{r_0(\theta_0 - \theta_i)}\right] \quad \textbf{[B-10]}$$

where γ is assumed equal to 0.75, but has a normal range between 0.6 and 0.8 (Haverkamp et al 1994). The values of b, θ_0 and θ_i are the same as in the Zhang (1997) analysis. The hydraulic conductivity is determined to be equal to

$$K = \frac{3}{2-0.55}\left[0.0092 - \frac{0.75(0.0681)^2}{1.58(0.46-0.37)}\right] = -.035\frac{cm}{s} = -35\times10^{-3}\frac{cm}{s}$$

Linear Methodology

Again, using Site 2, Mote 10, channel 1 as an example, hydraulic conductivity is calculated using the linear method. The simple linear method uses the simple infiltration rate and an assumption of the radius of the wetted disk for the dry and wet initial conditions. The radius of the wetted disk, r_d, for the dry initial condition is assumed to be 3.5 cm and for the wet is 4.5 cm. From a linear infiltration expression

$$I = C_1 t + C_2 \qquad \textbf{[B-11]}$$

K is found by multiplying C_1 by the ratio of the radii squared.

$$K = C_1\left(\frac{r_0}{r_d}\right)^2 \qquad \textbf{[B-12]}$$

For Site 2, Mote 10, channel 1, C_1 is 0.0078, and the initial condition is dry.

$$K = C_1\left(\frac{r_0}{r_d}\right)^2 = 0.0078\left(\frac{1.58}{3.5}\right)^2 = 0.0016\frac{cm}{s} = 1.6\times10^{-3}\frac{cm}{s}$$

Appendix C - Data and Analysis from the Field Measurements Using the Mini-Disk Infiltrometers

Site									
1	**2**	**3**	**4**	**5**	**6**	**7**	**8**	**9**	**10**
0.68	0.75	0.58	0.85	0.92	1.47	1.03	0.71	0.60	0.38
0.59	0.62	0.72	0.59	1.03	1.29	0.51	1.00	0.36	0.33
0.64	0.87	0.77	0.69	0.77	1.57	0.85	0.70	0.47	0.82
0.64	0.63	0.70	0.61	0.86	1.40	0.61	1.26	0.36	0.27
0.66	0.67	0.61	0.54	0.77	0.76	0.84	0.55	0.49	0.37
0.83	0.66	0.72	0.49	0.83	1.31	0.90	0.57	0.48	0.37
0.62	0.68	0.89	0.51	1.31	0.90	0.53	0.87	0.44	0.47
0.70	1.04	0.61	0.44	0.98	1.20	0.60	0.88	0.45	0.48
0.91	0.81	0.80	0.53	0.82	1.17	0.37	0.66	0.47	0.41
0.55	0.92	0.69	0.95	1.56	1.01	0.78	0.95	0.72	0.46
0.98	0.67	0.75	0.44	1.02	0.89	0.23	0.82	0.46	0.40
0.97	0.87	0.85	0.61	0.92	1.17	0.66	0.91	0.78	0.52

Table C.1. Hydraulic conductivity from the Zhang method with Carsel and Parish parameters, $K_{Z\text{-}CP}$ (cm s^{-1} x 10^{-3}).

Site									
1	**2**	**3**	**4**	**5**	**6**	**7**	**8**	**9**	**10**
0.16	0.17	0.13	0.20	0.21	0.34	0.24	0.16	0.14	0.09
0.14	0.14	0.17	0.14	0.24	0.30	0.12	0.23	0.08	0.08
0.15	0.20	0.18	0.16	0.18	0.36	0.20	0.16	0.11	0.19
0.15	0.15	0.16	0.14	0.20	0.32	0.14	0.29	0.08	0.06
0.15	0.15	0.14	0.12	0.18	0.18	0.19	0.13	0.11	0.09
0.19	0.15	0.17	0.11	0.19	0.30	0.21	0.13	0.11	0.09
0.14	0.16	0.21	0.12	0.30	0.21	0.12	0.20	0.10	0.11
0.16	0.24	0.14	0.10	0.23	0.28	0.14	0.20	0.10	0.11
0.21	0.19	0.19	0.12	0.19	0.27	0.09	0.15	0.11	0.10
0.13	0.21	0.16	0.22	0.36	0.23	0.18	0.22	0.17	0.11
0.23	0.16	0.17	0.10	0.24	0.21	0.05	0.19	0.11	0.09
0.22	0.20	0.20	0.14	0.21	0.27	0.15	0.21	0.18	0.12

Table C.2. Hydraulic conductivity from the Zhang method with Schaap and Leij (1998) parameters, $K_{Z\text{-}SL}$ (cm s^{-1} x 10^{-3}).

Site									
1	**2**	**3**	**4**	**5**	**6**	**7**	**8**	**9**	**10**
1.80	1.59	1.55	2.08	2.18	3.65	3.17	2.33	1.27	1.11
1.54	1.40	1.85	1.60	2.52	3.01	1.74	2.96	1.19	1.00
1.81	2.04	1.98	1.80	1.86	4.03	2.15	1.87	1.23	2.20
1.77	1.65	1.79	1.68	2.31	3.50	1.62	3.37	1.14	0.97
1.64	1.56	1.60	1.44	1.82	1.86	2.14	1.58	1.41	1.20
2.10	1.67	1.82	1.12	1.88	3.34	2.66	1.61	1.27	1.25
1.51	1.53	2.08	1.40	3.28	2.04	1.60	2.46	1.38	1.26
1.72	2.45	1.52	1.14	2.44	2.99	1.55	2.40	1.28	1.28
2.22	1.81	2.02	1.37	2.30	2.95	0.96	1.67	1.15	1.18
1.49	2.10	1.59	2.26	3.59	2.32	1.95	2.48	1.53	1.20
2.33	1.71	1.89	1.14	2.44	2.14	0.77	2.49	1.38	1.12
2.29	2.00	2.00	1.58	2.13	3.02	1.84	2.44	1.67	1.34

Table C.3. Hydraulic conductivity from the linear method, K_{LIN} (cm s^{-1} x 10^{-3}).

Site									
1	**2**	**3**	**4**	**5**	**6**	**7**	**8**	**9**	**10**
-14.5	-6.1	-11.6	18.9	22.3	25.4	-211.1	-253.5	-2.9	-50.0
-3.0	-6.4	4.6	-29.2	21.6	30.4	-218.5	-276.8	-106.6	-61.4
-70.0	12.6	4.0	-9.1	17.5	6.4	11.7	-26.4	0.7	-27.4
-48.3	-2.6	7.3	-86.3	-25.1	22.4	-6.6	-136.0	-76.1	-237.9
11.5	15.8	-0.1	-15.8	18.6	16.5	2.4	-60.0	-45.1	-174.9
2.7	13.1	7.6	4.3	12.9	5.6	-144.8	-61.7	-2.3	-177.6
-3.0	-0.4	21.1	-52.8	18.1	15.4	-75.3	-63.9	-81.4	-7.7
11.8	22.9	14.7	-0.4	15.6	23.9	6.6	-33.2	-26.6	-5.7
16.3	11.6	6.1	-0.3	-78.4	18.2	3.7	10.0	10.4	-35.1
-11.6	17.1	14.1	22.9	34.0	19.9	13.8	-5.8	-17.1	-10.9
23.6	11.7	10.3	-1.6	24.2	21.0	-89.3	-196.0	-44.5	9.4
23.4	14.0	20.4	-2.9	20.1	-6.0	-33.4	-23.7	-15.8	3.9

Table C.4. Hydraulic conductivity from the Vandervaere method, K_V (cm s^{-1} x 10^{-3})

	$K_{Z\text{-}CP}$		$K_{Z\text{-}SL}$		K_{LIN}		K_V	
Site	**X**	**SD**	**X**	**SD**	**X**	**SD**	**X**	**SD**
1	0.73	0.15	0.17	0.03	1.85	0.31	-5.08	28.50
2	0.77	0.13	0.18	0.03	1.79	0.30	8.59	9.81
3	0.72	0.09	0.17	0.02	1.81	0.20	8.21	9.01
4	0.61	0.16	0.14	0.04	1.55	0.36	-12.69	30.76
5	0.98	0.24	0.23	0.05	2.39	0.54	8.44	30.78
6	1.18	0.25	0.27	0.06	2.90	0.68	16.59	10.10
7	0.66	0.23	0.15	0.05	1.85	0.66	-61.73	86.73
8	0.82	0.20	0.19	0.05	2.30	0.55	-93.92	98.12
9	0.51	0.13	0.12	0.03	1.32	0.16	-33.95	37.35
10	0.44	0.14	0.10	0.03	1.26	0.32	-64.60	83.77

Table C.5. Mean, X, and standard deviation, SD, for hydraulic conductivity values (cm s^{-1} x 10^{-3})

Site	$K_{Z\text{-}SL}$	K_{LIN}	K_V
1	-77%	154%	-797%
2	-77%	134%	1023%
3	-77%	150%	1034%
4	-77%	156%	-2196%
5	-77%	144%	759%
6	-77%	147%	1308%
7	-77%	180%	-9454%
8	-77%	180%	-11501%
9	-77%	161%	-6814%
10	-77%	187%	-14789%

Table C.6. Percent change of hydraulic conductivity as compared to $K_{Z\text{-}CP}$.

Site									
1	**2**	**3**	**4**	**5**	**6**	**7**	**8**	**9**	**10**
0.061	-0.063	0.058	0.008	-0.007	0.026	0.174	0.193	-0.053	0.086
0.046	-0.059	0.039	0.068	0.013	-0.019	0.179	0.201	0.127	0.094
0.105	-0.040	0.041	0.050	0.007	0.049	0.030	0.076	0.037	0.073
0.090	0.047	0.033	0.073	0.071	0.029	0.052	0.145	0.109	0.177
0.021	-0.011	0.043	0.055	-0.003	0.012	0.045	0.101	0.088	0.153
0.044	0.017	0.035	-0.032	-0.036	0.050	0.148	0.102	0.043	0.154
0.010	-0.052	-0.012	0.082	0.030	-0.038	0.112	0.108	0.115	0.051
0.015	-0.024	0.002	0.033	0.025	0.020	0.032	0.085	0.073	0.047
0.011	-0.038	0.038	0.035	0.104	0.031	0.027	0.027	0.010	0.078
0.059	-0.032	-0.023	-0.005	-0.033	-0.033	0.023	0.060	-0.075	0.054
-0.003	0.021	0.029	0.035	0.001	0.003	0.119	0.175	0.089	0.006
-0.006	0.026	-0.009	0.042	-0.022	0.064	0.082	0.077	-0.076	0.032

Table C.7. Sorptivity from the Zhang method with Carsel and Parish parameters, $S_{Z\text{-}CP}$ (cm $s^{-0.5}$).

Site									
1	**2**	**3**	**4**	**5**	**6**	**7**	**8**	**9**	**10**
0.054	-0.055	0.051	0.007	-0.006	0.023	0.153	0.170	-0.046	0.075
0.040	-0.051	0.034	0.060	0.012	-0.017	0.157	0.176	0.112	0.082
0.092	-0.035	0.036	0.044	0.006	0.043	0.027	0.066	0.033	0.064
0.079	0.042	0.029	0.064	0.062	0.025	0.046	0.127	0.096	0.156
0.019	-0.009	0.038	0.048	-0.003	0.010	0.040	0.088	0.077	0.134
0.038	0.015	0.031	-0.029	-0.032	0.044	0.130	0.089	0.038	0.135
0.009	-0.045	-0.011	0.072	0.026	-0.033	0.099	0.095	0.101	0.045
0.013	-0.021	0.002	0.029	0.022	0.017	0.028	0.075	0.064	0.041
0.009	-0.034	0.033	0.031	0.091	0.027	0.024	0.024	0.009	0.069
0.052	-0.028	-0.020	-0.004	-0.029	-0.029	0.020	0.053	-0.066	0.047
-0.003	0.019	0.025	0.031	0.001	0.002	0.105	0.153	0.078	0.005
-0.005	0.023	-0.008	0.037	-0.019	0.056	0.072	0.068	-0.067	0.029

Table C.8. Sorptivity from the Zhang method with Schaap and Leij (1998) parameters, $S_{Z\text{-}SL}$ (cm $s^{-0.5}$).

Site									
1	**2**	**3**	**4**	**5**	**6**	**7**	**8**	**9**	**10**
0.049	-0.045	0.047	0.010	-0.001	0.029	0.142	0.154	-0.038	0.064
0.037	-0.043	0.033	0.050	0.015	-0.008	0.140	0.162	0.099	0.070
0.082	-0.027	0.035	0.039	0.008	0.050	0.027	0.062	0.030	0.058
0.071	0.039	0.029	0.076	0.056	0.030	0.043	0.121	0.085	0.131
0.019	-0.006	0.036	0.041	0.001	0.012	0.039	0.080	0.070	0.113
0.037	0.016	0.029	-0.021	-0.023	0.046	0.119	0.081	0.035	0.114
0.042	-0.036	-0.005	0.058	0.029	-0.025	0.090	0.090	0.092	0.040
0.022	-0.013	0.004	0.024	0.022	0.022	0.027	0.072	0.059	0.038
0.022	-0.025	0.033	0.026	0.078	0.031	0.022	0.024	0.010	0.062
0.050	-0.020	-0.015	0.001	-0.015	-0.021	0.022	0.052	-0.057	0.043
0.002	0.019	0.025	0.025	0.005	0.007	0.094	0.143	0.072	0.006
0.000	0.023	-0.003	0.030	-0.012	0.057	0.068	0.066	-0.057	0.027

Table C.9. Sorptivity from the Vandervaere method, S_V (cm $s^{-0.5}$).

	$S_{Z\text{-}CP}$		$S_{Z\text{-}SL}$		S_V	
Site	**X**	**SD**	**X**	**SD**	**X**	**SD**
1	0.038	0.036	0.033	0.031	0.036	0.025
2	-0.017	0.037	-0.015	0.032	-0.010	0.028
3	0.023	0.026	0.020	0.023	0.021	0.020
4	0.037	0.033	0.033	0.029	0.030	0.026
5	0.012	0.041	0.011	0.036	0.014	0.029
6	0.016	0.033	0.014	0.029	0.019	0.027
7	0.085	0.059	0.075	0.052	0.069	0.046
8	0.112	0.055	0.099	0.048	0.092	0.043
9	0.041	0.074	0.036	0.065	0.033	0.057
10	0.084	0.053	0.074	0.046	0.064	0.038

Table C.10. Mean, X, and standard deviation, SD, for sorptivity values

Site	$S_{Z\text{-}SL}$	S_V
1	-12%	-4%
2	-12%	-43%
3	-12%	-9%
4	-12%	-19%
5	-12%	11%
6	-12%	20%
7	-12%	-19%
8	-12%	-18%
9	-12%	-18%
10	-12%	-24%

Table C.11. Percent change of sorptivity values as compared to $S_{Z\text{-}CP}$

Appendix D - Alternate Analyses for the Mini-Disk

The negative sorptivity values are a result of the second term of the cumulative infiltration equation being negative. The regression of the data to the infiltration model occasionally results in negative sorptivity values which are physically impossible. I have examined two options to try to resolve this issue.

Two options to resolve the issue are presented. The first option to consider is a variation of the segmentation of the cumulative infiltration equation from Madsen and Chandler (2007). Instead of segmenting the data set into the early time sorptivity dominated infiltration and the later time steady-state infiltration, only the early time was examined. The second option is to add data to the regression analysis representing an assumed infiltration value out in the future. By adjusting the future assumed value, the negative component of the cumulative infiltration equation could be eliminated.

First, the length of the sorptivity of the cumulative infiltration was determined by examining Site 2, Mote 10, Channel 1. This is the same infiltration run shown in Chapter 2 and in the calculation in Appendix B. The cumulative infiltration equation for this site for the entire time series is

$$I = C_1 t - C_2\sqrt{t} = 0.008780t - 0.04767\sqrt{t}$$

Note that the second term for Site 2, Mote 10, Channel 1 is negative.

The cumulative infiltration equation was examined at increasing intervals of about 120 second. For example, the first segment of the cumulative infiltration equation is from 0 to 121 second, and the second segment of the cumulative infiltration equation is from 0 to 242 seconds, and so on. The resulting coefficients, sorptivity, and hydraulic conductivity are shown in Table D.1.

From results of the interval analysis, the second term, C_2, is positive for the intervals up to an end time of 725 seconds, after that the second term is negative. For this particular infiltration run, the sorptivity dominated time is less than 725 seconds. The second term, C_2, seems to fluctuate greatly, while the first term, C_1, seems to remain near 0.006 cm s^{-1} for the early sorptivity time and increases as C_2 becomes negative.

Time		Cumulative Infiltration			Zhang (1997)		Haverkamp (1994)	
start	end	C_1	C_2	R^2	S	K	S	K
(s)	(s)	(cm s^{-1})	(cm $s^{-.05}$)	-	(cm $s^{-.05}$)	(cm $s^{-1}x10^{-3}$)	(cm $s^{-.05}$)	(cm $s^{-1}x10^{-3}$)
0	121	0.0064	0.0019	0.708	0.0025	0.55	0.0019	13.28
0	242	0.0060	0.0087	0.841	0.0114	0.51	0.0087	11.55
0	363	0.0068	0.0002	0.921	0.0003	0.57	0.0002	13.99
0	484	0.0057	0.0141	0.950	0.0185	0.49	0.0141	9.53
0	604	0.0060	0.0095	0.971	0.0125	0.51	0.0095	11.40
0	725	0.0065	0.0016	0.982	0.0021	0.55	0.0016	13.38
0	846	0.0071	-0.0091	0.986	-0.0120	0.60	-0.0091	13.64
0	967	0.0075	-0.0188	0.989	-0.0247	0.64	-0.0188	11.47
0	1088	0.0079	-0.0271	0.991	-0.0357	0.67	-0.0271	7.79
0	1209	0.0082	-0.0321	0.993	-0.0422	0.69	-0.0321	4.80
0	1330	0.0085	-0.0397	0.994	-0.0522	0.72	-0.0397	-0.95
0	1451	0.0087	-0.0457	0.995	-0.0602	0.74	-0.0457	-6.50

Table D.1. Interval analysis for sorptivity dominated infiltration for Site 2, Mote 10, Channel 1.

The two methods employed to determine the sorptivity and the hydraulic conductivity are the Zhang (1997) method and the Haverkamp et al (1994) method. The Zhang (1997) method is described in Chapter 3 and shown in Appendix B. The Haverkamp et al (1994) method uses the same cumulative infiltration equation as Zhang (1997), but the equation to determine sorptivity and hydraulic conductivity are the same as Vandervaere et al(2000).

Since the Zhang (1997) method of analysis uses the coefficient divided by a constant value, the sorptivity and hydraulic conductivity are similar to the coefficients C_1 and C_2. The sorptivity values vary greatly and become negative as the end time interval increases. The hydraulic conductivity values generally increase.

The Haverkamp et al (1994) method of analysis, which is very similar to Vandervaere et al (2000), has the same fluctuations of sorptivity as the Zhang (1997) method. The hydraulic conductivity values are positive and realistic for much of the analysis. This is an improvement on previous results from the Vandervaere et al (2000) analysis as it is assumed that the Vandervaere et al(2000) analysis would exhibit similar results.

Modifying the interval of analysis, the values for sorptivity using the Zhang (1997) and Haverkamp et al (1994) methods are improved as are the values for hydraulic conductivity using the Haverkamp et al (1994) method. It is unclear if the modified interval of analysis improves the Zhang (1997) calculation of hydraulic conductivity as the value seems to increase as the interval increases.

Not every infiltration run is the same as Site 2, Mote 10, Channel 1. The coefficients, C_1 and C_2, vary as does the length of infiltration. Instead of performing an individual analysis for each infiltration run in order to determine the most ideal time interval, a single interval is used for all infiltration runs. That time interval is approximately 5 minutes or 300 seconds. From Table D.1, 300 seconds is within the range of positive C_1 values, and it is assumed that 0 to 300 seconds will encompass the sorptivity dominated infiltration.

Applying the Zhang (1997) and Haverkamp et al (1994) methods of analysis on the first 300 seconds of all infiltration runs results in the following figures:

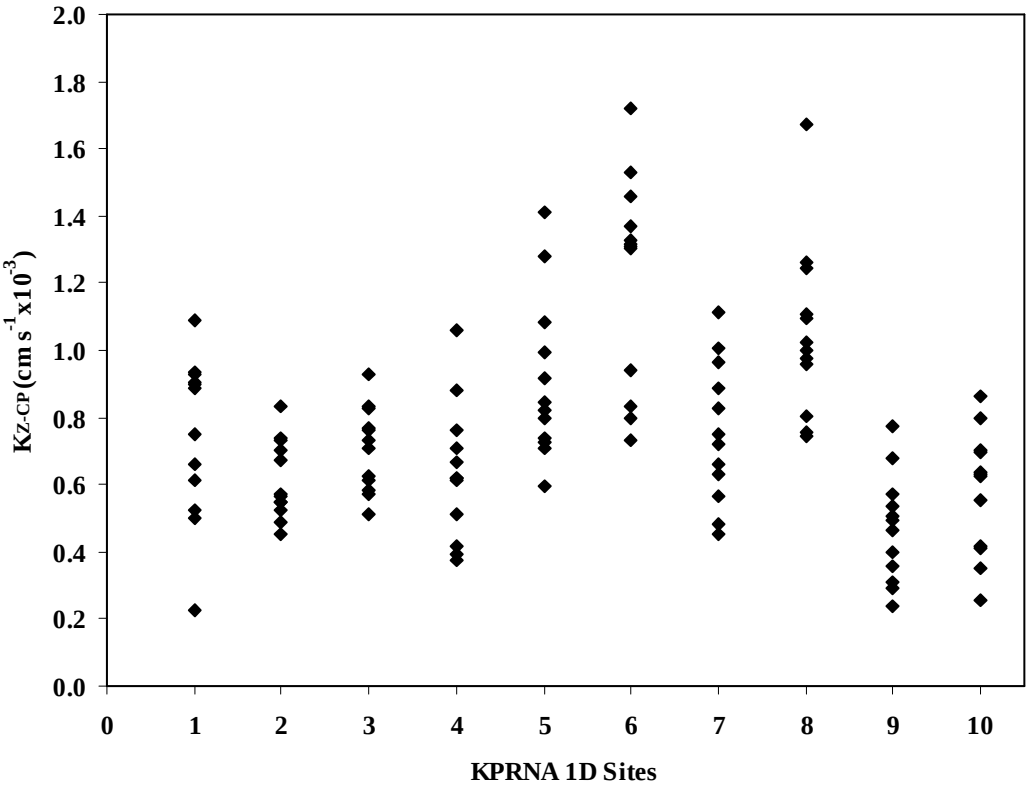

Figure D.1. Hydraulic conductivity using the method from Zhang (1997) for the first 5 minutes of infiltration.

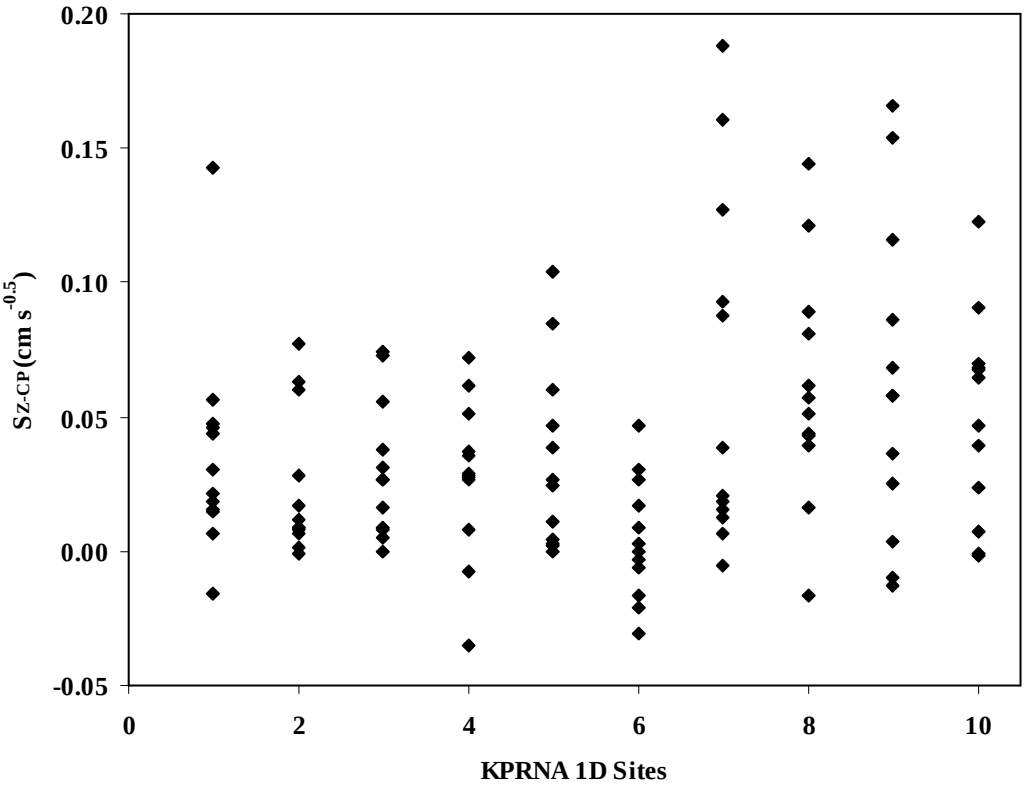

Figure D.2. Sorptivity using the method from Zhang (1997) for the first 5 minutes of infiltration.

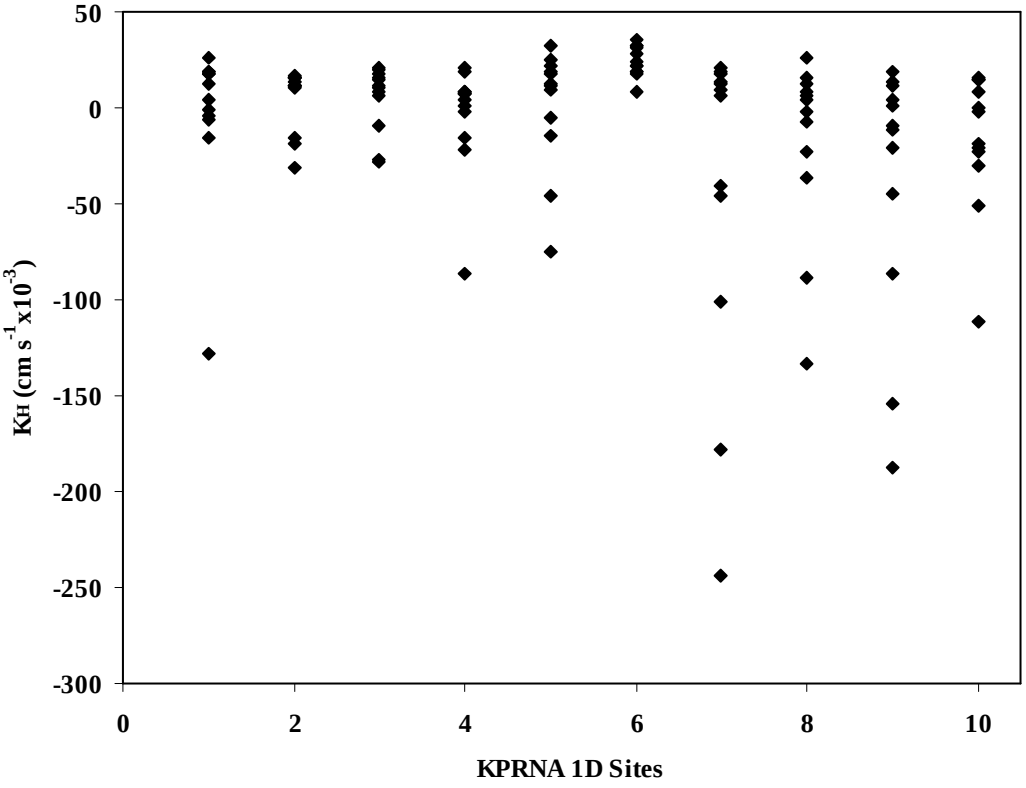

Figure D.3. Hydraulic conductivity using the method from Haverkamp et al (1994) for the first 5 minutes of infiltration.

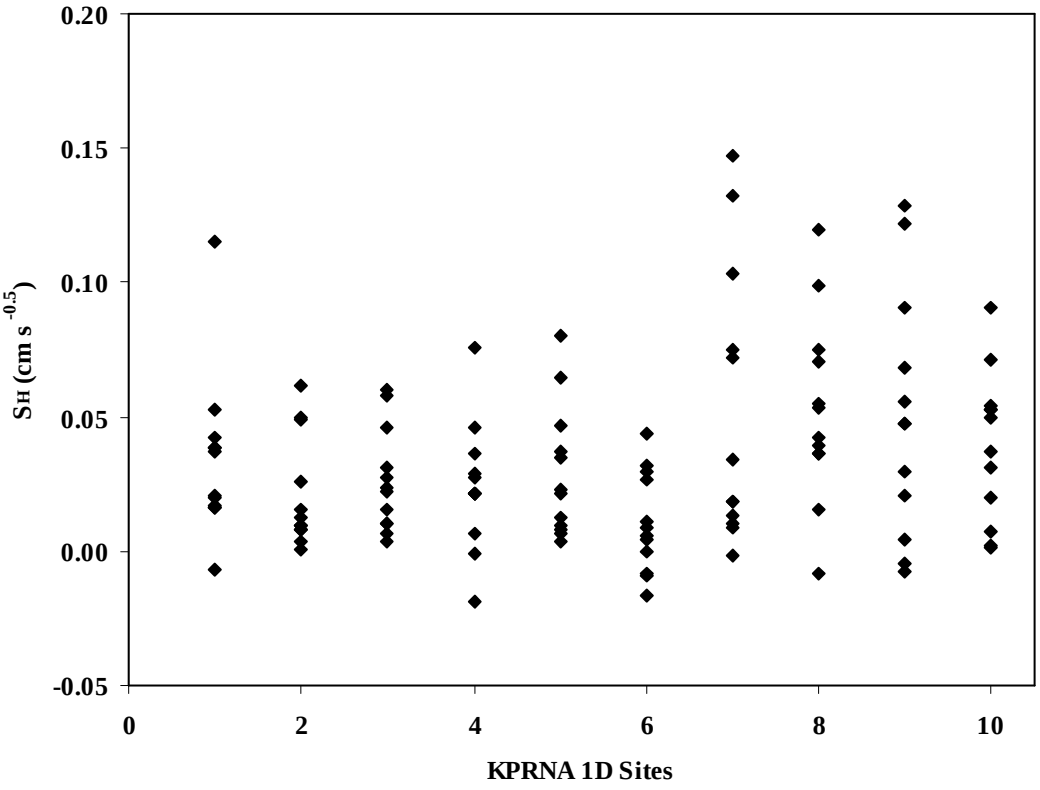

Figure D.4. Sorptivity using the method from Haverkamp et al (1994) for the first 5 minutes of infiltration.

The number of negative sorptivity values, or negative C_2 coefficients, has been reduced from 26 to 17. The hydraulic conductivity values from the Zhang (1997) analysis with the adjusted time interval are similar to the unadjusted time interval. The hydraulic conductivity values from the Haverkamp et al (1994) with the adjusted time interval are similar to the results from Vandervaere et al (2000) with the unadjusted time interval. Haverkamp et al (1994) has 45 negative hydraulic conductivity values, while Vandervaere et al (2000) has 62, thus the adjusted time intervals reduced the number of negative values for hydraulic conductivity. The extremely negative values of hydraulic conductivity are still seen with the adjusted time interval. Perhaps with further adjustments to the time interval, improvements can continue to be made.

The second option to eliminating the negative sorptivity coefficient is to add fixed points to the regression analysis. An added data point (in addition to the point setting time at zero to zero infiltration) representing an assumed infiltration value in the future would impact the

polynomial regression. By adjusting the future assumed value, the negative component of the cumulative infiltration equation could be eliminated.

A fixed point in the future would either result in no change to the negative sorptivity value or an underestimation of the infiltration values at the end of the infiltration run. If the infiltration values at the end of the infiltration run are not being satisfied with this second option, then that is similar to ignoring the end time values. Ignoring the end time values is what occurred under the first option.

A third option in trying to resolve the negative sorptivity issue is to reexamine the model. The infiltration model is a two term polynomial with coefficients for the square root of time and time. It is possible, for example, that the data would fit a three term polynomial infiltration model with the third term being time to the 3/2 power ($t^{3/2}$). With redefining the model, the values of the coefficients would need to be confirmed, redefined or defined in the case of the new third term.

Appendix E - Sample Calculations for the Large Disk

Three-Dimensional Methods

The equations used in the three-dimensional infiltration analysis proposed by Reynolds and Elrick (1991) are as follows:

$$\overline{K}_{x,y} = \frac{G_d \overline{\alpha}_{x,y} Q_x}{r\left(1 + G_d \overline{\alpha}_{x,y} \pi r\right)\left(Q_x / Q_y\right)^P} \qquad \textbf{[E-1]}$$

where x = 1,2,3,… and y = x+1, G_d is assumed to be equal to 0.25, Q_x and Q_y are the flow rates at two consecutive tensions, r is the radius of the disk and equal to 4 cm, and

$$P = \frac{h_x}{h_x - h_y} \qquad \textbf{[E-2]}$$

where h_x and h_y are two consecutive tensions, and

$$\overline{\alpha}_{x,y} = \frac{\ln\left(Q_x / Q_y\right)}{h_x - h_y} \qquad \textbf{[E-3]}$$

Using Site 2 at depth 1 cm as an example, the flow rate at -3 cm tension, Q(h=-3 cm), is 0.0126 $cm^3\ s^{-1}$ and at -2 cm tension, Q(h=-2 cm), is 0.0276 $cm^3\ s^{-1}$. With the above equations,

$$\overline{\alpha}_{x,y} = \frac{\ln\left(Q_x / Q_y\right)}{h_x - h_y} = \frac{\ln\left(0.0126/0.0276\right)}{-3-(-2)} = \frac{\ln(0.457)}{-1} = 0.783 cm^{-1}$$

$$P = \frac{h_x}{h_x - h_y} = \frac{-3}{-3-(-2)} = \frac{-3}{-1} = 3$$

$$\overline{K}_{x,y} = \frac{G_d \overline{\alpha}_{x,y} Q_x}{r\left(1 + G_d \overline{\alpha}_{x,y} \pi r\right)\left(Q_x / Q_y\right)^P} = \frac{(0.25)(0.783)(0.0126)}{4[1 + (0.25)(0.783)(3.14)(4)](0.0126/0.0276)^3}$$

$$\overline{K}_{x,y} = \frac{0.00247}{4[1 + 2.459](0.457)^3} = \frac{0.00247}{4[3.459](0.0954)} = \frac{0.00247}{1.321} = 0.00187 cm \cdot s^{-1}$$

The equations proposed by Zhang (1997) are as follows:

$$I = C_1 t + C_2 \sqrt{t} \qquad \textbf{[E-4]}$$

$$K(h_0) = C_1 / A_1 \qquad \textbf{[E-5]}$$

$$S(h_0) = C_2 / A_2 \qquad \textbf{[E-6]}$$

with coefficients, A_1 and A_2 defined based on soil-water retention function, soil texture, and infiltrometer properties. The sorptivity was not determined for the laboratory measurements of the large disk. The equation used for the calculation of A_1 is dependent on n, a soil parameter defined by van Genuchten (1980). For a silt loam the n value is less than 1.9, and the equation to determine the dimensionless coefficient for hydraulic conductivity is

$$A_1 = \frac{11.65(n^{0.1} - 1)e\left[7.5(n - 1.9)\alpha h_0\right]}{(\alpha r_0)^{0.91}} \qquad \textbf{[E-7]}$$

where α and n are the retention parameters of the van Genuchten (1980) soil-water retention curve. Using the laboratory results of the large core from the cumulative infiltration of site 2, depth 1 cm, tension -2 cm, the first coefficient is 0.000493. From Carsel and Parish (1988), the α value for a silt loam is 0.02 cm^{-1} with n equal to 1.41. The applied tension was set to -2 cm, and r_0 is equal to 4.5 cm. The b value is assumed to be 0.55 (Warrick and Broadbridge, 1992).

$$A_1 = \frac{11.65((1.41)^{0.1} - 1)\exp\left[7.5((1.41) - 1.9)(0.02)(-2)\right]}{\left[(0.02)(4.5)\right]^{0.91}} = 3.54$$

From the graphical analysis, C_1 is 0.000493, and then hydraulic conductivity is computed thusly,

$$K(h_0) = C_1 / A_1$$

$$K(h_0) = 0.000493/3.54 = 0.000139\frac{cm}{s} = 0.139\times10^{-3}\frac{cm}{s}$$

Appendix F - Data and Analysis for the Large Core

Exponential regression of the large disk infiltration

The information in the following figures populates Table 4.1 for site 2, Table 4.2 for site 6, and Table 4.3 for site 9.

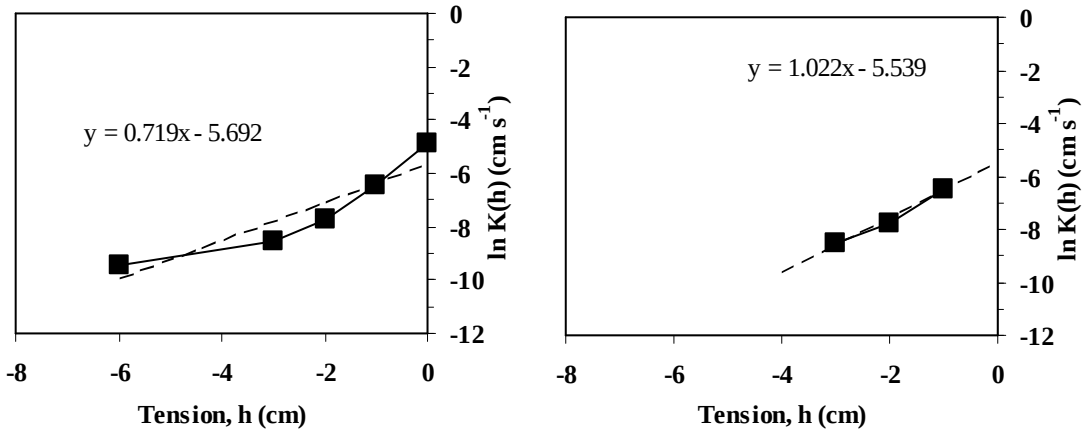

Figure F.1 Exponential Regression of the large disk infiltration at site 2, Depth 1 cm

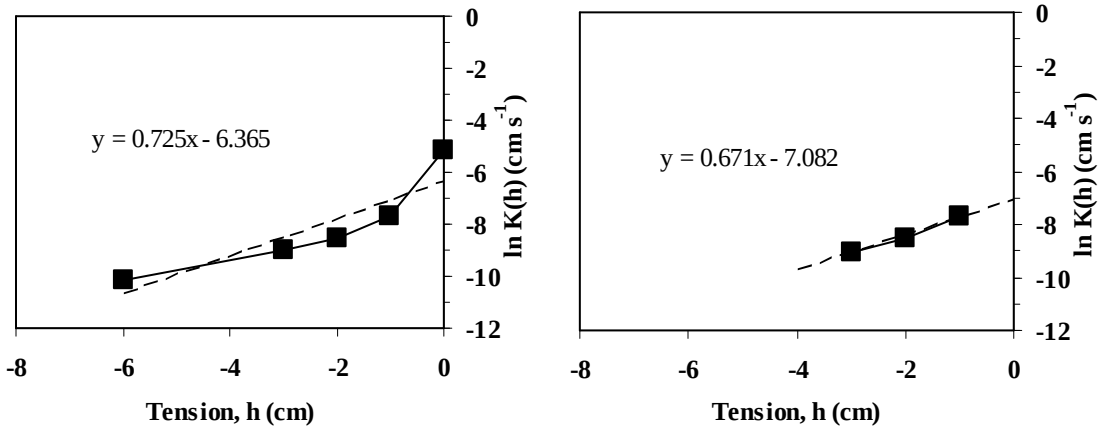

Figure F.2. Exponential Regression of the large disk infiltration at site 2, Depth 11 cm

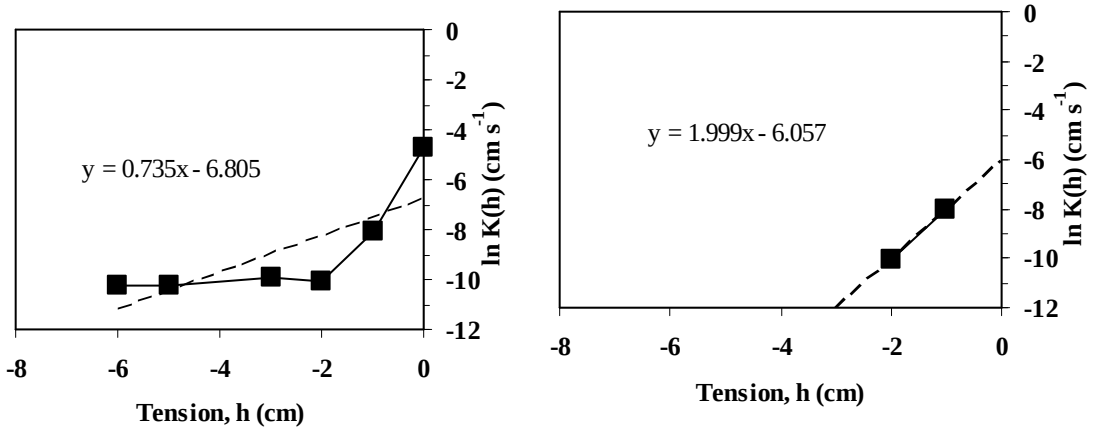

Figure F.3. Exponential Regression of the large disk infiltration at site 2, Depth 21 cm

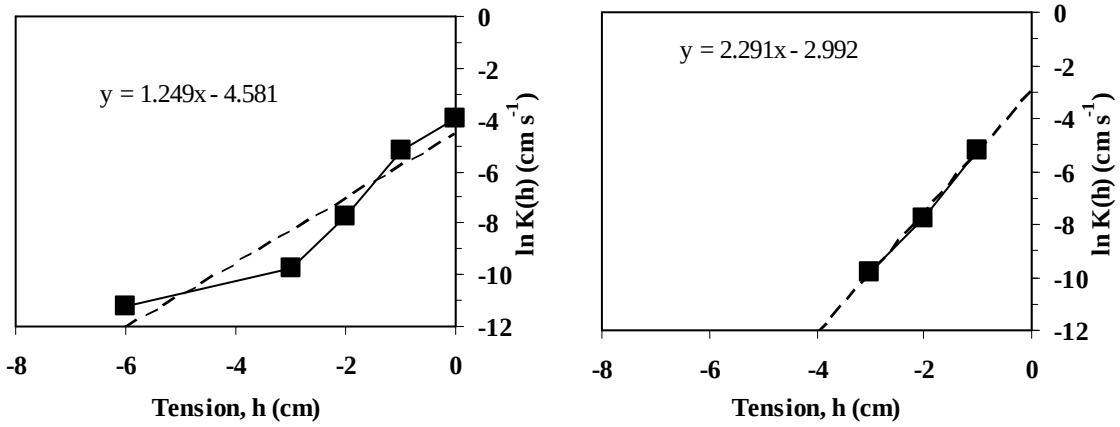

Figure F.4. Exponential Regression of the large disk infiltration at site 2, Depth 31 cm

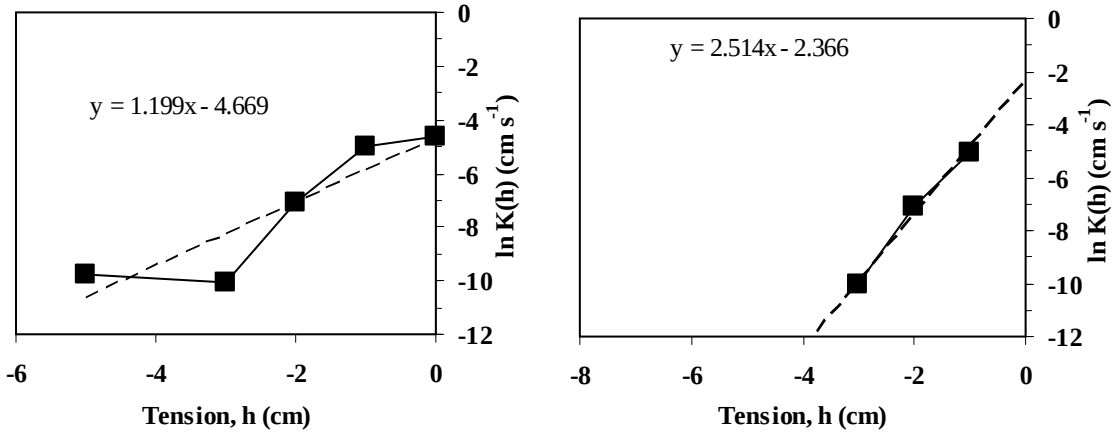

Figure F.5. Exponential Regression of the large disk infiltration at site 2, Depth 41 cm

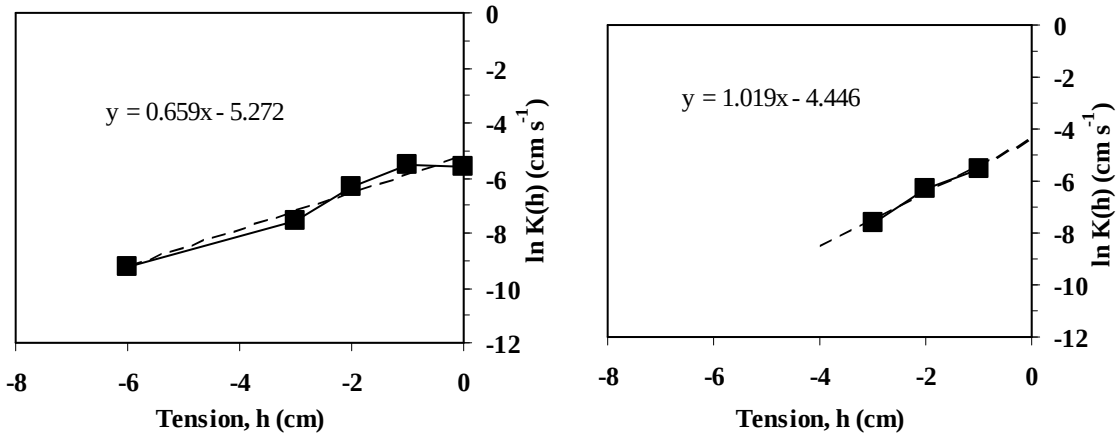

Figure F.6. Exponential Regression of the large disk infiltration at site 2, Depth 51 cm

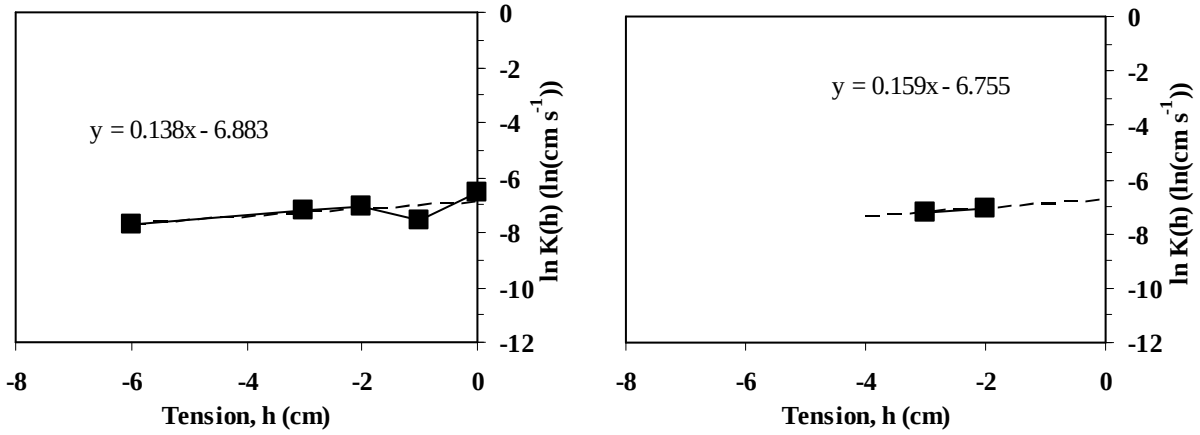

Figure F.7. Exponential Regression of the large disk infiltration at site 6, Depth 1 cm

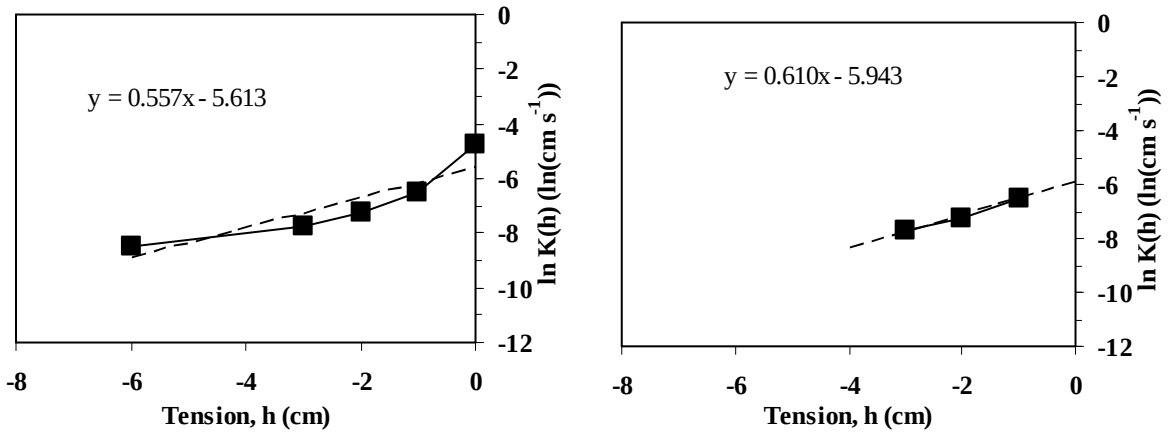

Figure F.8. Exponential Regression of the large disk infiltration at site 6, Depth 11 cm

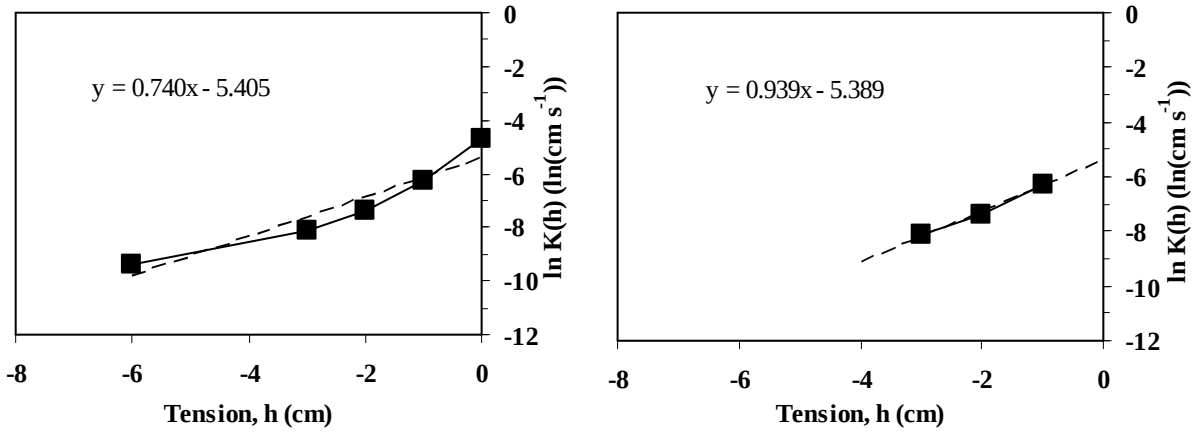

Figure F.9. Exponential Regression of the large disk infiltration at site 6, Depth 21 cm

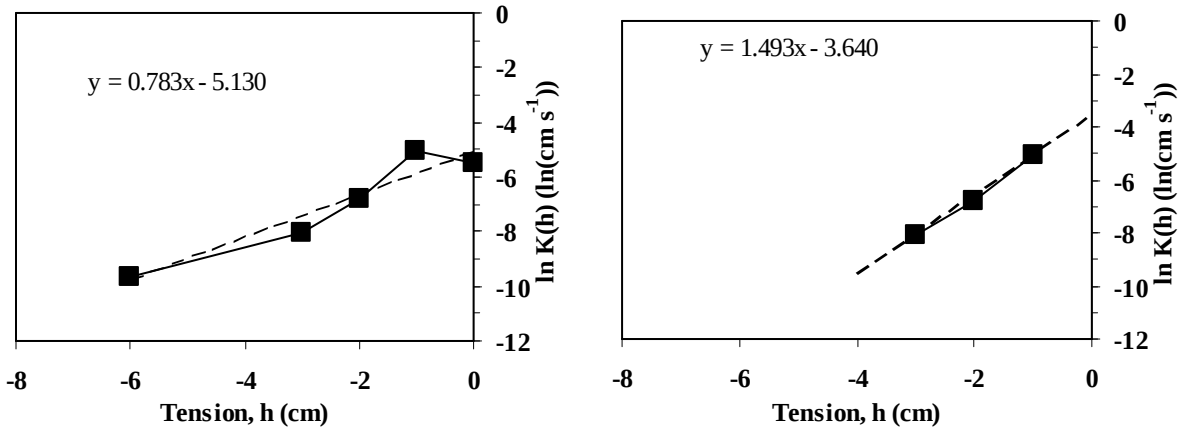

Figure F.10. Exponential Regression of the large disk infiltration at site 6, Depth 31 cm

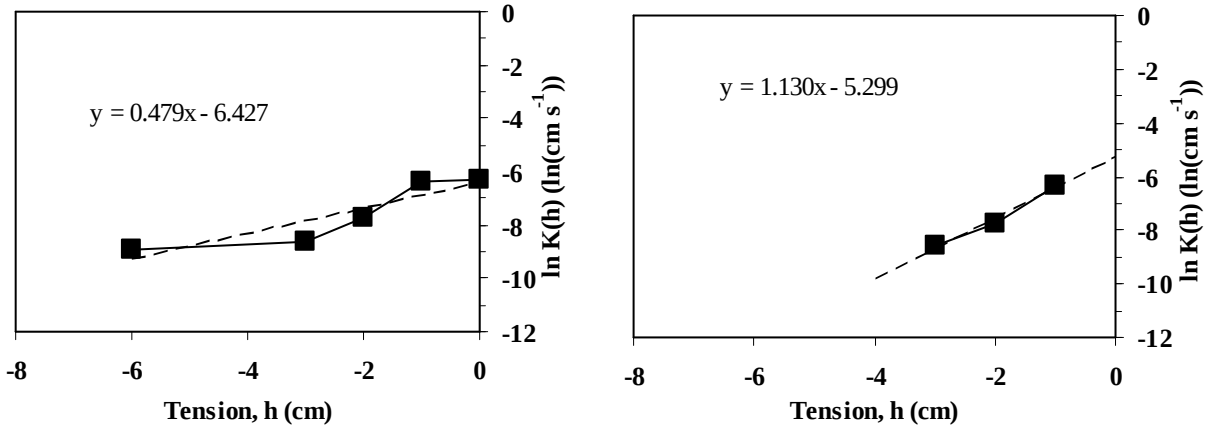

Figure F.11. Exponential Regression of the large disk infiltration at site 6, Depth 41 cm

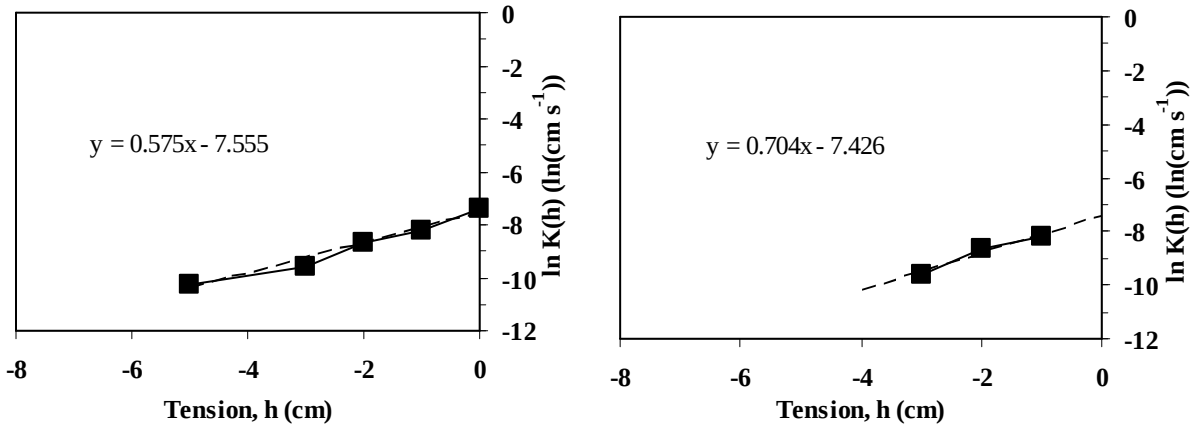

Figure F.12. Exponential Regression of the large disk infiltration at site 6, Depth 53 cm

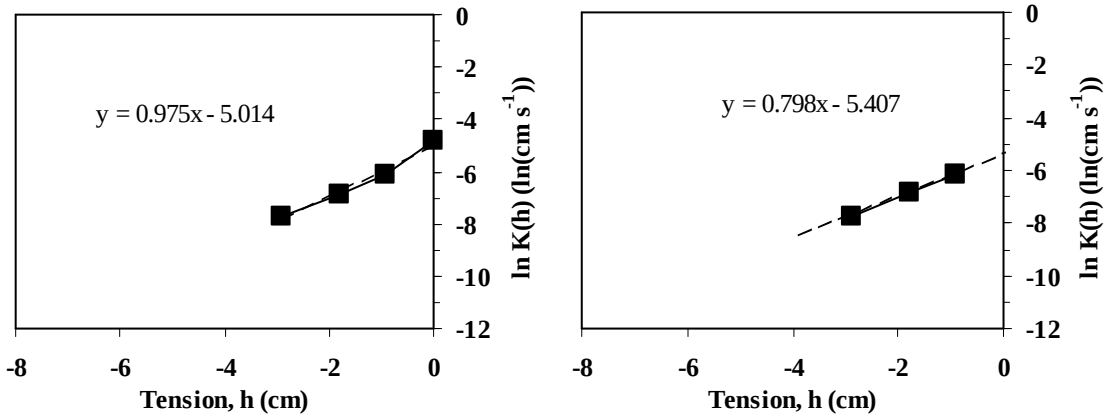

Figure F.13. Exponential Regression of the large disk infiltration at site 9, Depth 0 cm

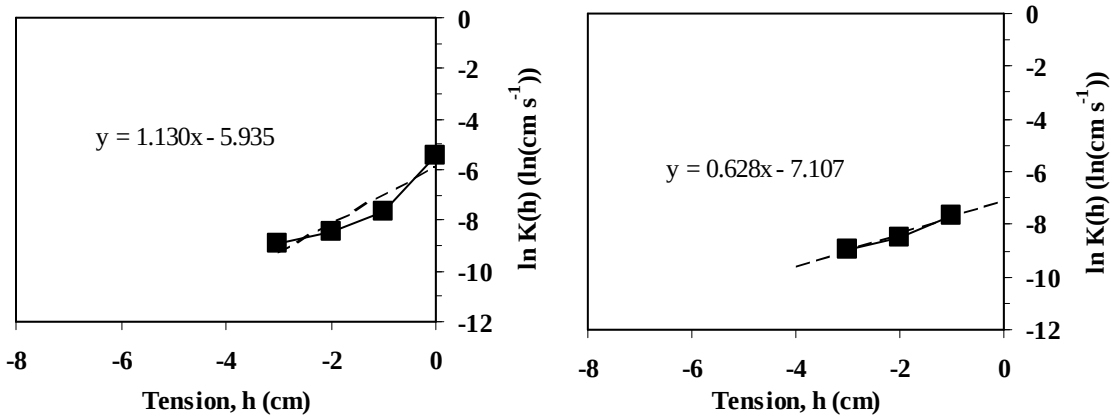

Figure F.14. Exponential Regression of the large disk infiltration at site 9, Depth 11 cm

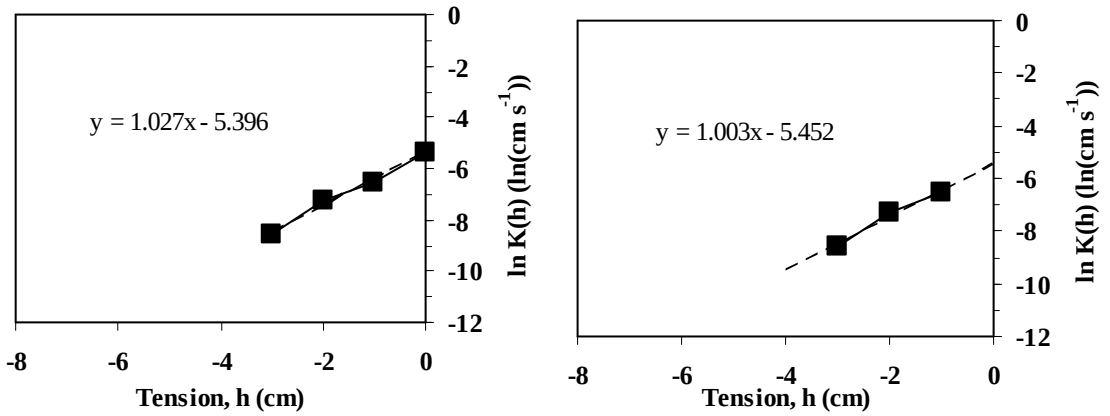

Figure F.15. Exponential Regression of the large disk infiltration at site 9, Depth 21 cm

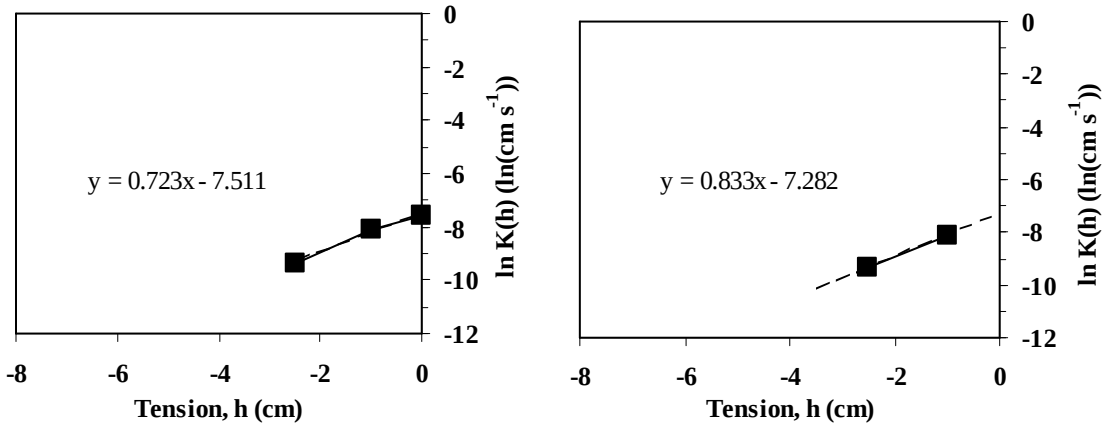

Figure F.16. Exponential Regression of the large disk infiltration at site 9, Depth 31 cm

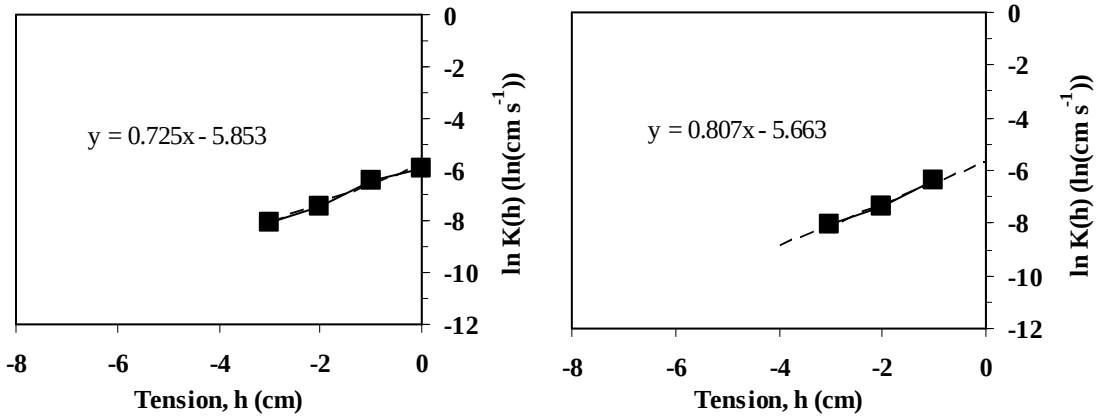

Figure F.17. Exponential Regression of the large disk infiltration at site 6, Depth 41 cm

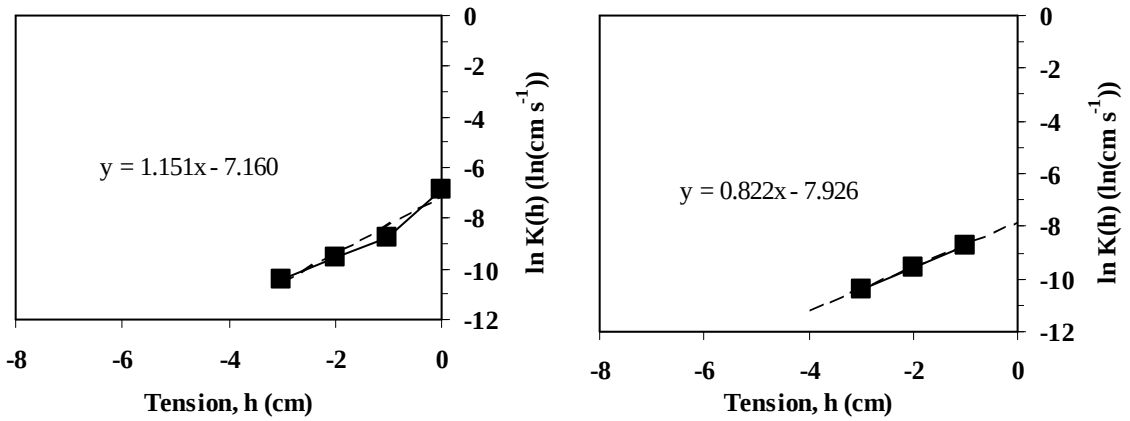

Figure F.18. Exponential Regression of the large disk infiltration at site 6, Depth 51 cm

Laboratory mini-disk analysis

Site	Depth (cm)	$K_{Z\text{-}CP}$	$K_{Z\text{-}SL}$	K_{lin}	K_V
			($cm\ s^{-1} \times 10^{-3}$)		
2	1	0.217	0.050	0.578	-5.0
	11	0.154	0.036	0.383	3.7
	21	0.028	0.006	0.112	0.9
	31	0.145	0.034	0.395	4.0
	41	0.271	0.063	0.595	-350.7
	51	0.113	0.026	0.315	-0.9
6	0	0.141	0.033	0.597	-90.4
	11	0.119	0.028	0.383	-38.4
	21	0.367	0.085	0.897	-4.3
	31	0.235	0.055	0.608	4.9
	41	0.251	0.058	0.676	6.4
	51	0.014	0.003	0.207	-33.9
9	11	0.065	0.015	0.176	-4.8
	21	0.002	0.000	0.050	-36.9
	31	0.006	0.001	0.078	-2.6
	41	0.026	0.006	0.127	-20.1
	51	0.054	0.012	0.144	1.4

Table F.1. Summary of K(h=-3cm) from the laboratory measurements of the mini-disk infiltrometers using the Zhang (1997) approach with Carsel and Parrish (1988) parameters, $K_{Z\text{-}CP}$, with Schaap and Leij (1998) parameters, $K_{Z\text{-}SL}$, the simple linear analysis, K_{lin}, and the Vandervaere et al (2000) approach, K_V.

Site	Depth (cm)	$K_{Z\text{-}SL}$	K_{lin} ($cm\ s^{-1} \times 10^{-3}$)	K_V
2	1	-77%	166%	-2379%
	11	-77%	149%	2326%
	21	-77%	301%	3260%
	31	-77%	172%	2648%
	41	-77%	120%	-129531%
	51	-77%	178%	-882%
6	0	-77%	323%	-64226%
	11	-77%	222%	-32416%
	21	-77%	144%	-1262%
	31	-77%	159%	1970%
	41	-77%	170%	2449%
	51	-77%	1425%	-249494%
9	11	-77%	169%	-7470%
	21	-77%	2827%	-2174230%
	31	-77%	1214%	-43376%
	41	-77%	383%	-76621%
	51	-77%	169%	2597%

Table F.2. Percent change in K(h=-3cm) for the Zhang (1997) approach with Schaap and Leij (1998) parameters, $K_{Z\text{-}SL}$, the simple linear analysis, K_{lin}, and the Vandervaere et al (2000) approach, K_V, compared to the Zhang (1997) approach with Carsel and Parrish (1988), $K_{Z\text{-}CP}$.

Site	Depth (cm)	S_{ZCP}	S_{ZSL} (cm $s^{-0.5}$)	S_V
2	1	0.040	0.035	-0.022
	11	0.011	0.010	0.003
	21	0.042	0.037	-0.003
	31	0.036	0.031	0.001
	41	-0.038	-0.033	-0.086
	51	0.042	0.036	-0.012
6	0	0.147	0.129	0.076
	11	0.081	0.071	0.036
	21	0.017	0.015	-0.017
	31	0.042	0.037	0.003
	41	0.046	0.040	-0.006
	51	0.148	0.130	0.033
9	11	0.016	0.014	0.020
	21	0.048	0.042	-0.034
	31	0.068	0.059	0.010
	41	0.063	0.055	0.029
	51	0.017	0.015	-0.001

Table F.3. Summary of sorptivity (cm $s^{-0.5}$) from the laboratory measurements of the mini-disk infiltrometers using the Zhang (1997) approach with Carsel and Parrish (1988) parameters, $S_{Z\text{-}CP}$, with Schaap and Leij (1998) parameters, $S_{Z\text{-}SL}$, and the Vandervaere et al (2000) approach, S_V.

Site	Depth (cm)	$S_{Z\text{-}SL}$	S_V ($cm\ s^{-0.5}$)
2	1	-12%	-155%
	11	-12%	-76%
	21	-12%	-108%
	31	-12%	-96%
	41	-12%	126%
	51	-12%	-128%
6	0	-12%	-48%
	11	-12%	-56%
	21	-12%	-201%
	31	-12%	-92%
	41	-12%	-113%
	51	-12%	-78%
9	11	-12%	26%
	21	-12%	-172%
	31	-12%	-85%
	41	-12%	-54%
	51	-12%	-108%

Table F.4. Percent change of sorptivity for the Zhang (1997) approach with Schaap and Leij (1998) parameters, $S_{Z\text{-}SL}$, and the Vandervaere et al (2000) approach, S_V, compared to the Zhang (1997) approach with Carsel and Parrish (1988), $S_{Z\text{-}CP}$.